SU-SEL-65-064

Backscatter of Radio Waves from the Ground

by

J. G. Steele

June 1965

Technical Report No. 109

Printed (but not supported) under
Office of Naval Research Contract
Nonr-225 (64), NR 088 019, and
Advanced Research Projects Agency ARPA Order 196-65

This report is a thesis submitted for the degree of
Doctor of Philosophy at the University of Queensland,
Brisbane, Australia.

RADIOSCIENCE LABORATORY

STANFORD ELECTRONICS LABORATORIES

STANFORD UNIVERSITY · STANFORD, CALIFORNIA

SEL-65-064

BACKSCATTER OF RADIO WAVES FROM THE GROUND

by

J. G. Steele

June 1965

Technical Report No. 109

Printed (but not supported) under
Office of Naval Research Contract
Nonr-225(64), NR 088 019, and
Advanced Research Projects Agency ARPA Order 196-65

This report is a thesis submitted for the degree of
Doctor of Philosophy at the University of Queensland,
Brisbane, Australia.

Radioscience Laboratory
Stanford Electronics Laboratories
Stanford University Stanford, California

AUTHOR'S PREFACE, MAY 1965

The author welcomes the reprinting of this work for distribution by the Office of Naval Research.

This work was completed in December 1964 and has since been favourably received by examiners appointed by the University of Queensland.

The main results have now been accepted for publication in the Australian Journal of Physics, under the title "Backscatter of 16-Mc/s Radio Waves from Land and Sea." A Research Note entitled "Ground Backscatter and the Ionosphere" is to be submitted to the Journal of Atmospheric and Terrestrial Physics. Both of these articles contain material which corrects and enlarges upon sections of this thesis.

ERRATA

Page	Line	Should Read
14	12	Pattern of Antenna.
149	18	... at 18.75 m ...
173	20	... below 8°, at the sounder. This may mean ...
	23	... sounder. However, tilts in the ionosphere may allow the low angle rays to reach the scattering area at high angles.
190	10	... AP-13, 179.

ABSTRACT

At 16 Mc/s, the backscatter coefficient for sea is found to be 10 dB higher than for land for angles of elevation between 25^{o} and 15^{o}. At lower angles there is a knee effect, and the backscatter coefficient decreases very rapidly. The knee angle is lower for sea than for land. For a given surface, and at angles above the knee, the variation of backscatter coefficient with elevation angle is consistent with the type of scatter expected from upright objects such as trees or wave crests, and the fading of the echoes is ascribed to the Doppler movement of these objects.

The frequency of observation of Sporadic-E by backscatter sounding is strongly influenced by whether the backscatter occurs on the land or on the sea. Sporadic-E itself appears to be uniformly distributed.

In observations of F region propagation by the backscatter technique, the nature of the terrain should be taken into account. This is particularly important in the case of trans-equatorial one-hop propagation.

The experimental procedures developed here include a new method of measuring the vertical radiation patterns of large high frequency antennas, a computer program to calculate the power of backscatter echoes, and the application of

vertical incidence data to oblique propagation. New insights are gained into the interpretation of backscatter records.

PREFACE

The research described in this thesis was carried out while the author was a candidate for the degree of Doctor of Philosophy in the University of Queensland. The investigation forms part of a program of ionospheric research within the Physics Department, directed by Professor H. C. Webster, to whom the author is especially grateful. Dr J. A. Thomas and Dr J. D. Whitehead also supervised the work and made many valuable suggestions.

The work was financially assisted by the Australian Radio Research Board and made use of equipment purchased with funds supplied under Research Contract AF 64(500) - 9 by the United States Air Force.

Particular thanks are due to the academic staff and research students of the Physics Department, especially Mr B. A. McInnes, Mr M. Akram, Mr E. W. Dearden, Miss E. M. Matthew (now Mrs G. Swenson) and Mr K. S. White.

The experimental work was made possible by the co-operation of the Commonwealth Bureau of Meteorology, the Commonwealth Department of Civil Aviation, the Ionospheric Prediction Service of the Department of the Interior, the Physics Department (R.A.A.F. Academy) of Melbourne University and the technical staff of the Physics and Surveying Depart-

ments, University of Queensland. Data analysis was assisted by Mrs D. Nielson and Miss B. Roes.

The work described in this thesis is, to the best of my knowledge and belief, original, except as acknowledged in the customary form. I declare that I have not submitted this material, either in whole or in part, for a degree at any university.

J. G. Steele

TABLE OF CONTENTS

BACKSCATTER OF RADIO WAVES FROM THE GROUND

1. INTRODUCTION

Ground backscatter is the process by which high frequency waves are scattered at the ground, so that some of the energy goes back along its original path to the transmitter. This process is used in oblique incidence sounding of the ionosphere. A pulse of radio energy may undergo backscatter at the ground after one or more hops via the ionosphere, and the time the echo takes to return is a measure of the range at which backscatter occurs. The various uses of backscatter sounding are outlined in PETERSON (1954).

Calculations of the strength of backscatter echoes have been hampered by the lack of information about the backscatter coefficient. This coefficient is a parameter similar to the radar cross-section per unit area. Its relation to other parameters will be considered in Chapter 4.

The composition and roughness of the ground where backscatter takes place may be expected to influence the backscatter coefficient. An understanding of the variation of the backscatter coefficient with elevation angle and type of ground is essential to the correct interpretation of backscatter records, and is the main concern of this project.

(a) Variation with angle of elevation :- For a given backscatter sounder, a particular type of echo is not normally detectable beyond a certain maximum range, and this range may be determined by the angular variation in the backscatter coefficient. A knowledge of this variation facilitates the identification of echo types and the recognition of anomalous behaviour of such types. This will be discussed with special reference to Sporadic-E echoes.

(b) Variation with type of ground :- Neglect of any variation with ground type may result in misleading conclusions on the nature of the ionosphere in certain directions. For example, as a result of backscatter observations, it has been thought that E_s occurs more frequently over the sea than over the land (EGAN and PETERSON, 1961, 1962), and that transequatorial one-hop propagation occurs preferentially to the north-east of Brisbane rather than to the north-west (THOMAS, 1962). Knowledge of the backscatter coefficient may cause these conclusions to be modified.

In the present investigation, the 16 Mc/s backscatter sounder at Brisbane was used (THOMAS and McNICOL, 1960a, 1960b, 1962). It consists of a rotating array of four horizontally-polarized Yagi antennas mounted half a wavelength above the ground (Fig. 1). The antennas were directed to the east and to the west, to obtain echoes from the sea and the land in turn. Rectangular pulses of 600 microseconds duration were transmitted, at a peak power of 5 kW. Back-

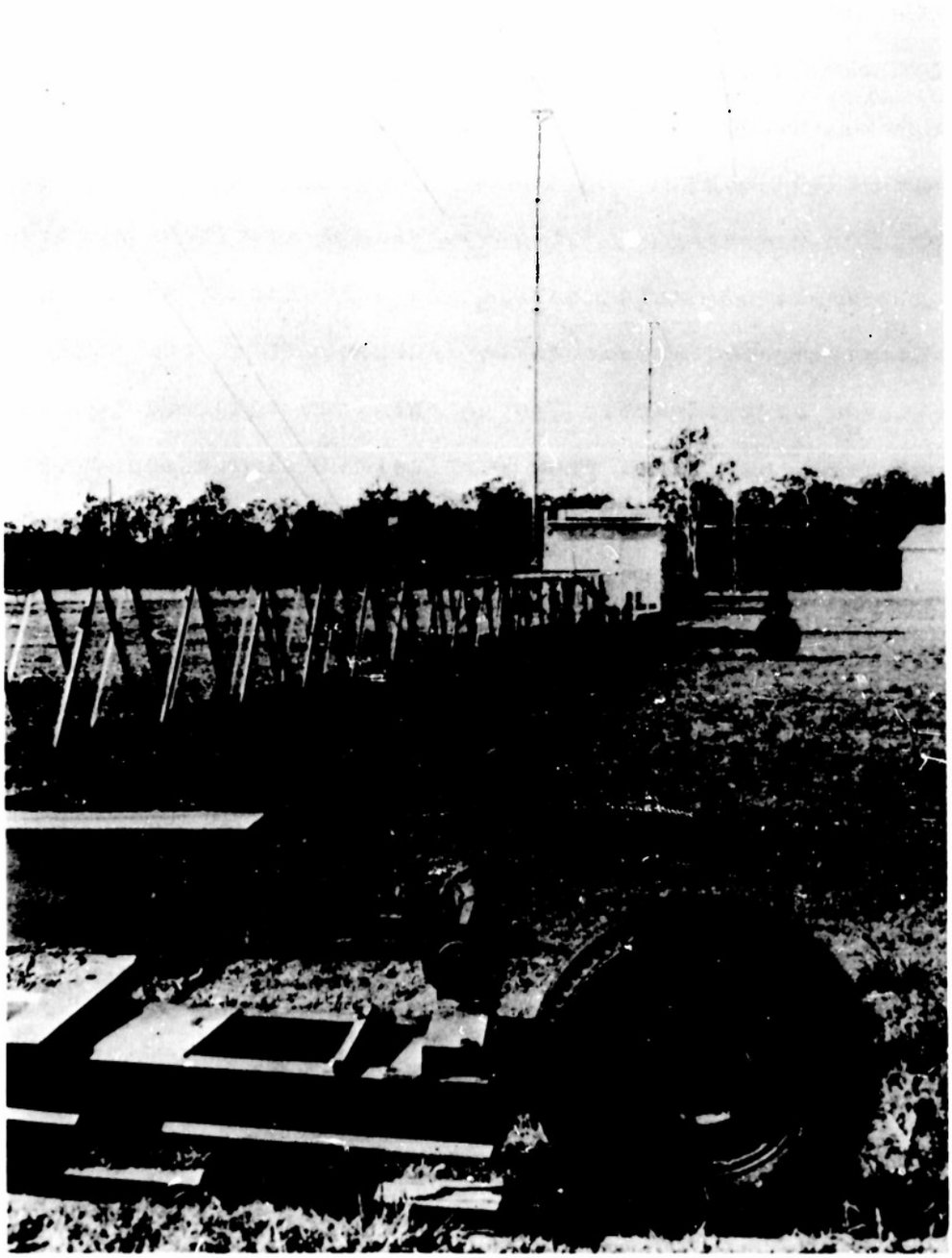

Fig. 1. 16 Mc/s rotating array.

scatter echoes were recorded on a range —amplitude display, by the use of a swept-gain unit. As the recording film moved slowly past the brightness-modulated oscilloscope trace the echo intensity in dB was plotted against the oblique range of the echo.

For comparison with these range—amplitude records, the range—amplitude relationship was calculated, assuming the backscatter coefficient to be independent of the angle of elevation of the rays. The calculation involved ionospheric parameters, estimated from vertical incidence soundings at Brisbane, and the vertical radiation pattern of the antenna array, measured by means of a balloon-borne transmitter. The results of the calculations were compared with the corresponding observed backscatter records to deduce the relative backscatter coefficient at the calculated angle of elevation.

2. PREVIOUS WORK

2.1 Variation with angle of elevation

DIEMINGER (1951), experimenting at Lindau between 1 and 20 Mc/s, found that the echo amplitude decreases rapidly with range, and reasoned that this could only occur if the backscatter coefficient depends mainly on the number and areas of surfaces larger than a wavelength. As such areas usually have a very small angle of tilt, the backscatter coefficient should decrease very rapidly as the angle of elevation decreases.

SHEARMAN (1961) at Slough recorded 15 and 21 Mc/s backscatter echoes on a range—amplitude display. For comparison, he calculated the echo pattern, neglecting any angular dependence of backscatter coefficient, and making other simplifying assumptions, and found fairly good agreement with observations. In reply to discussion he stated that the major unknown was the variation of backscatter with the angle of incidence, and that this could only be measured satisfactorily from an aircraft. Meanwhile, NIELSON et al. (1960) published some results of measurements made with an airborne radar. They pointed out that when ground-based backscatter sounders are used to find ground backscatter parameters, at least two ionospheric reflections are involved, and the precise nature of

these reflections cannot be determined. To avoid these ionospheric reflections, they installed a 4 kW backscatter radar operating at 32.8 Mc/s in an aircraft, which was flown over California, the Pacific Ocean, Alaska and the Arctic Ocean. Echoes were recorded on an A-scope display, and compared with echo strengths calculated on the basis of a constant backscatter coefficient of one. The ratio of the observed to the calculated values was taken as a measure of the backscatter coefficient. They constructed curves of backscatter coefficient against angle of elevation from 60^{o} to 4^{o}, showing a slope of about 0.6 dB per degree for horizontally polarized waves. At angles below 20^{o}, the slope was greater than 0.6 dB per degree for ice, and less than 0.6 for desert. The antennas, which were attached to the nose and tail of the aircraft, were difficult to calibrate accurately, as the calibration had to be done while the aircraft was in flight, using a receiver on the ground. It was difficult to know the aircraft's position and orientation during the calibration, and the overall errors amounted to perhaps 6 dB (NIELSON et al. page 34, errata), and therefore 12 dB for transmission and reception.

HAGN (1962) analysed the work of NIELSON et al. (1960). He published a revised set of curves for the backscatter coefficient. He rejected results below angles of 10^{o} for sea and 20^{o} for land, because at lower angles the curves show a "knee" effect (HAGN, 1962, p.8 and p.85) where the

backscatter coefficient decreases very rapidly. This knee did not always occur at the same angle, even for the same terrain. Further, the presence of mountains at the horizon often made it impossible to assume that the ground was uniformly rough for rays near the tangent ray. Towards higher angles of elevation, the backscatter coefficient increased rapidly for horizontal polarization (about 1 dB per degree), but decreased very slowly for vertical polarization (about -0.1 dB per degree).

2.2 Variation with type of ground

VILLARD and PETERSON (1952a, 1952b), at 3-30 Mc/s, found no noticeable change in echo amplitude from land to sea. They suggested that, unlike u.h.f.(300-3000 Mc/s) echoes which do show some change, h.f.(3-30 Mc/s) backscatter echoes involve comparatively long wavelengths and comparatively enormous echoing areas. Both these factors would tend to prevent any discrimination between land and sea in backscatter records.

DIEMINGER (1951), while observing backscatter echoes at 1-20 Mc/s swept frequency, identified an echo group which remained at almost constant range, in contrast to the group associated with the skip focusing area, which was varying in range. The range of the fixed group corresponded to backscatter from the Northern slopes of the Alps. SILBERSTEIN (1954), using 3-25 Mc/s swept frequency backscatter, found a similar group of echoes constant in range, thought to be due to the Rocky Mountains. McCUE (1956) found that at angles of elevation near 30^{o} land is a more prominent source of backscatter than sea, for frequencies near 6 Mc/s.

SHEARMAN (1956b) reported that observations at Slough between 10 and 27 Mc/s confirmed the lack of dependence on terrain found by VILLARD and PETERSON. He considered that this was surprising, in view of the large difference between sea and land echoes noticed with airborne centimetric radar equipment. He suggested that any differences are masked by

the large variations in echo amplitude introduced by the ionosphere. In the discussion following this paper it was pointed out (by W. R. Piggott) that the ordinary countryside is quite rough from the radio point of view, and that a mountain is not necessarily a better echoing object than the ground as a whole. The only cases which have been reported of abnormal backscatter from distant mountain masses are those for which the phase of the reflected wave is held constant over a wide area, so that we have a coherent mirror-type reflection. For example, the ionospheric station at Lindau is almost at the centre of curvature of the Alps, and frequently receives an abnormal echo coming from that arc. The beginning of the Alps forms a sort of curved mirror, and while the mountains themselves do not contribute much, the gradual rise at their beginning does. In contrast, no echo from the Alps was received at Slough.

SHEARMAN considered vertically polarized waves, and developed a model for the scattering source, namely a system of hemispherical bosses on a perfectly conducting ground, and found that a density of about 1000 bosses /km^2 could account for the observed strength of a backscatter echo from a ground range of 670 km West of Slough, that is, from the Atlantic Ocean. In the discussion it was noted that these scattering sources would be common for average sea conditions, and a serious decrease in scattering would only be expected for exceptionally calm conditions. SHEARMAN concluded the dis-

cussion by stating that there was a clear need for a thorough investigation of the relative amplitude of scatter from land and sea, and that the direct measurement from an aircraft of the scattering properties of various types of terrain at these wavelengths would provide much useful evidence.

WILKINS and SHEARMAN (1957) reasserted the view that, in general, terrain effects tend to be masked by much larger variations of echo strength due to the variable efficiency of the ionosphere as a propagation medium. They added that with the wide beams in use with rotating aerials, azimuthal resolution of geographical features is unlikely to be practicable. SHEARMAN (1961) said that the variation with the type of ground appears surprisingly small, and that the only objects which have so far been identified are large mountain ranges.

RANZI and DOMINICI (1959), although using a wide beam, observed that 22.3 Mc/s backscatter echoes from continents, and especially from the Sahara Desert, have a considerably lower intensity than those from the sea. They suggested a difference of about 10 dB between land and sea. DOMINICI (1962, 1963) qualified this by remarking that the intensity distribution of echoes was influenced by the variation in the vertical radiation pattern of the antenna, owing to the varying topography around the antenna.

NIELSON et al. (1960) found that for horizontal polarization, and at 32.8 Mc/s, the backscatter coefficient for

desert was about 6 dB less than that for smooth ice or sea at angles of elevation above 30^{o}, but that at about 10^{o} desert gives stronger backscatter than sea. Vertical polarization gives stronger return than horizontal from sea, but land is indifferent to polarization. As the roughness of the sea increases, polarization effects become less noticeable.

HAGN (1962), in revising the results of NIELSON et al., found that for both horizontal and vertical polarizations, the backscatter coefficient for land is about 20 dB below that for sea. Owing to the uncertainty concerning the knee in the curves, no comparison could be made at angles lower than 20^{o}.

2.3 Summary

After many years during which ground-based sounders found no difference between sea and land scatter, one exception emerged in which the sea appeared to give stronger backscatter.

The widely publicized need for aircraft measurements of the backscatter coefficient has been fulfilled, and the results show two major effects, the existence of a knee in the curve of backscatter coefficient against elevation angle, and the predominance of sea scatter strength over that of land scatter. However, only comparatively smooth surfaces were considered. Also, the calibration of air-

borne antennas proved to be quite difficult and the results may contain large errors.

3. THE RELATIONSHIP OF THE PRESENT INVESTIGATION TO PREVIOUS WORK

The present work concerns elevation angles from about 7° to 30°, and the polarization at the echoing area is elliptical and variable, owing to Faraday rotation in the ionosphere.

Concerning the variation of the backscatter coefficient with angle of elevation, the knee effect has been discovered independently of HAGN (1962), and the angle at which this occurs has been investigated for the terrain types available. For angles above the knee, the coefficient decreases, and this trend agrees with HAGN's results for vertical polarization.

The variation with the type of ground is quite marked, and the present work indicates that for land, the backscatter coefficient is about 10 dB less than for sea. This supports the observations of RANZI and DOMINICI (1959). For low angles, HAGN's reappraisal of NIELSON et al. has removed the most serious disagreement with the present work.

The method used here has certain advantages over previous methods.

(a) Narrow Azimuthal Beam.

(i) As the antenna beam is narrower than in previous in-

investigations, there is less azimuthal spread of the rays in the ionosphere, and therefore the ionospheric parameters in the path of the rays can be estimated more precisely.

(ii) The minimum group range of a backscatter echo serves as a guide to the ionospheric configuration at the control point, and this range is well defined when the antenna beam is narrow.

(iii) Owing to the narrower beam, it is easier to discriminate between different areas of the ground from which backscatter is received.

(b) Vertical Radiation Pattern of Antenna.

(i) A ground-based antenna is easier to calibrate than an airborne antenna.

(ii) Changes in the topography near the antenna can be taken into account, so that the variations of the vertical pattern with azimuth are well understood.

(c) Location of the Sounder.

(i) The sounder is well placed for comparing land and sea backscatter, as the land and sea extend without interruption for several thousand kilometers to the west and east respectively.

(ii) It is particularly easy to observe the boundary between land and sea scatter, as the coastlines recede almost radially from Brisbane at ranges beyond 500 km.

(iii) The absence of noise such as that due to aircraft

engine ignition facilitates good recording of echoes.

(d) Applicability of Results.

(i) The polarization of the waves at the echoing area is typical for operating conditions of backscatter sounders, therefore the backscatter coefficient derived here should be more applicable to normal backscatter sounding than that derived from airborne experiments.

(ii) The frequency used here (16 Mc/s) is typical for backscatter sounding, whereas the results obtained at higher frequencies cannot confidently be extrapolated to this region.

(iii) The echoes may include returns from many large topographical features, as the echoing area is large. In contrast, aircraft measurements involve a much smaller sample of terrain, and therefore comparatively smooth surfaces only were selected (HAGN, 1962).

4. DISCUSSION ON THE BACKSCATTER COEFFICIENT

4.1 Definitions

Backscatter coefficient

The radar equation is of the form

$$P_R = \frac{\sigma G^2 P_o \lambda^2}{(4\pi)^3 R^4}$$ (CLAPP, 1946; SHEARMAN, 1956b; COSGRIFF et al., 1960; NIELSON et al., 1960),

where P_o = power transmitted

P_R = power received

R = range of target

G = antenna gain

σ = radar cross-section

$$= \frac{4\pi \cdot \text{Power scattered per unit solid angle}}{\text{Power incident per unit area}}$$

(NIELSON et al., 1960).

A parameter commonly used in radar is σ_o, the radar cross-section per unit area of the surface.

The backscatter coefficient γ (COSGRIFF et al., 1960) is related to σ_o, and is the radar cross-section per unit area normal to the direction of propagation at the scattering area (HAGN, 1962).

For an element of scattering area, the incident rays

are nearly parallel, and Fig. 2 illustrates the relationship between γ and σ_o. Let

Δ = angle of elevation of the rays

$\varphi = \frac{\pi}{2} - \Delta$ = angle of incidence

A_s = area of scattering surface

$A_n = A_s \sin\Delta$ = area projected normal to the rays = "incidence area"

Then $\sigma_o = \frac{\sigma}{A_s}$

and $\gamma = \frac{\sigma}{A_n} = \frac{\sigma_o A_s}{A_n} = \frac{\sigma_o}{\sin\Delta}$, or $\frac{\sigma_o}{\cos\varphi}$.

NIELSON et al.(1960) and HAGN (1962) use the symbol $\rho = \frac{\gamma}{2}$. SHEARMAN (1956b) uses the symbol $A_o = \sigma_o$. The parameters γ, ρ, σ_o and A_o are independent of the radar parameters such as transmitted power, pulse width, antenna pattern and receiver gain. They depend only on the terrain and the angle of elevation.

Isotropic scatter

If energy is scattered uniformly into the space available the scattering is called isotropic. For isotropic scattering into the hemisphere above the scattering surface, γ is constant for all angles of elevation. If all the incident energy is scattered in this way, $\gamma = 2$ and $\rho = 1$.

To show this, let

P_s = power scattered

P_i = power incident

$d\theta$ = element of azimuthal angle

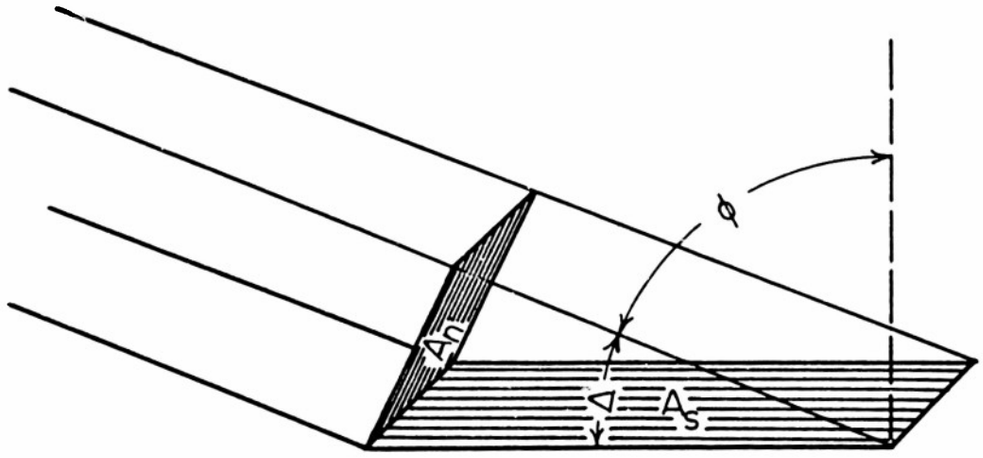

Fig. 2. Rays falling on element of scattering area.

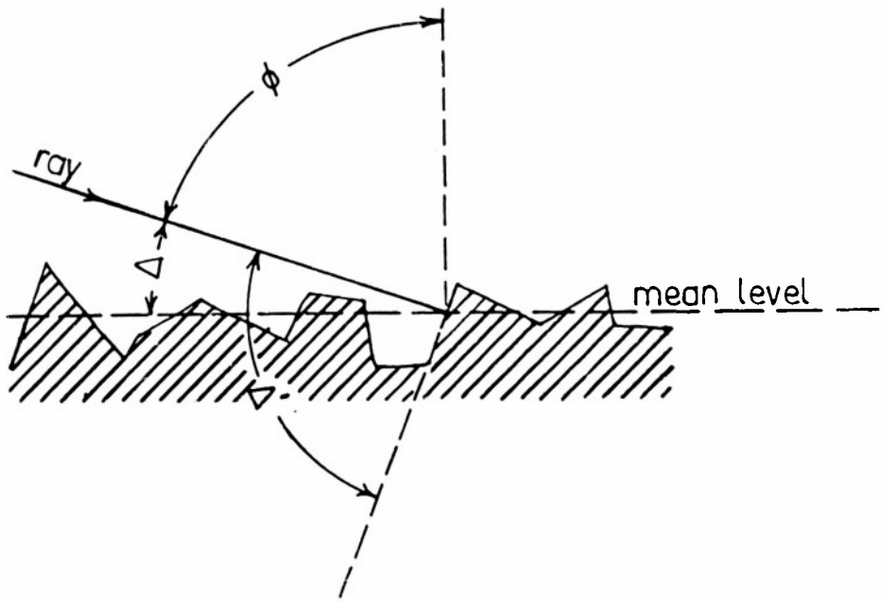

Fig. 3. Quasispecular scatter from suitably inclined surface.

$d\Omega$ = element of solid angle,

$= d\Delta d\theta$.

From the definition of σ ,

$$\sigma = 4\pi \frac{\frac{dP_s}{d\Omega}}{P_i/A_s} .$$

Therefore, $$dP_s = \frac{P_i}{4\pi} \frac{\sigma}{A_s} d\Omega$$

$$= \frac{P_i}{4\pi} \gamma \sin \Delta \, d\Delta d\theta .$$

If energy is scattered uniformly into the volume above the surface,

$$\text{total } P_s = \frac{P}{4\pi} \gamma \int_0^{\pi/2} \int_0^{2\pi} \sin \Delta \, d\Delta \, d\theta$$

$$= \tfrac{1}{2} P_i \gamma .$$

If $P_s = P_i$, $\gamma = 2$.

Some workers, for lack of information about γ , have assumed isotropic scatter (SHEARMAN, 1961; THOMAS and McINNES, 1962), and others, when investigating γ, have assumed it constant for comparison with experimental results (CLAPP, 1946; COSGRIFF et al. 1960; NIELSON et al. 1960). An exception is SHEARMAN (1956b), who assumed A_o constant.

Relative backscatter coefficient

The present work concerns the relative backscatter coefficient. To find the absolute backscatter coefficient, it is necessary to find absolute values of the radar parameters, but that is to be dealt with in another project.

The relative backscatter coefficient does, however, make possible a comparison of backscatter from different terrains and at different angles of elevation.

Angular power spectrum

For radar echoes, some authors (EVANS and PETTENGILL, 1963; LYNN et al., 1964) use the parameter $P(\varphi)$, the angular power spectrum, which is defined as the angular distribution of echo power per unit area of surface. It is the angular part of σ_o.

4.2 Laws of illumination and emission

In the formulation of echo power, use is made of the following laws, which apply to a unit element of surface area, that is, for the case when $A_s = 1$, and hence

$$A_n = \sin \Delta = \cos \varphi \ .$$

Let F = incident flux.

Cosine law of illumination

Power incident on unit element of surface = $F A_n$

$$= F \cos \varphi \ .$$

Lambert's cosine law

The flux emitted from a unit element of surface is the same in all directions.

Hence, power emitted in any direction from unit area of surface = (emitted flux) . A_n

= (constant) . $\cos \varphi$

For the echo power, the above laws are combined, so that $P(\varphi) = \cos^2 \varphi$.

Lommel-Seelinger law

For diffuse reflection, $P(\varphi, \theta) = \dfrac{\cos \varphi \cos \theta}{\cos \varphi + \cos \theta}$

where θ = angle of emission. For backscatter, $\theta = \varphi$, hence $P(\varphi) = \cos \varphi$.

Specular scatter

If $\varphi = 0$, the above laws reduce to $P(\varphi) = 1$.

For some surfaces, this may hold even when φ is not zero. φ is the angle between the ray and a line normal to the mean level of the terrain, and Fig.3 shows that even if φ is not zero, the local angle of incidence $\boldsymbol{\varphi}'$ on any given scatterer may be zero. For example, if a surface is covered with hemispheres, $P(\varphi)$ does not vary with φ, since provided the radius a is greater than 0.2λ, σ_o is approximately equal to πa^2 for each scatterer. This type of specular scatter from suitably orientated surfaces of sufficient extent is referred to as "semispecular" or "quasi-specular" scatter.

The relationship of γ and σ_o to the scattering laws

$P(\varphi)$ is the angular part of σ_o, so

$$P(\varphi) \propto \sigma_o$$

$$\propto \gamma \cos \varphi .$$

If σ_o is independent of φ, $P(\varphi)$ is constant, that is, specular type.

If γ is independent of φ (i.e. isotropic scattering), $P(\varphi) \propto \cos \varphi$, that is, Lommel-Seelinger scattering.

Table 1 gives a summary of the laws:

TABLE 1

SUMMARY OF SCATTERING LAWS

Scattering Law	$P(\varphi)$ or σ_o	$\gamma = \frac{\sigma o}{\cos \varphi}$
Lambert	$\propto \cos^2 \varphi$	$\propto \cos \varphi$
Lommel-Seelinger	$\propto \cos \varphi$	$\propto$ constant
Specular	$\propto$ constant	$\propto 1/\cos \varphi$

The use of the scattering laws in the present work

The calculations follow the method of SHEARMAN (1956b), with one difference. He assumed A_o constant; here γ is assumed constant.

In SHEARMAN, we find the equivalent of $dP \propto A_o \, dS$, where dP = power returned from an element of ground area dS, and $A_o = \sigma_o$. A_o was taken as the radar cross-section of n hemispherical bosses per unit area of the ground, which is $n \pi a^2$ (a = radius of boss), independent of φ .

In the present work, A_o has been replaced by $\gamma \sin \Delta$. As a first assumption, γ is taken to be independent of Δ . This brings the presentation into line with NIELSON et al. (1960), HAGN (1962) and COSGRIFF et al. (1960), and therefore the results will be easily comparable with theirs. The difference between observations and calculations will be a measure of the deviation of the backscatter coefficient γ from isotropic scattering.

4.3 Attempts to find γ theoretically

The usual approach is to assume a statistical model of the surface and derive an expression for γ that depends on φ and the wavelength λ, and on the statistical parameters assumed, such as the distribution of heights of surface irregularities and the auto-correlation coefficient of the irregularities across the surface. The classical work in this field is by DAVIES (1954, 1955), and most work subsequent to his merely alters the statistics. DAVIES considered a statistical model of a surface with height z following a Gaussian distribution with standard deviation σ. For radiation scattered from a "slightly rough" surface (z and $\sigma \ll \lambda$), he deduced that the radiation can be divided into a coherent and an incoherent component. For the latter, $P(\varphi) = \cos^2 \varphi$, which corresponds to Lambert's Law. For a "very rough" surface ($\sigma \gg \lambda$), DAVIES had some success in predicting the sea clutter of centimetric radar from $\varphi = 0^\circ$ to 30°. His treatment failed to predict $P(\varphi)$ near $\varphi = \pi/2$, which would be of greater interest.

KATZ and SPETNER (1958), quoted by COSGRIFF et al. (1960), produced a theory for angles near grazing. The theory takes account of the fact that there is a tendency for scatter to be specular in type, from upright objects such as tree trunks. Their result is of the form

$$\gamma \propto \frac{1}{\cos \varphi \ (A + \cos^2 \varphi)}$$

which, depending on the value of A, will be between $1/\cos\varphi$

and $1/\cos^3 \varphi$. An experimental result given by KATZ and SPETNER (1960) is of this type. A similar theoretical result was derived by PEAKE (1957a, 1957b, 1958); it applies to a model consisting of vertical cylinders, and for φ near $\pi/2$, $A \gg \cos^2 \varphi$, so $\gamma \propto 1/\cos \varphi$.

The usefulness of a statistical approach is doubtful. HAGN (1962) held the view that no simple mathematical model would suffice to describe the actual physical process. COSGRIFF et al. (1960) pointed out that even with satisfactory theoretical models, there would be no unique way of associating a given type of terrain with one of the models. The theories do, however, give some idea of the ways in which γ might be expected to vary with φ . It is to be expected that different types of surfaces and different radio wavelengths will give rise to laws ranging from Lambert to various forms of specular, and γ will correspondingly depend on powers of $\cos \varphi$ ranging from 1 to -3.

4.4 Summary

The backscatter coefficient is a parameter similar to the radar cross-section per unit area, and is related to it by the expression $\gamma = \sigma_o / \cos \varphi$. For isotropic scattering, γ is constant, and in the present work this is assumed in the calculations, so that the difference between observations and calculations will be a measure of the deviation of γ from isotropic scattering. Theoretical considerations suggest angular dependencies ranging from $\gamma \propto \cos \varphi$ to $\gamma \propto 1/\cos^3 \varphi$.

5. SPECULAR AND DIFFUSE ECHOES

Specular and diffuse echoes correspond to the coherent and incoherent components derived theoretically by DAVIES (1954, 1955).

5.1 Evidence from lunar echoes

Various authors (BROWN, 1960, HAGFORS, 1961, WINTER, 1962) consider that the total lunar return at any instant of time is composed of two components, which are the result of two general types of terrain features. The specular component arises from an area where $\varphi = 0$, or from a large-scale irregularity giving a coherent echo such that φ is effectively zero. The diffuse component is predominant as φ approaches 90°, and follows a law such as $P(\varphi) \propto \cos^2 \varphi$ (PETTENGILL, 1960) or $\cos \varphi$ (EVANS and PETTENGILL, 1963, LYNN et al., 1964), or some intermediate law such as $\cos 3/2\varphi$ (BROWN, 1960, EVANS and PETTENGILL, 1963). The diffuse component is presumably due to a small-scale roughness superimposed on the large-scale structure (HAGFORS, 1961).

The relative importance of specular and diffuse components depends on the wavelength. At optical wavelengths, the moon is a completely diffuse scatterer. Moon radar experiments (LYNN et al., 1964) show that as the wavelength

is increased from 8 mm to 68 cm, the diffuse component becomes weaker relative to the specular component. As might be expected, the longer waves are insensitive to the small-scale irregularities. The specular component, which at 8 mm is predominant only for φ close to zero, becomes predominant at longer wavelengths for values of φ up to 50°. While it is risky to extrapolate this trend to higher values of φ at yet longer wavelengths, it is tempting to predict that at 16 Mc/s (λ= 18.75 m) the specular component of lunar echoes would predominate at all angles. Recent work by DAVIS and ROHLFS (1964) at wavelengths between 11m and 22m confirms the virtual absence of any diffuse component.

5.2 Terrestrial echoes at u.h.f.

COSGRIFF et al. (1960), using wavelengths near 1 cm, found that for surfaces such as grass, that appeared rough in terms of λ, γ was fairly independent of incidence angle between 10° and 80°. This corresponds to a predominance of the diffuse component. For a smooth surface such as a concrete road, γ decreased by as much as 25 dB (COSGRIFF et al. page 43) when Δ varied from 80° to 10°, indicating a decrease in the diffuse component. A longer wavelength would have the same effect as a smoother surface (neglecting changes in dielectric constant). It might therefore be expected that at longer wavelengths, the diffuse component of ground scatter will be small, and therefore the echo will depend mainly on irregularities contributing specular type

returns.

5.3 Terrestrial echoes at h.f.

NIELSON et al. (1960, page 2) assumed specular echoes to be negligible except near vertical incidence, although it was noted that W. S. Ament believed that there is a transitional range between specular (at vertical incidence) and diffuse (at grazing incidence) (BLAKE, 1950). The subsequent report (HAGN, 1962) admitted that a large return could come from a combination of specular and diffuse components; no attempt was made to distinguish between them, apart from cases where mountains and coastlines gave obvious specular enhancements. Such cases were not used to determine ρ, and only smooth surfaces such as flat deserts and icefields were studied. If we combine HAGN's results for horizontal and vertical polarizations, we find that for mixed polarizations there is a marked decline in ρ as Δ varies from 50^{o} to 20^{o}, indicating a weak diffuse component. In addition, a knee effect cuts off the echo at still lower values of Δ.

In the present work, the knee effect is also observed. Above the knee, however, γ increases as Δ decreases from 30^{o} to 10^{o}. This increase cannot be due to a diffuse component alone, since for diffuse scattering γ should be constant (Lommel-Seelinger) or vary as $\cos \varphi$ (Lambert), but here it varies approximately as $1/\cos^{2}\varphi$. The conclusion may be that the echoes are predominantly quasi-specular. The difference from HAGN's result probably lies in the fact that he

selected smooth surfaces only, for which the specular component is concentrated near vertical incidence; the present work involves very large areas with a mixture of many types of surfaces, the more rugged of which could cause specular type scattering even at angles near grazing incidence.

5.4 The nature of the irregularities

If the irregularities are hemispheres (SHEARMAN, 1956b), we should observe specular type echoes such that $\gamma \propto 1/\cos\varphi$, but in fact we get $1/\cos^2\varphi$. It is therefore considered that the irregularities responsible for the strong quasi-specular component are more rugged in shape than hemispheres, and cause comparatively stronger backscattering at low angles of elevation. It has been observed that at low angles, vertically polarized signals are scattered back more strongly than horizontally polarized signals (HAGN, 1962). In the present work, with polarization elliptical after reflection in the ionosphere, it seems likely that the echo consists of a large quasi-specular component due to the vertical component of the radiation at the scattering sources, superimposed on a much weaker, and perhaps negligible, diffuse component.

The theory of KATZ and SPETNER (1958) and also of PEAKE (1957a, 1957b, 1958) considers scatterers which are primarily vertical, such as vertical cylinders. Trees would vary in shape from approximate hemispheres to vertical cylinders analogous to top-loaded vertical antennas. The form-

er would be expected to give $\gamma \propto 1/\cos\varphi$, and the latter probably $1/\cos^3\varphi$, as it resembles the type of antenna most effective at low angles. An average of $1/\cos^2\varphi$ is consistent with this picture. For the sea, it is likely that backscatter arises primarily at the wave crests (KERR, 1951). The scatterers would then be conical in shape, that is, intermediate between hemispheres and vertical cylinders, and again probably consistent with $\gamma \propto 1/\cos^2\varphi$.

In terms of irregularities such as trees and wave crests, certain phenomena mentioned elsewhere in this work may be interpreted:

(i) Sea echoes are stronger than land echoes. In general, the sea is rougher than the land, and there are more wave crests effective in producing backscatter than effective trees, per unit area.

(ii) Sea echoes fade regularly, but land echoes fade in a random fashion, giving a patchy appearance on the records. This may be because the wave crests tend to move with a constant velocity, and therefore give rise to a constant Doppler fading of the echoes. On the other hand, the trees move to and fro in the wind in a random fashion, so that the Doppler frequency is never constant. Fading is discussed in Section 7.2.

(iii) The knee in the γ (Δ) curve occurs at about 13° for land and at lower angles for sea. Although re-radiation from a short vertical dipole is most effective at low angles

of elevation, ground losses seriously diminish the radiation near the grazing angle. Ground losses are greater for land than for sea, hence the higher knee angle for land. The variation in the knee angle for sea may be due to variations in the height of the wave crests above the surrounding surface. This is discussed in Section 9.4.

5.5 Summary

Table 2 compares the theories and experiments mentioned in this chapter.

Both lunar and terrestrial echoes show a trend away from diffuse scattering as the wavelength is increased from 1 cm to about 30 m. The scattering irregularities at 16 Mc/s are therefore considered to be quasi-specular scatterers. They are probably most sensitive to vertically-polarized waves, and are probably to be identified with trees and the crests of sea waves. Such a picture is consistent with other observed features of backscatter echoes.

TABLE 2

SUMMARY OF THEORIES AND EXPERIMENTS

Type	γ	Theory	Experiment
Diffuse	$\cos \varphi$	Lambert; DAVIES, "slightly rough", u.h.f.	Optical frequencies.
	1	Lommel-Seelinger. "isotropic"	LYNN et al., diffuse component of lunar echoes at u.h.f.; COSGRIFF et al., rough terrestrial surfaces at u.h.f.
	$1/\cos \varphi$	SHEARMAN, hemispheres.	HAGN, smooth sea and land at 32 Mc/s, vert. poln, low angles.
Specular	$1/\cos^2 \varphi$	PEAKE, and KATZ and SPETNER, vertical cylinders, low angles.	Present work, random sea and land at 16 Mc/s, probably vert. poln., low angles.
	$1/\cos^3 \varphi$		

6. ANTENNA CALIBRATION

6.1 Introduction

In the calculation of the power returned in backscatter echoes it is necessary to know the vertical radiation pattern of the antenna system. The antenna comprised a rotating array of four three-element Yagi antennas, horizontally polarized. The Yagis were spaced 1.1 λ apart and were designed to produce a narrow azimuthal beam. The height of the Yagis was 0.47 λ above the ground, with the intention of achieving a broad lobe in the vertical plane with its maximum at about 25^{o} (THOMAS and McNICOL, 1960a).

The vertical radiation pattern could not be calculated simply, as the ground was level to only about 100 feet from the centre of the array (about 1.5 λ), and also because the electrical properties of the ground were not known. The radiation pattern in a southerly direction was measured using a transmitter in a helicopter hovering at selected heights at a distance of 2 km (THOMAS and McNICOL, 1960b). The pattern in a northerly direction was measured using a transmitter in an aeroplane traversing a line to the north at a series of fixed heights and fixed distances (THOMAS and McINNES, 1962). The maximum radiation was found to occur at an elevation of 35^{o} to the south, and 20^{o} to the

north. The discrepancy between these results, as well as tne need for measurements to the east and west, necessitated a more accurate method.

With a helicopter or aeroplane the main errors arise in plotting the position of the aircraft during the experiment. The helicopter was not capable of hovering at a constant altitude. The aeroplane did not fly exactly on the desired course. In both cases theodolite readings of the position of the aircraft could not be taken at the antenna site for elevation angles below about 20^{o}, as the view was obscured by trees and haze. The aeroplane was particularly difficult to track with a theodolite owing to its speed. These problems were overcome by tethering a balloon at a range of up to 5000 feet (80 λ), and operating a balloon theodolite at the tethering point. The height of the balloon was calculated from the amount of tethering line released, and when possible this was checked by another theodolite near the antenna. In calm weather, the balloon remained in any desired position for long periods.

6.2 Equipment

(a) Balloon. Meteorological balloons of 300, 500 and 800 g were used, the most suitable being a 500 g neoprene balloon specially designed for use as a captive (tethered) balloon. The balloon was filled with Hydrogen to a diameter of 6 or 7 feet, that is, to a volume of about 150 cubic feet. This provided a free lift of over 10 pounds; as the balloon,

transmitter and tethering line weighed about 4 pounds, the tension on the tethering line was about 6 pounds. It was found from experience that a nylon line of 50 pounds breaking strain was needed, to allow for wind gusts and braking during ascent, as well as damage to the line due to snags. The line was wound manually by means of a heavily-constructed reel one foot in diameter. Figure 4 illustrates the balloon and reel. In good weather the balloon could be recovered after its flight and taken by truck to another site for further use.

(b) Transmitter. The transmitter is illustrated in Fig.5. The box contained a 16 Mc/s crystal-controlled oscillator, modulated by a 130 c/s signal. Fig. 6 shows the miniaturized construction of the circuit, and Fig. 7 is the circuit diagram. The 9 volt battery shown was capable of operating the transmitter for several hours. It was found that after the first few minutes of operation, the transmitter output decreased at the rate of about 8% per hour, and this correction was applied to the data taken during the experiment.

The transmitter was suspended 25 feet below the balloon on a separate line, to allow it to hang free of the tethering line, and to allow it to rotate about a vertical axis with the aid of a swivel. The signal was radiated by a short horizontal dipole of length 1.25 m. As this is much shorter than a wavelength, its radiation pattern was assumed to be the same as for an elementary dipole in free

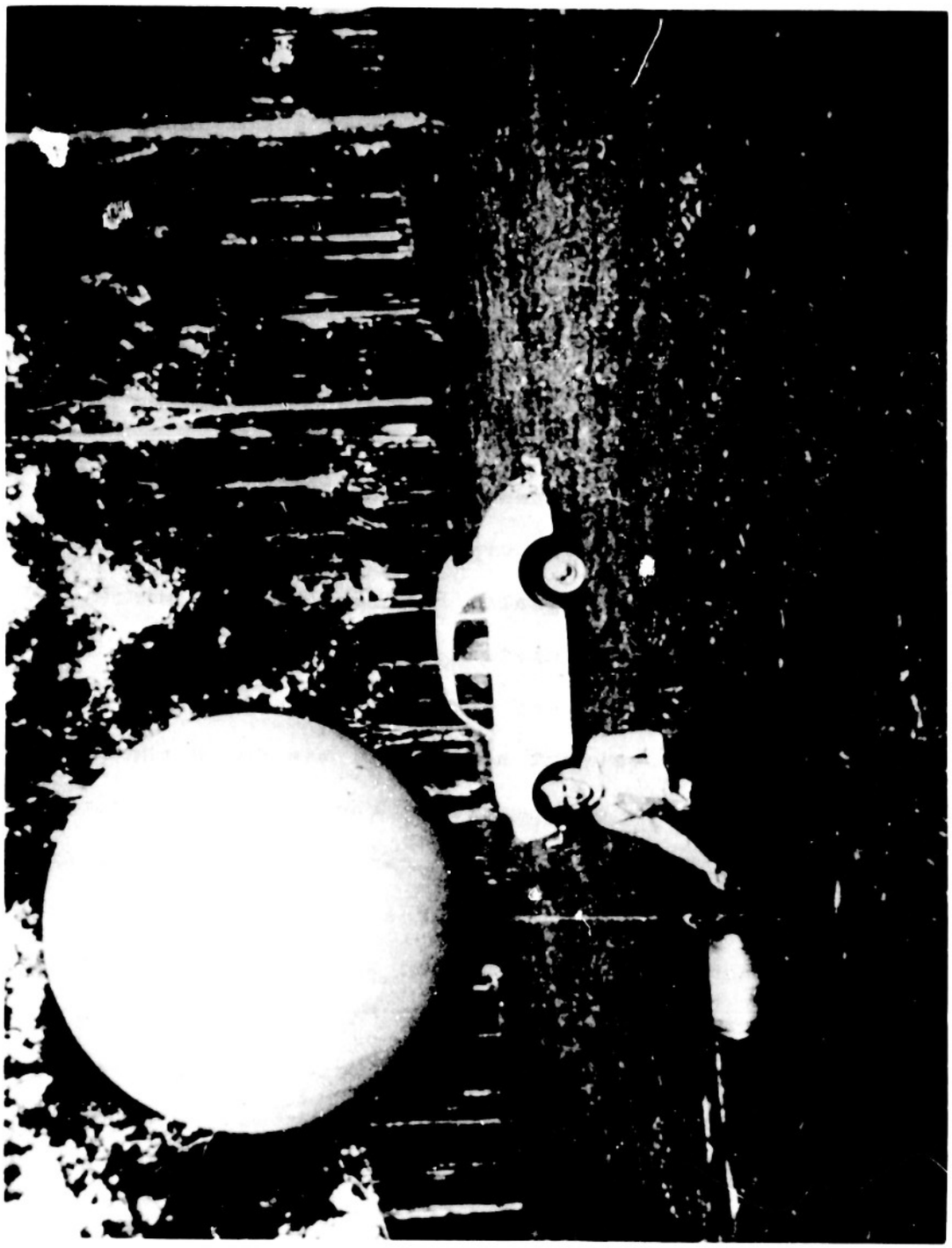

Fig. 4. Balloon and reel used in antenna measurements.

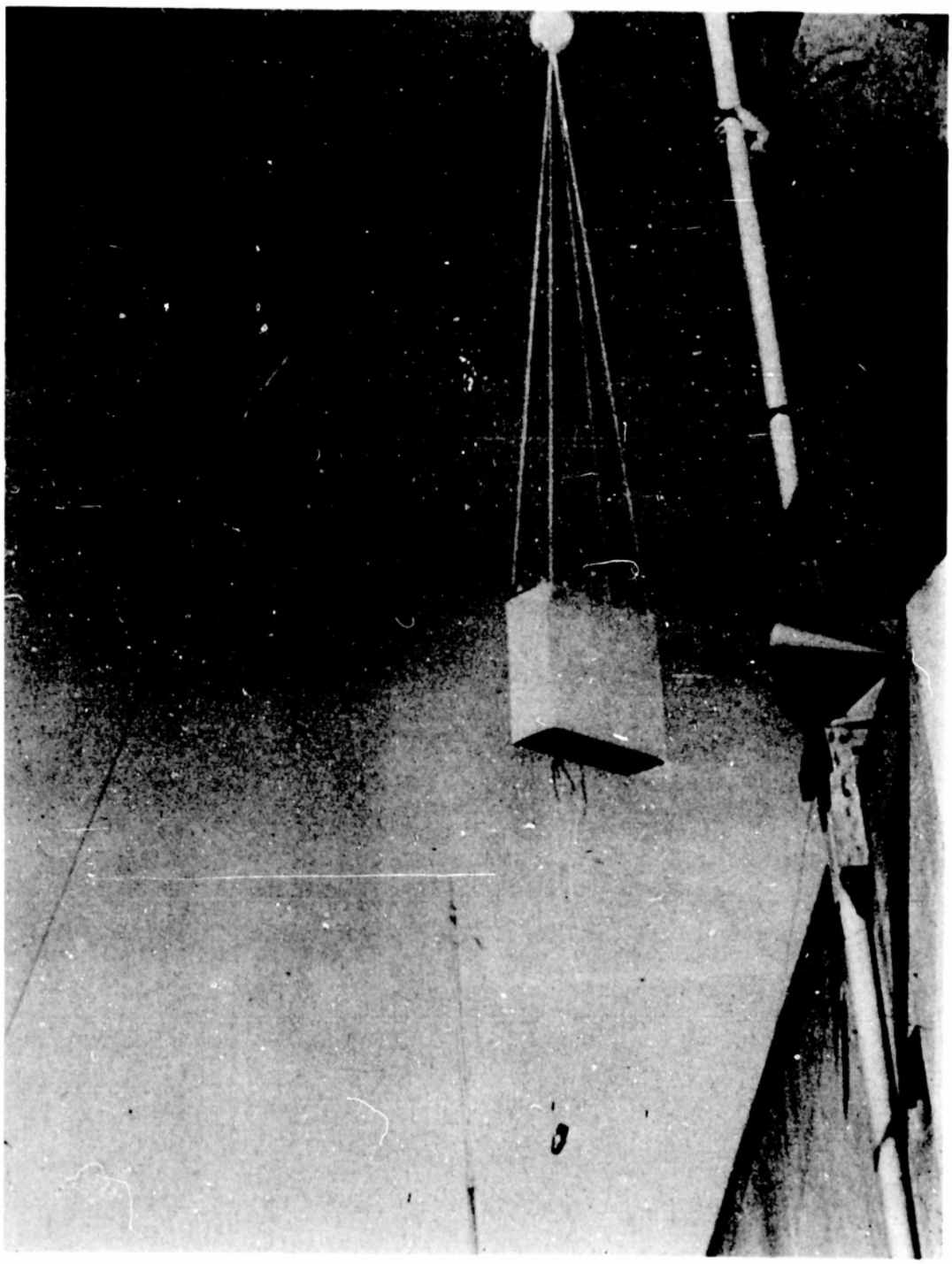

Fig. 5. Balloon-borne transmitter, showing wind vanes.

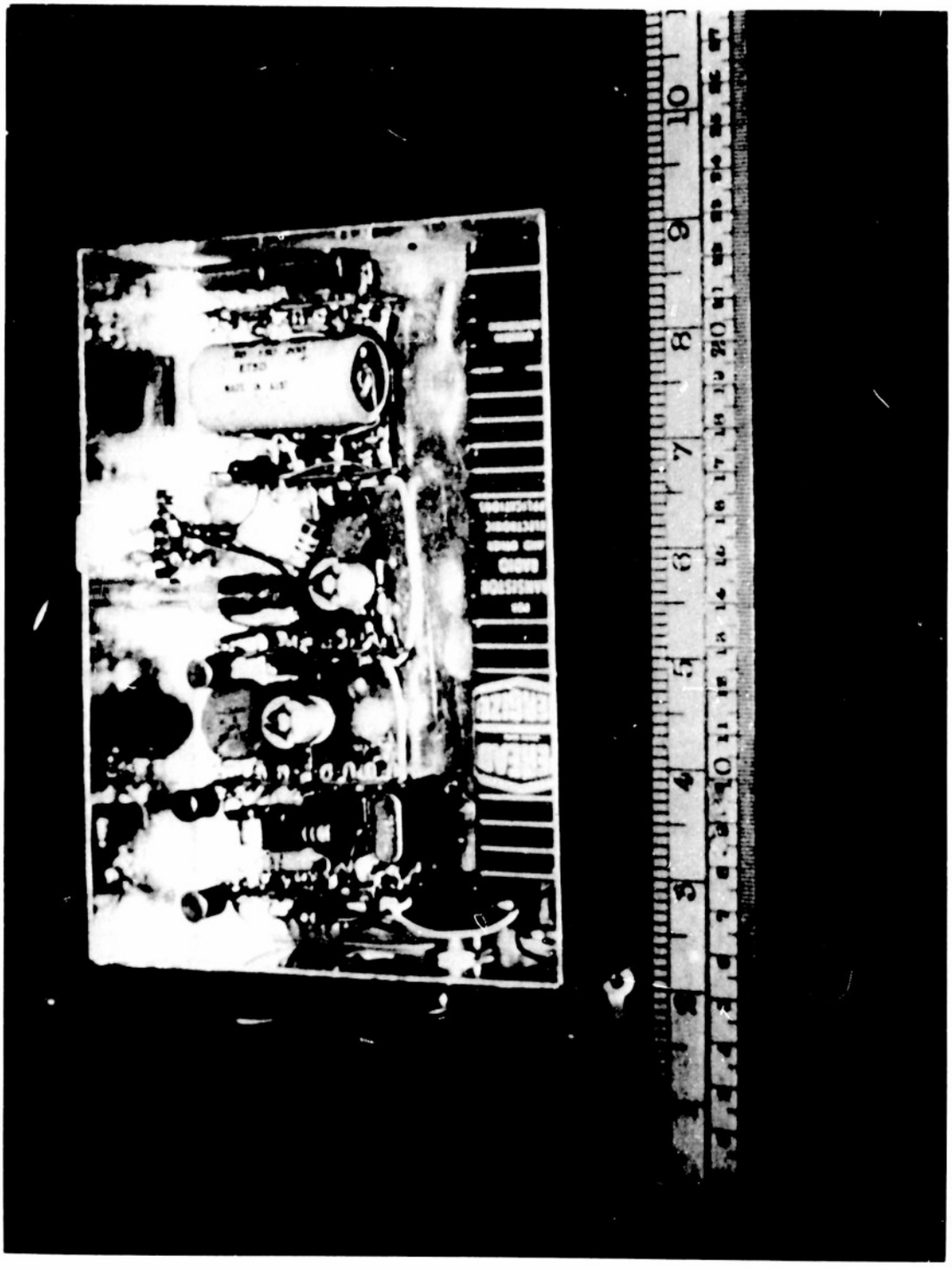

Fig. 6. Balloon-borne transmitter, circuit construction.

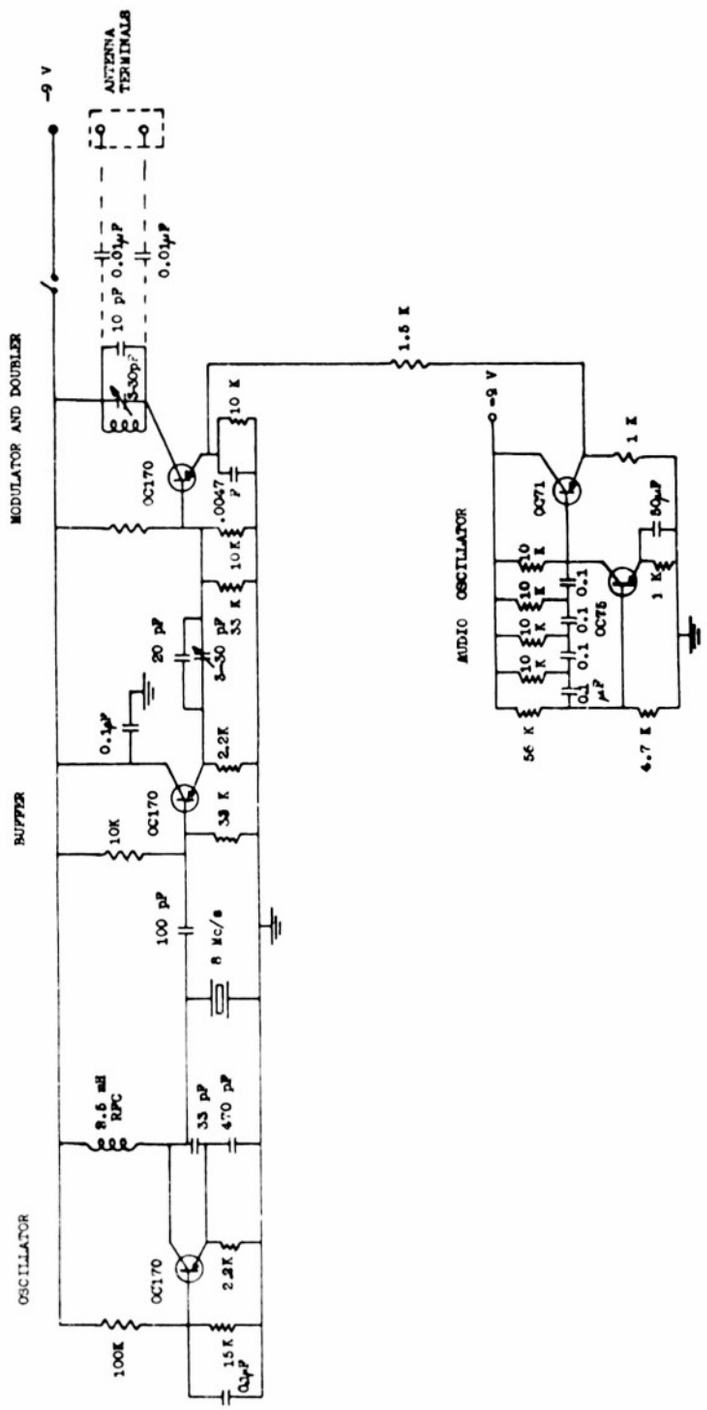

Fig. 7. Circuit diagram for 16 Mc/s balloon-borne transmitter with 130 c/s modulation.

space, that is, radiating isotropically in the vertical plane, and having maximum azimuthal radiation in the broadside directions. Two celluloid cones were used as wind vanes to keep the dipole rotating, and the result was a kind of turnstile antenna. BRUECKMANN (1963) had a similar idea when he proposed that an artificial earth satellite be equipped with a turnstile antenna for use in calibrating large antenna systems.

6.3 Recording

The signal was received at the array on the ground, and the 130 c/s waveform was displayed on an oscilloscope. Earphones were used to aid identification and tuning. The array was rotated continuously, to ensure that every reading was taken with the maximum of the azimuthal pattern of the array directed towards the balloon. This rotation took nearly 4 minutes, whereas the balloon transmitter rotated about once per second. Twice in each rotation of the turnstile antenna, its maximum was directed towards the array, and this maximum was independent of the angle of elevation of the transmitter with respect to the receiver, because of the uniform vertical pattern of the turnstile antenna. The effect of rotating both antennas was that the fast (2 c/s) fading of the transmitted signal was modulated by the slow fading due to the rotation of the array. When the received signal reached a maximum during any one rotation of the array, the peak voltage was read from the oscilloscope

screen.

To allow time for rotation of the array and for the winding of the reel, the balloon was raised or lowered at 5 minute intervals. Each new position corresponded to some new angle of elevation, so new theodolite readings were taken. Theodolite tracking was made possible at night by attaching a small 6 volt bulb to the transmitter, with a separate battery supply. A red globe was used so that the light could be distinguished from the stars, and the regular twinkling due to rotation of the transmitter also aided identification. Most of the work had to be done at night to satisfy aviation regulations, but it was found that at night the calm atmospheric conditions were much superior to daytime conditions, and so night flying was preferred.

Communications between the balloon site and the rotating array were effected by means of a radio link from a truck at the balloon site to a hut near the rotating array, and thence by underground telephone to the control cabin of the array. The schematic diagram of Fig. 8 shows this arrangement.

6.4 Geometry

The range and elevation angle of the pilot transmitter were obtained by graphical construction based on theodolite readings and the length of the tethering line. The length of the line was measured by counting the number of revolutions of the winding reel. Although the line was sub-

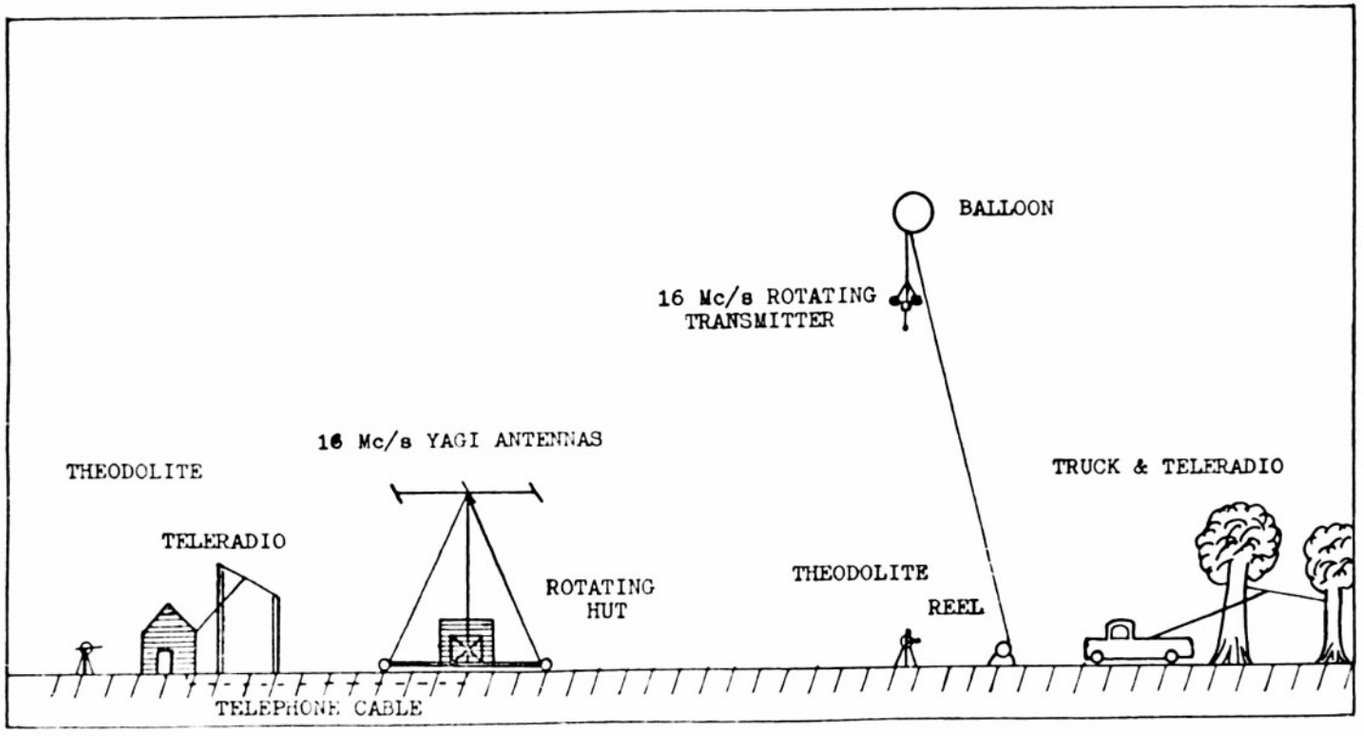

Fig. 8. Schematic diagram of method of measuring vertical pattern of array.

ject to stretching, it was found that after the first use of the line no correction for stretching was needed, as the line was then permanently in tension on the reel and further stretching was negligible under normal conditions.

Figure 9 is a scale drawing illustrating the graphical construction. In the elevation at the right of the figure, the line length and theodolite elevation were used to give the height of the transmitter and its ground range from the reel. This range was then used in conjunction with the theodolite azimuth to construct the plan and thereby find the ground range of the balloon from the array. Finally, this ground range and the balloon height were used to construct the left-hand elevation, from which the range r and elevation Δ of the transmitter with respect to the array were read. The elevation with respect to a second theodolite near the array was also read from the figure, and found to agree with readings from that theodolite to within 1^{o}. In the figure, the crosses represent positions of the transmitter; the line and balloon are sketched in, and Δ is indicated, for the highest position only.

Figure 9 is taken from an actual balloon flight, with the balloon tethered to the west of the array at a point 277^{o} from true north.

Figure 10 shows another flight, with the tethering point 44^{o} from true north. The dots represent positions of the transmitter, and the numbers represent minutes after

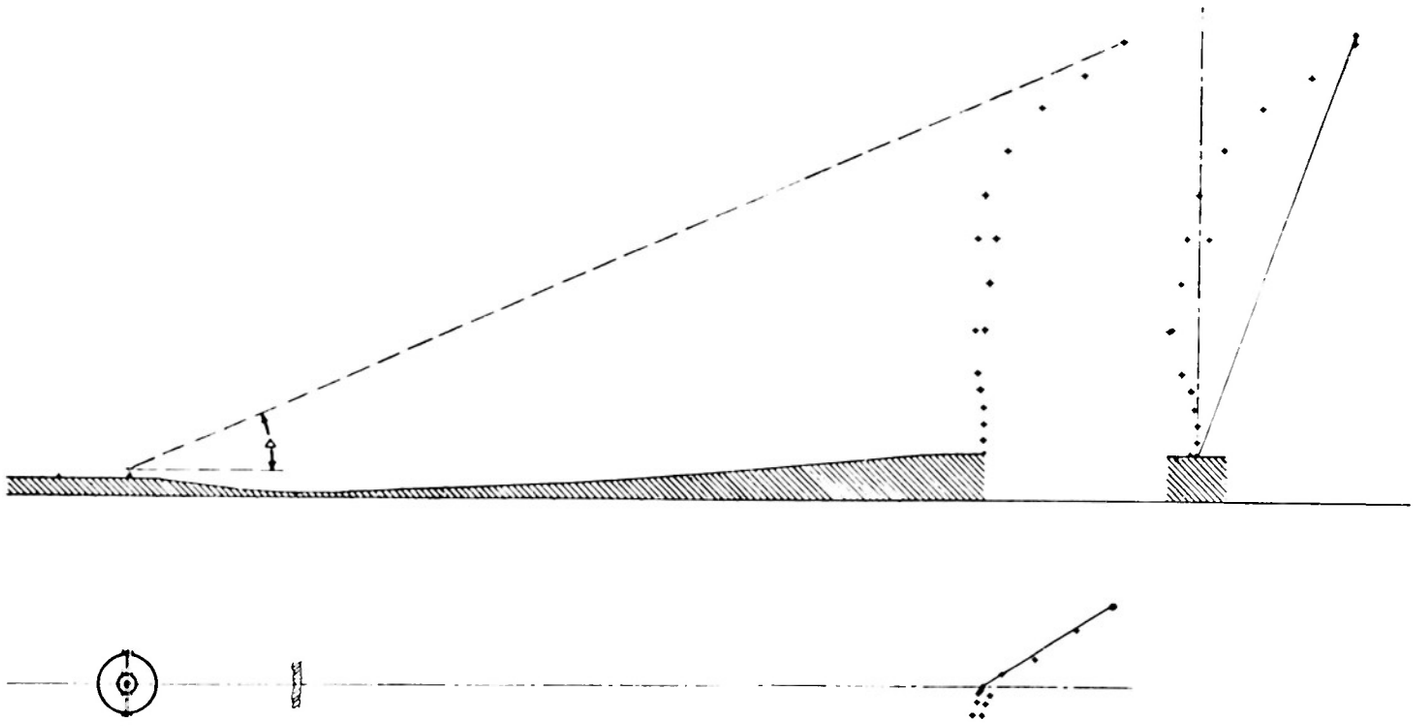

Fig. 9. Graphical construction to obtain elevation and range of balloon during flight W.

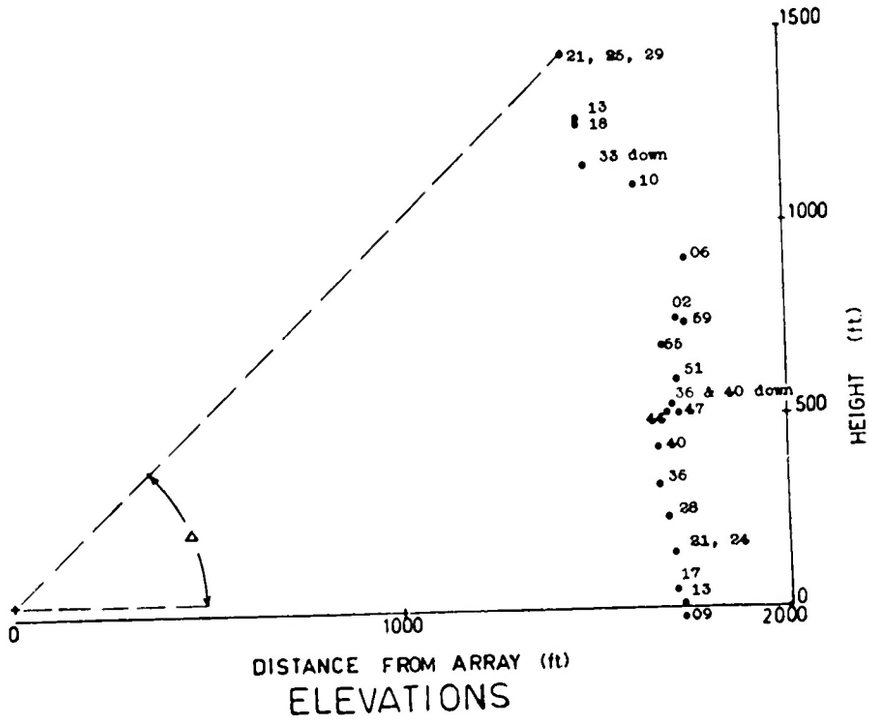

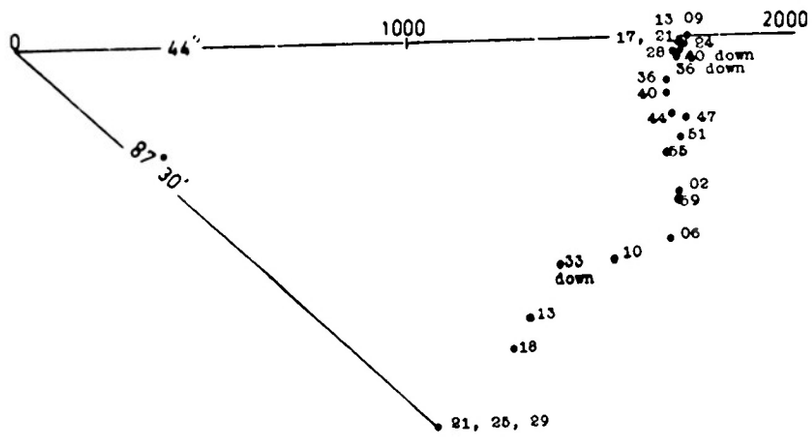

PLAN

Fig. 10. Balloon flight NE.

the hour, the times at which readings were taken at the array. Three points represent readings taken during descent of the balloon, the remainder during ascent. The elevations show heights above ground level at the array, which was 55 feet above sea level. The azimuth of the balloon with respect to the array varied by more than 40°, but this did not invalidate the results, as the ground in a north-easterly direction near the array was of fairly constant slope, and also because the greatest deviation from 44° was for high angles of elevation. Provided Δ was less than 20°, the azimuthal deviation was less than 10°. For higher angles the ground ray was reflected well within the level circle of radius 100 feet, so the vertical pattern was considered to be azimuthally invariant above 20°.

Table 3 summarizes the main balloon flights.

TABLE 3

BALLOON FLIGHTS

Designation	Date	Time of Start (hours)	Azimuth (degrees)	Range (ft)	Max. Ht. (ft)	Max. Elev.
N1	28.11.62	0044	1	4900	1200	$22^{\circ}30'$
N2	4.12.62	2252	355	1940	750	$51^{\circ}30'$
NE	5.12.62	0209	44	1730	1450	$44^{\circ}00'$
SE	6. 2.63	2248	143	1890	1600	$25^{\circ}45'$
W	7. 2.63	0212	277	2800	1500	$23^{\circ}00'$

The aerial photograph of Fig. 11 shows the five sites. The rotating array appears as a circle in the centre of the picture. The main topographical feature in the vicinity of the array is a small creek that flows from the south-west in a clockwise direction to the north-east, as far as the river which is itself comparatively unimportant in the formation of the radiation patterns owing to its greater range.

The ground profiles between the array and the balloon sites are plotted in Fig. 12. The vertical scale is greatly magnified, and heights are measured above sea level. The proximity of the creek on the western side of the array is particularly apparent.

The Fresnel zone condition requires the range of the pilot transmitter to be greater than $2D^2/\lambda$, where D is the lateral dimension of the antenna (BRUECKMANN, 1955; KEAY and GRAY, 1964). The horizontal length of the array = 3.8λ, so $2D^2/\lambda$ = 1728 feet. For the five balloon flights, the balloon was tethered at ranges greater than this, although on one occasion, N2, the balloon was blown to half this range by the wind. The measured vertical pattern may therefore be in error for the higher angles of elevation in this instance.

6.5 Results

$G(\Delta)$, the antenna power gain, was obtained as follows.

$$P(\Delta) \propto G(\Delta) / r^2,$$

Fig. 11. Aerial photograph of Radio Research Station, Moggill, and environs. Arrows indicate sites at which the balloon was tethered.

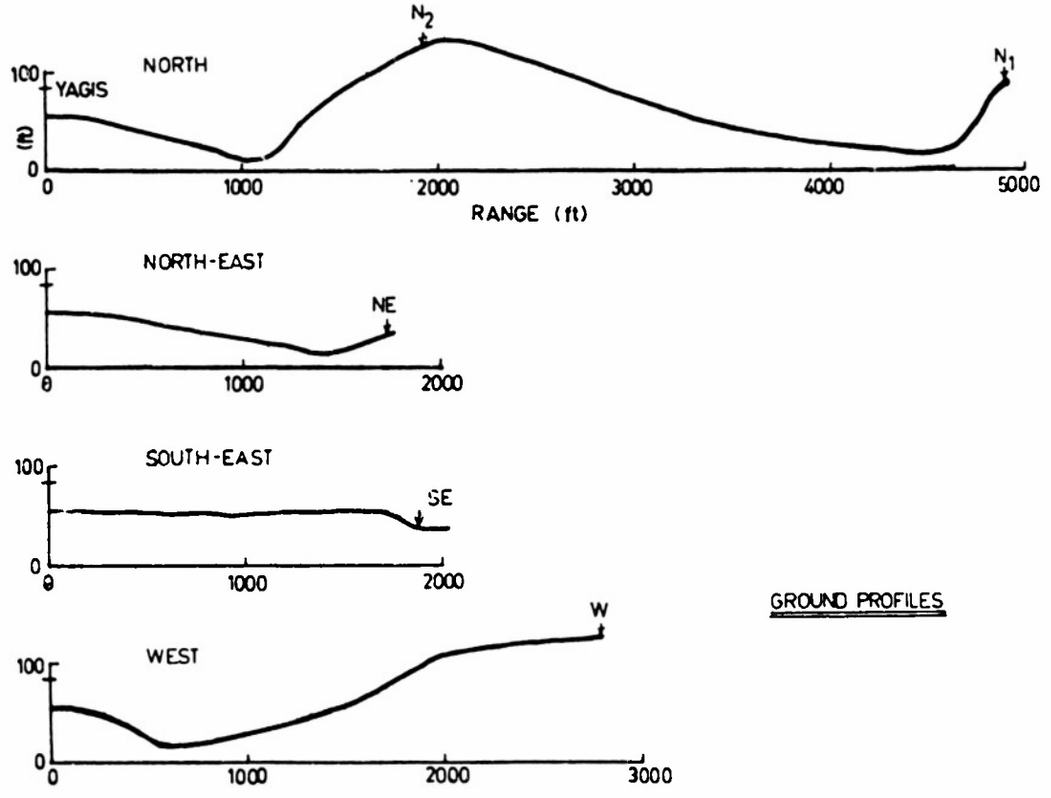

Fig. 12. Ground profiles between array and balloon sites.

where $P(\Delta)$ = power received at the array

$G(\Delta)$ = antenna power gain

r = oblique range of pilot transmitter.

But $P \propto S^2$,

where S = signal strength received (in volts).

Hence, $G(\Delta) \propto S^2 r^2$.

For the five flights, $G(\Delta)$ was plotted against Δ, and for comparison the five curves were normalized at the maximum of the main lobe, which occurred at about 25°. The results are presented in Fig. 13, giving G in dB relative to the gain at the maximum of the lobe. Also shown is a curve obtained by measuring the pattern of a model Yagi at v.h.f. (A.R.R.L., 1956, Fig. 4——55). The model was of similar proportions to the Yagis on the array, and was mounted 0.5λ above a flat, perfectly conducting surface, and its maximum radiation was at 28°.

Only N2 and NE extend the measurements to high angles above the lobe maximum, and their lack of agreement can be attributed to the declining accuracy of the measurements as the balloon ascends. As most backscatter echoes at 16 Mc/s arrive at angles below 30°, the results are adequate for the purpose of the present project.

Interest centres on the disagreements between the curves below the maximum of the main lobe. NE and SE follow the v.h.f. result fairly closely, as the ground is fairly level in those directions in the neighbourhood of the

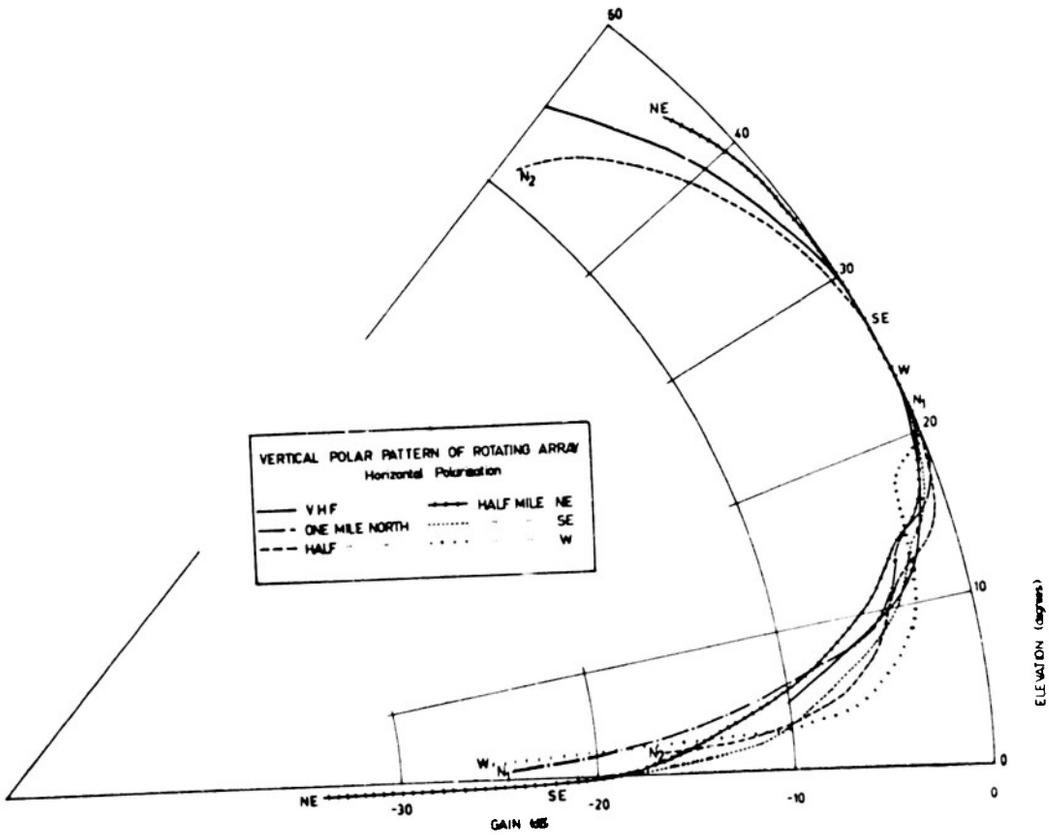

Fig. 13. Vertical radiation pattern of 16 Mc/s array.

array. N1 agrees well with the v.h.f. result down to 5^{o}, and the diminishing radiation below 3^{o} is probably due to shadowing by the intervening hill (See Fig. 12).

In contrast, N2 and W show enhancement of the pattern between 10^{o} and 4^{o}. This is thought to be due to focusing of the ground-reflected rays in the concave mirror formed by the creek. The western pattern will be discussed in greater detail in a later section.

6.6 Correction for the Finite Range of the Balloon

Owing to the finite range of the balloon from the array, it is not always a good approximation to assume that the rays from the pilot transmitter arriving at the array are parallel. If the ground is flat, it is fairly easy to calculate the error in the measured pattern due to this assumption, for various balloon ranges. This was done for the case of a half-wave dipole at a height of $0.5\,\lambda$ above the ground, and assuming a ground reflection coefficient of -1. The correction terms obtained should be sufficiently applicable to the vertical pattern of the array.

The geometry is shown in Fig. 14. It is seen that

$$\tan \varepsilon = \frac{h+\lambda}{L} = \tan \Delta + \lambda / L.$$

Path difference between the direct and ground-reflected rays is

$$d = \frac{L}{\cos \varepsilon} - \frac{L}{\cos \Delta}$$

$$= L (\sec \varepsilon - \sec \Delta)$$

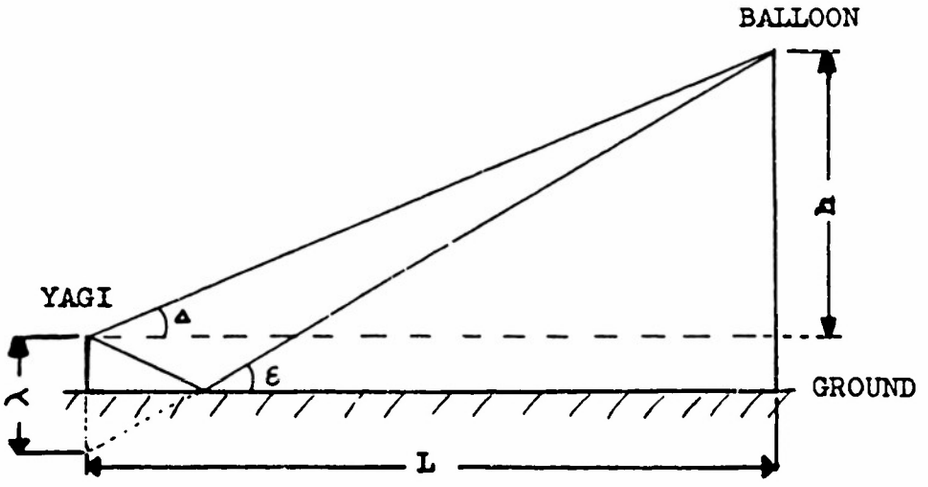

Fig. 14. Ray geometry for finite range of balloon.

$$= L \left\{ \sec \tan^{-1} (\tan \Delta + \lambda / L) - \sec \Delta \right\}$$

Phase difference $\varphi = 2 \pi d / \lambda$.

Let the field at the array due to the direct ray = $E_o \sin \omega t$

Then, for a reflection coefficient of -1,

field at the array due to the reflected ray = $-E_o \sin(\omega t + \varphi)$,

since the assumed dipole is isotropic in the vertical plane.

Total field $E = E_o \left\{ \sin \omega t - \sin (\omega t + \varphi) \right\}$

$$= 2 E_o \cos (\omega t + \varphi /2) \sin (- \varphi /2),$$

i.e., the amplitude of the field varies as $- \sin \varphi /2$,

i.e., $E \propto - \sin \pi d / \lambda$,

$$\propto - \sin \frac{\pi L}{\lambda} \left\{ \sec \tan^{-1} (\tan \Delta + \lambda/L) - \sec \Delta \right\}.$$

This amplitude was calculated on a computer for different values of L/λ from 15 to 1000, and for Δ varying from 1^o to 34^o. The results were plotted as a set of curves of E (in dB) against Δ (Fig. 15). The $L/\lambda = 1000$ curve was taken to be approximately the situation for parallel rays, and it was found that the necessary correction to be applied to the experimental results was greatest at low angles of elevation, and negligible at the maximum of the lobe. For $L/\lambda = 30$, which is the case for measurements N2, NE and SE, the correction was 0.7 dB at 10^o, 1.5 dB at 5^o, and 3 dB at 2^o. This correction was applied to the measured antenna patterns. In cases where the ground slopes away from the array at an angle of, say, 2^o, the correction normally applicable at 5^o, say, would apply at about 3^o. As angles below 5^o were not used in calculating the

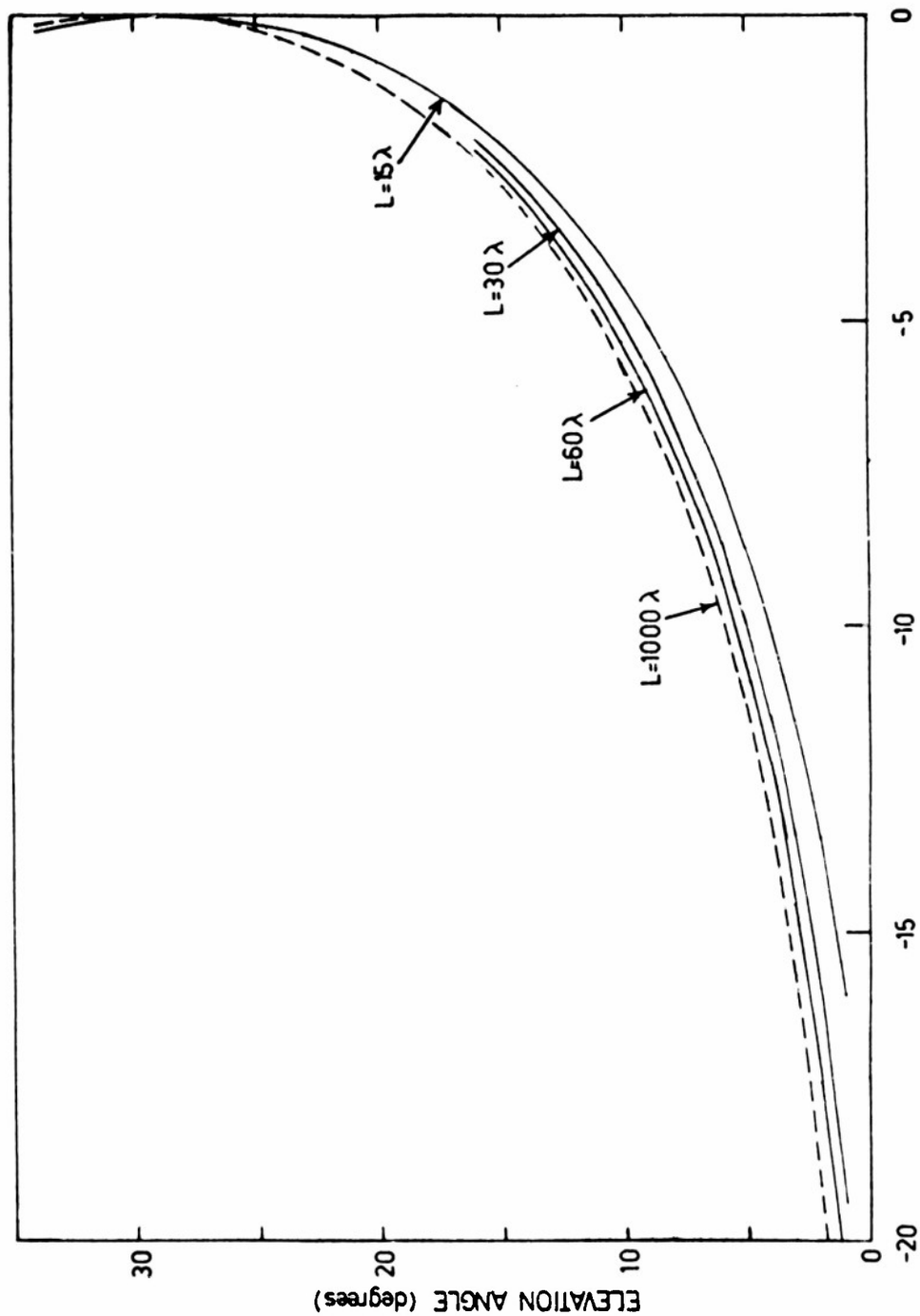

Fig. 15. Theoretical antenna patterns for various balloon ranges.

strengths of backscatter echoes, the correction is important chiefly between 5^{o} and 10^{o}.

To compare the magnitude of this correction with the experimental accuracy, Fig. 16 shows the experimental points obtained from the balloon flight SE ($L = 30.8\ \lambda$), as well as the v.h.f. result referred to above. Also shown are two curves from Fig. 15 , those calculated for $L = 1000\ \lambda$ and $L = 30\ \lambda$. Above 15^{o}, the scatter of points about a mean is $\pm$ 0.5 dB, which is greater than the correction calculated for $L = 30\ \lambda$. Below 15^{o} the experimental points, though fewer, are probably more accurate, and the correction becomes significant compared to the experimental error.

The v.h.f. result illustrates the performance of a typical Yagi under ideal conditions. Even when the experimental points are corrected, they differ from the v.h.f. result, because of the uneven ground and the slightly different nominal height of the antennas.

6.7 Influence of the Western Ground Profile

For the western pattern, the ground near the array is so irregular that it was doubted whether a correction for the finite range of the balloon as described above would suffice. A calculation similar to the above, but taking into account the western ground profile, was carried out. The geometry is shown in Fig. 17. The ground profile was specified in terms of x, y and α , and the figure shows a ground-

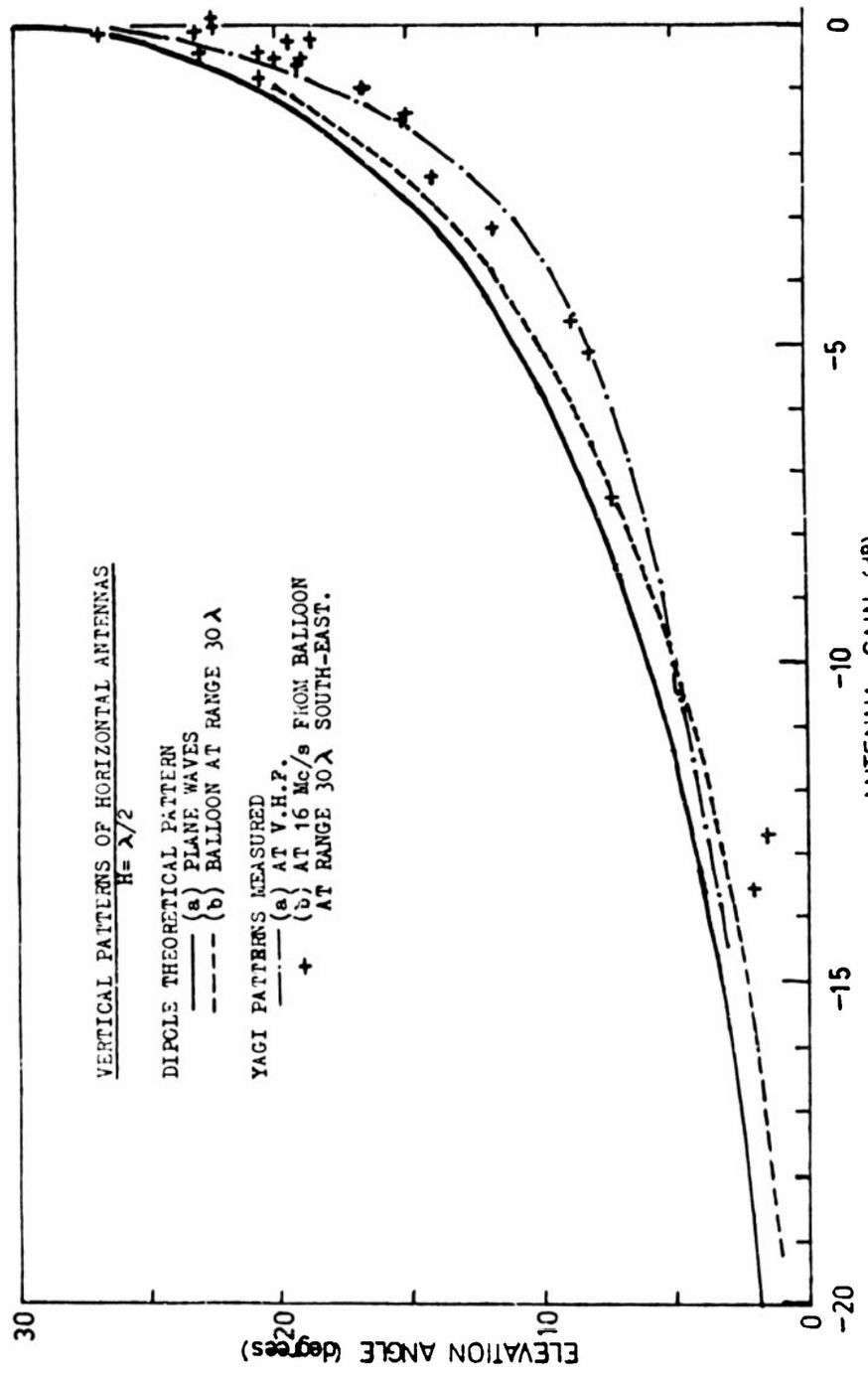

Fig. 16. Relative importance of range correction and experimental accuracy.

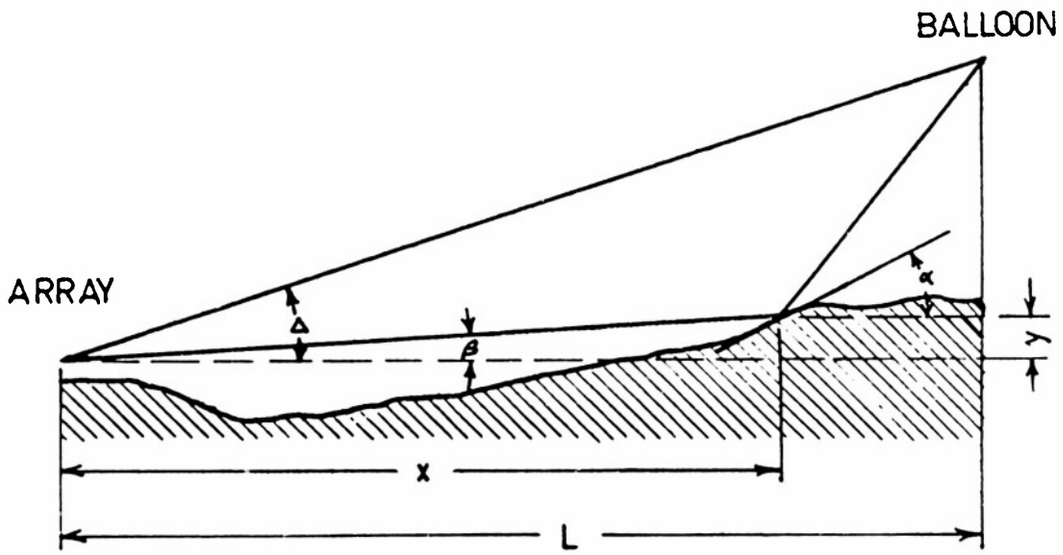

Fig. 17. Ray geometry for western ground profile.

reflected ray, reflected at the point (x, y) where the slope of the ground is α . Double reflections of the ground ray were neglected, and the antenna pattern was calculated for a horizontal dipole, $\lambda/2$ above the ground, with the ground range L equal to 2800 feet and 10^7 feet, representing the balloon flight W and the case for parallel rays respectively.

The results are shown in Fig. 18. Curve (a) is the pattern measured at a range of 2800 feet, and the dots denote actual points measured. Curve (b) was calculated for a flat earth and a range of 2800 feet, and also applies for the western pattern down to 15°, as the area of the ground where reflection occurs is flat for the higher angles. Curves (c) were calculated for the western ground profile and indicate the pattern below 15°, for a balloon range of 2800 feet. Curves (d) were calculated for the western profile and a range of 10^7 feet. Discontinuities in curves (c) and (d) were prominent, and where gaps were left in the patterns they may be taken to be 6 dB, being the contribution of the direct ray only.

It appears from Fig. 18 that the correction for the finite range of the balloon may be best achieved by raising the pattern at 3° by about 3°, similar to the way in which curves (c) are raised to (d). The correction would be smaller at higher angles.

The method did not, however, give a very accurate

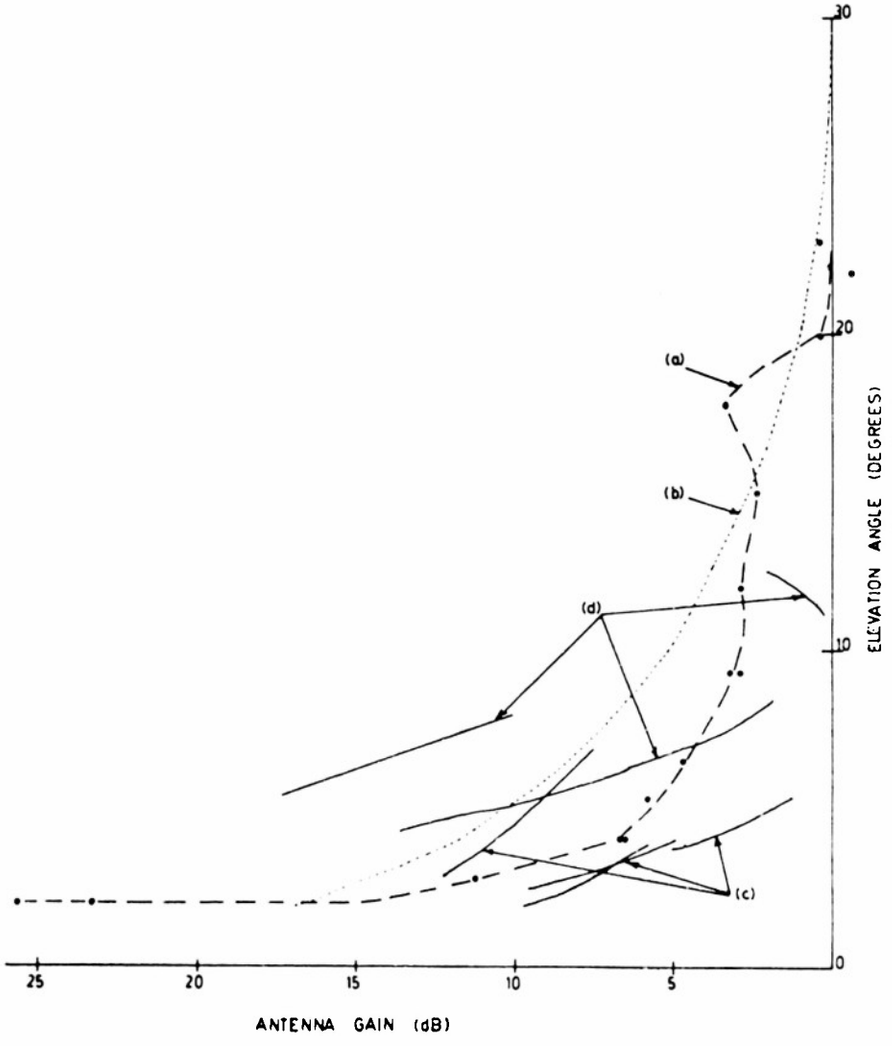

Fig. 18. Antenna patterns for various ranges, west.
(a) Pattern measured with balloon at 2800 ft.
(b) Pattern calculated for 2800 ft, flat earth.
(c) Pattern calculated for 2800 ft, western profile
(d) Pattern calculated for 10^7 ft, western profile.

picture of the vertical radiation pattern, even though it sufficed to give an idea of the correction to be applied to the measured pattern. It was possible to improve the calculation of the pattern, provided parallel rays only were considered. The improved calculation had four advantages over the earlier method:

(i) The gain of the Yagi antenna at different angles in free space (WILLIAMS, 1950, page 115) was tabulated in the computer and used to modify the simple dipole result.

(ii) The ground profile was taken at smaller intervals of range, and the slope at each point was calculated from the adjacent heights.

(iii) The focusing of the ground ray due to the curvature of the ground was taken into account.

(iv) Where more than one reflected ray contributed to the pattern at a given angle of elevation, all were added vectorially with the direct ray.

Fig. 19 shows the calculated pattern (Curve (a)), with the points measured at 2800 feet plotted for comparison. Above 16^{o} the curve is due to the sum of the direct and reflected rays. Between 16^{o} and 10^{o}, only the direct ray is involved. At 10^{o} the reflected ray reappears, in such a phase that it strongly enhances the pattern, and at 8^{o} a second reflected ray gives further enhancement. The discontinuities involve jumps as large as 6 dB.

The discontinuities do not, however, appear in the

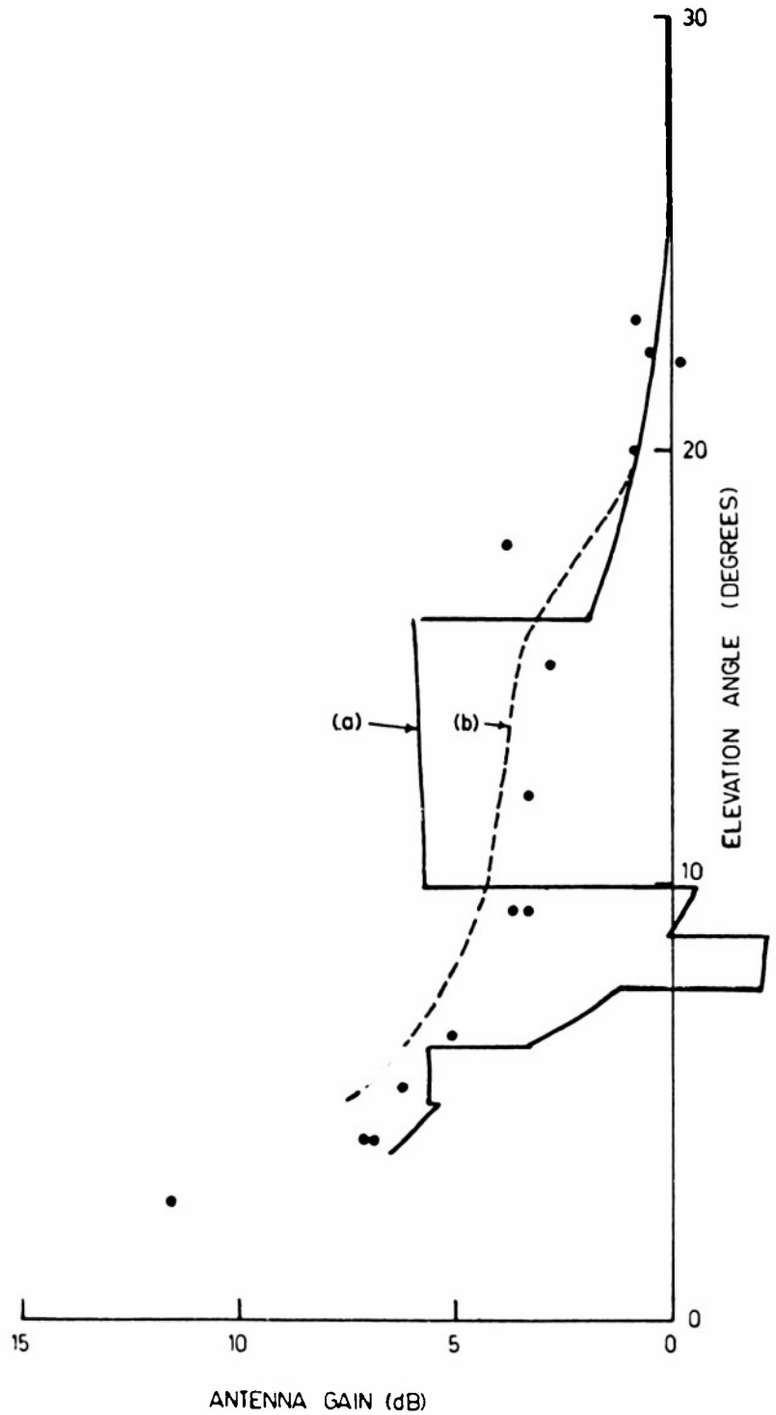

Fig. 19. Antenna patterns, west.
Dots represent pattern measured with balloon at 2800 ft.
(a) Pattern calculated for 2800 ft, western profile.
(b) Most probable corrected pattern.

measured pattern. The measured curve is fairly smooth, and even if corrected for the finite range of the balloon, would still be a smooth curve. The fact that the discontinuities do not appear in practice is probably due to a combination of causes:

(i) The ground profile is not constant across the lateral dimension of the antenna. The ground 100 feet on either side of the assumed profile line will have a different profile, and this is particularly important close to the array at the edge of the levelled circle, where the rays contributing to the pattern at about 16^{o} are being reflected. The actual pattern is therefore the average of a number of different patterns, hence the observed smoothness of the measured pattern.

(ii) Fresnel diffraction at an edge causes appreciable illumination in the shadow region. KNIGHT et al. (1964) showed that calculated antenna patterns which exhibited sharp discontinuities could be smoothed by taking the diffracted energy into consideration in the calculations. They were concerned with relatively simple profiles, and it is doubtful whether their treatment could be applied to the present problem, but it does at least justify the smoothing of a calculated pattern.

The curve (b) was taken as the most probable corrected pattern.

The corrected patterns for both east and west, as

adopted for use in calculating relative backscatter coefficients, are given in Fig. 20.

6.8 Summary

The vertical radiation patterns of the 16 Mc/s antenna array at Moggill have been measured, using a new method involving a balloon-borne transmitter with a rotating antenna. The patterns differ according to the azimuthal orientation of the array, and the differences have been interpreted as due to the ground profiles between the array and the pilot transmitter.

For fairly smooth ground, the measured pattern can be quite simply corrected for the finite range of the balloon.

For the western ground profile, the theoretical pattern of the array is in general agreement with the measured pattern, and contains discontinuities which can be explained away.

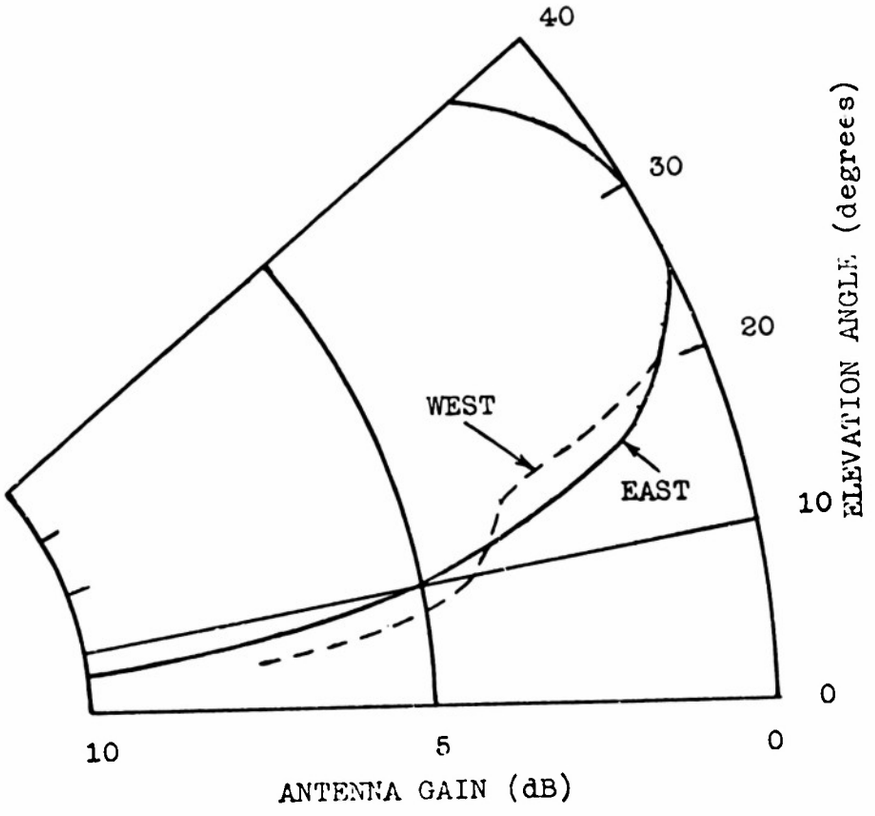

Fig. 20. Corrected patterns adopted for use in calculating relative backscatter coefficients.

7. BACKSCATTER RECORDS

7.1 Production of records

The various facilities of the 16 Mc/s backscatter sounder have been described by THOMAS and McNICOL (1962). In the present work, the sounder was operated with rectangular pulses of 600 microseconds duration, a pulse repetition frequency of 25 pulses per second, and peak pulse power of about 5 kW. The antennas were aimed in a fixed direction, usually to the east or to the west.

The type of data presentation was a rectangular range—time display, with an amplitude sweep superimposed. The basic range——time display was formed in a similar way to a type B presentation in radar (range——azimuth), but without rotation of the antennas. Backscatter echoes to a range of 4500 km were displayed on an oscilloscope screen by brightness- or blackout-modulation of the time-base trace, and were recorded on film moving continuously past the trace at 1/2 inch per minute. Such a record enlarged three times is illustrated in Fig. 21 (20/12/63, 1530 hours, 192° mag. az., no gain sweep). The strong horizontal lines are at intervals of 1000 km, and the weaker ones at intervals of 250 km. The echo has its leading edge at about 1900 km (p'_{min}, where p' designates equivalent free-space range).

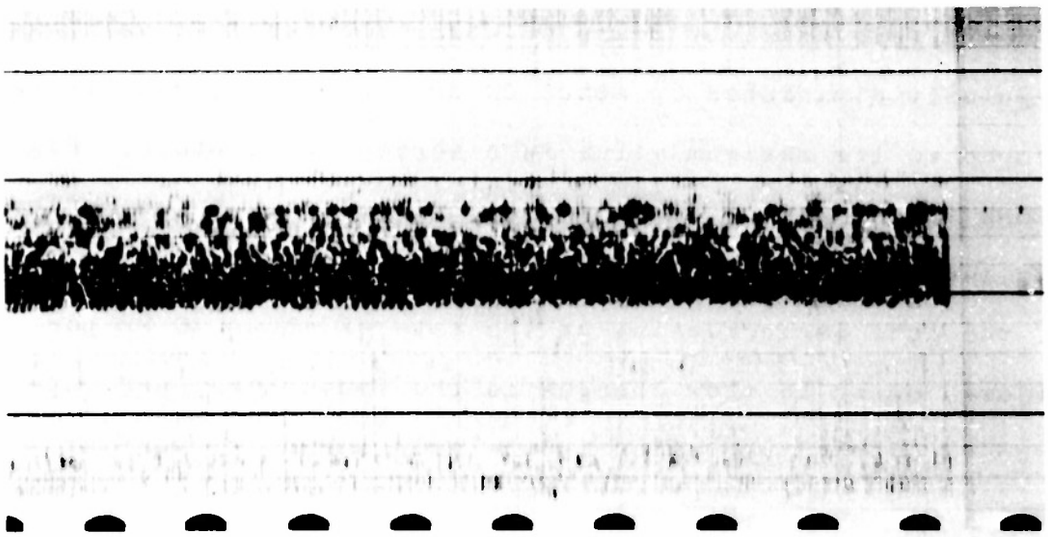

Fig. 21. Backscatter range—time record, 20/12/63, 1530 hours, 192° mag. az., no gain sweep. Horizontal scale is about 1½ inches per minute in this enlargement. Leading edge of echo is at 1900 km.

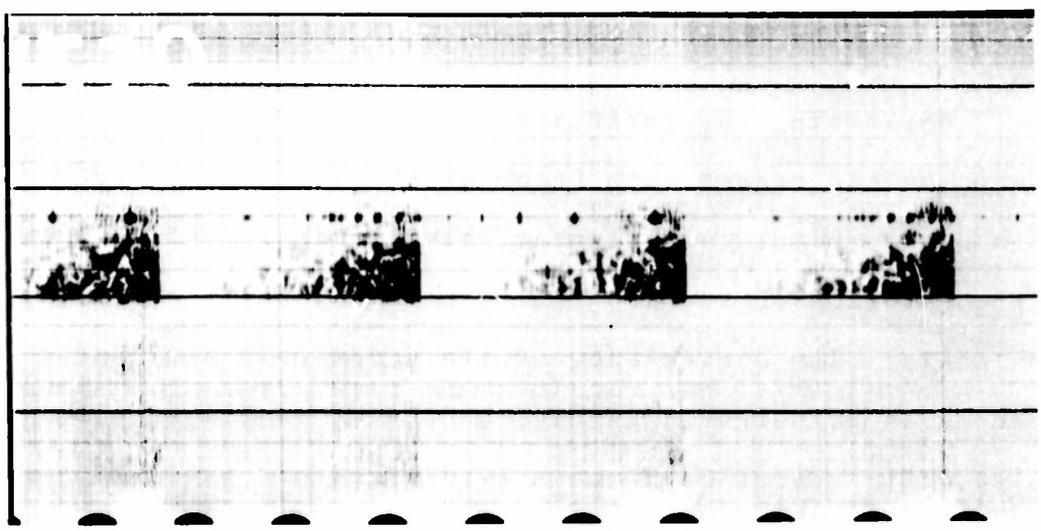

Fig. 22. As for Fig. 21, but with swept-gain unit operating continuously. Each sweep traverses 40 dB in 1 minute, producing a range—amplitude frame.

This range——time display was modified by the use of a swept-gain unit, by means of which the receiver gain was regularly diminished by about 40 dB, and then gradually restored to its maximum value in a series of 11 steps. Fig. 22 shows the same film as Fig. 21, a few minutes later, after the swept-gain unit had been switched on. The minimum range of the echo is increasing at the rate of about 10 km per minute, owing to slow changes in the ionosphere, and superimposed on this variation is the gain sweep, traversing 40 dB per minute every minute. Each stage of the gain sweep lasts 5 seconds, as this was found to be the minimum time needed to average out fading effects. The 1 minute sweep is therefore a compromise between two requirements, the need to record at maximum gain at least once per minute, and the need to record each gain stage for at least 5 seconds duration.

Neglecting any variation in range during one gain sweep, we can regard each frame of the swept-gain records as a range——amplitude display, similar in format to a type A presentation of the echo pulse with a logarithmic amplitude scale. The equivalence of the swept-gain and A-scan records is illustrated in Fig. 23 for an idealized echo pulse. The advantage of this type of record over the A-scan lies in the fact that in practice, blackout-modulation as used here appears to be a more satisfactory way of averaging out the echo pulse shapes than is possible with A-scan.

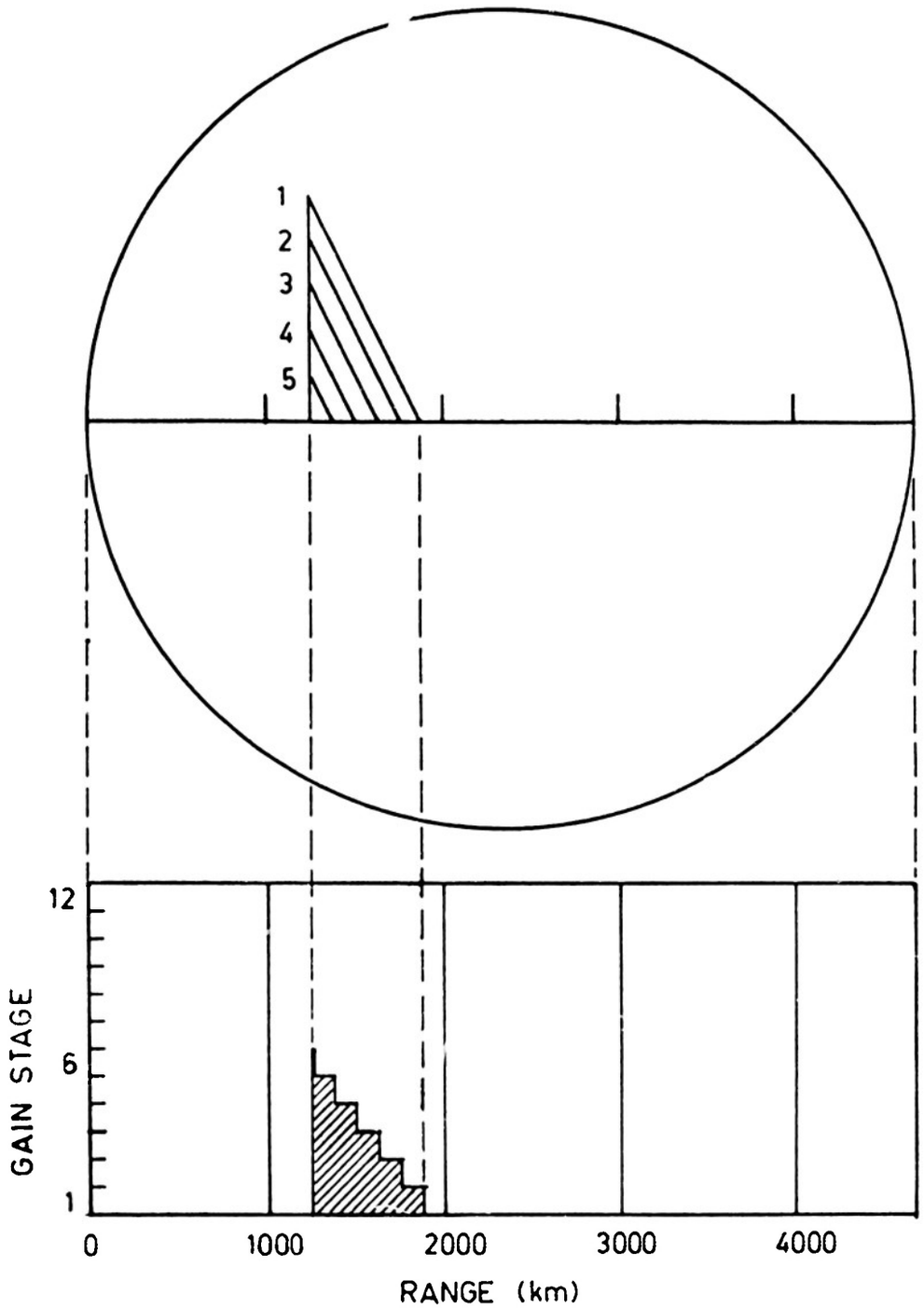

Fig. 23. Illustrating the equivalence of swept-gain and A-scan records.

Successive pulses are returned with different shapes as a result of fading, and some averaging process is required. NIELSON et al. (1960) relied on film exposures long enough to superimpose a large number of fading shapes on the A-scan frame. This has the disadvantage that the larger echo pulses obscure the smaller ones, and what remains is an envelope of the larger pulses. The present method is thought to provide a more useful type of averaging, as the limits of the strong and weak echoes can be discerned, even if the echo fades to zero, and some estimate of the fading rate can also be obtained.

In the present work, the maximum amplitude visible on the film was chosen, for the desired swept-gain frame. Other frames nearby were checked to see if the reading was constant over a few minutes. Although the echo appeared very faint at the edges of the swept-gain films, different people scaling the films were able to obtain consistent results. It may be noted that the films would be easier to scale if there were a greater contrast between the recorded signal and that which falls below the recording threshold determined by the film sensitivity. A steeper threshold could be achieved by making the receiver reject all signals below a given level for each stage of the swept-gain unit.

The error in reading the films was probably $\pm$ 2 dB, so the amplitude——time curves were smoothed, as in Fig.49, and the smoothed values were used in the calculations.

The readings obtained depend on the depth of fading (ADAM and WHITEHEAD, 1960). The present work assumes that the depth of fading is fairly constant (See Section 7.2).

7.2 Fading Types

The example given in Figures21 and 22 show a typical F-region-propagated one-hop backscatter echo (designated 1F) from a direction of 192° magnetic. At the range shown, the backscattering occurs on the Southern Ocean near Tasmania. The fairly regular fading (about 1 c/s) noticeable at the leading edge and the trailing edge of the echo is fairly typical of sea scatter (SHEARMAN, 1962). The fading is fairly constant in phase across the range spread of the echo.

By contrast, Fig. 24 (9/4/63, 1800 hours, 260° mag. az.) is a 1F echo from the land near Birdsville. The fading in general has no preferred frequency, and the phase is irregular, giving rise to a patchy appearance of the echo. It is considered that this fading is due to the motion of the trees, which are thought to be the main scattering objects. CLAPP (1946, p.4) refers to the "wind in the trees" observed by radar at u.h.f. In contrast, SHEARMAN (1962) believed that any fading of echoes from land must be due to the ionosphere alone, while fading of sea scatter represents a combination of ionospheric and sea wave effects. SHEARMAN's opinion is probably correct for land surfaces bare of vegetation or other moving objects.

Fig. 25 (20/12/63, 1200 hours, 192° mag. az.) gives

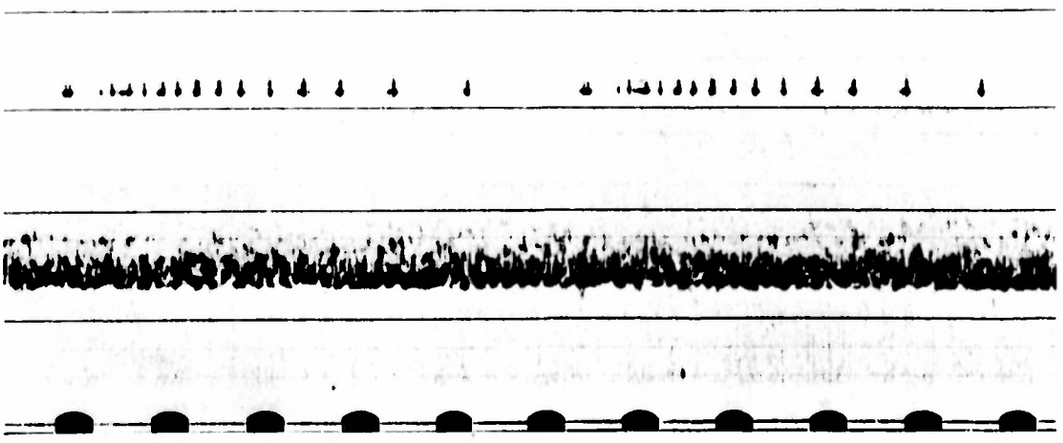

Fig. 24. Backscatter from land. Range—time record, 9/4/63, 1800 hours, 260° mag. az., no gain sweep. Horizontal scale is about 1½ inches per minute. Leading edge of 1F echo is at 1300 km.

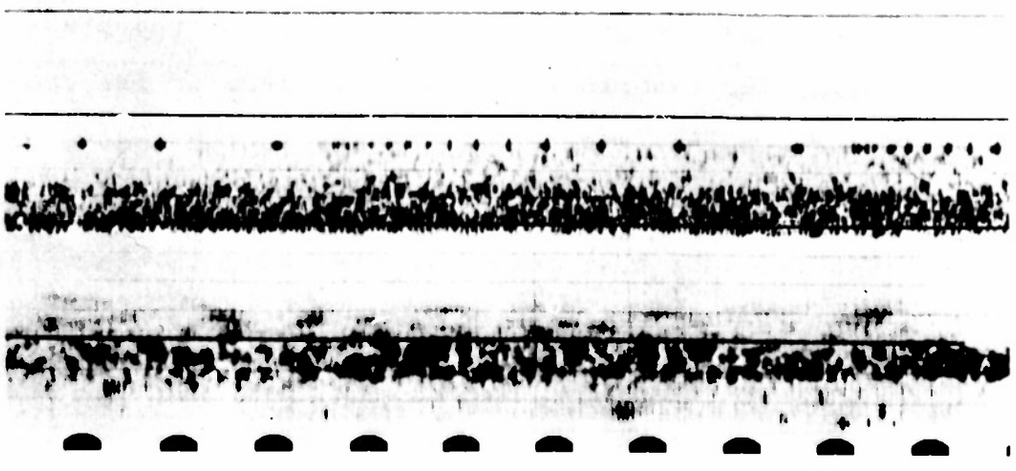

Fig. 25. Backscatter from land and sea. Range—time record, 20/12/63, 1200 hours, 192° mag. az., no gain sweep. Echo at 700 km is $1E_s$ from land. Echo at 2000 km is 1F from sea.

an interesting comparison of land and sea backscatter. The echo from 600 to 1000 km is E_s-propagated ground scatter (designated $1E_s$) from the eastern highlands of New South Wales, and shows the patchiness characteristic of land scatter. The echo at 2000 to 2600 km is a 1F echo from the Southern Ocean.

The possibility that the regular fading attributed to sea scatter originates in the ionosphere is ruled out by the fact that when $1E_s$ and 1F echoes are both present in the east, the same kind of fading appears in both echoes (Fig. 26, 5/4/63, 1620 hours, 80^o mag. az.). Even if the phenomenon causing the fading could occur simultaneously in both the E and F regions, the control points for E_s and F propagation are at different ranges from the sounder. The fading is probably due to the motion of the sea waves.

A similar fading record, obtained by direct backscatter from the sea at low angles, was reported by DOWDEN (1957), but his explanation, based on the beat between Doppler-shifted echoes from opposite directions, will not suffice here, as the sea is viewed in only one direction. Nevertheless, the fading frequency is similar to the Doppler shift expected for 16 Mc/s, if sea waves of length $\lambda / 2$ are considered (CROMBIE, 1955).

The velocity of a sea wave of length L is given by $v = \frac{gL}{2\pi}$, g being the acceleration due to gravity. The Doppler shift Δf produced by sea waves of length $L = \lambda / 2$

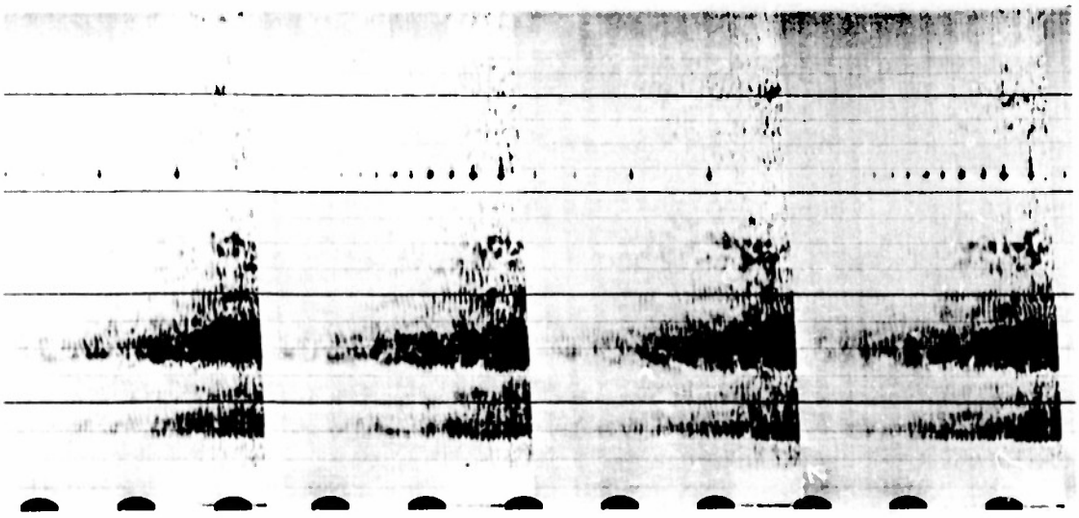

Fig. 26. Backscatter from sea. Swept-gain record, 5/4/63, 1620 hours, 80° mag. az. Duration of each frame is 1 minute, and fading rate is approximately 48 cycles per minute. Similar fading occurs in both 1F and $1E_s$ echoes.

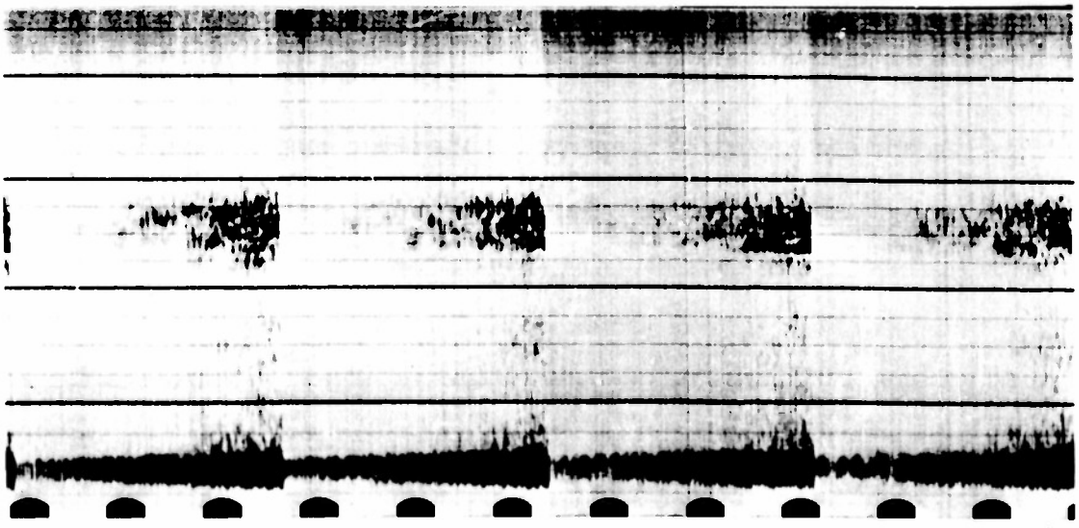

Fig. 27. Direct backscatter from field-aligned E_s. Swept-gain record, 20/13/63, 1700 hours, 192° mag. az. Range of echo is about 400 km, and a 1F sea echo appears at 2400 km, showing possible magneto-ionic splitting.

travelling radially to the observer will be

$$\Delta f = \frac{2v}{\lambda} = \frac{2}{\lambda}\sqrt{\frac{g}{2\pi}\frac{\lambda}{2}} = \sqrt{\frac{g}{\pi\lambda}} .$$

At 16 Mc/s, $\Delta f = 0.41$ c/s.

In a Fourier analysis of the sea waves there will be two components with wavelength $L = \lambda/2$. These will have velocities +v and -v, and so there will arise two Doppler-shifted echoes with frequencies f + 0.41 and f - 0.41 c/s. The fading can be attributed to the beat between these two signals, as follows:

(a) The fading rate for sea echoes in Figures 22, 25 and 26 is about 48 per minute, or 0.8 c/s. This compares well with 2 Δf.

(b) The depth of fading may be as great as 20 dB between maximum and minimum. This implies that there are two signals of approximately equal intensity interfering with each other.

INGALLS and STONE (1957) measured the Doppler power spectrum of sea echoes at 18 and 24 Mc/s, and found three spectrum peaks. One peak was at the carrier frequency, and the others were narrow sidebands shifted by Δf. The bandwidth of the Doppler-shifted sidebands was about 10^{-2} c/s, and the distribution of the echo power among the three peaks was a function of sea state.

In the present work, it would seem that when deep fading occurs, the sidebands are of equal power and the carrier frequency component is negligible. This appears to corre-

late with fairly calm conditions. When the fading is not pronounced, one of the sidebands is probably suppressed in favour of the other. The carrier frequency component is again negligible, as fading is not observed at the frequency Δf but only at $2 \Delta f$.

It is important to note that the fading can be explained almost entirely in terms of the terrain. Any fading due to ionospheric effects is normally slow and weak, indicating that the ionosphere is a comparatively stable medium.

Direct backscatter from field-aligned irregularities in E_s is illustrated in Fig. 27 (20/12/63, 1700 hours, 192° mag. az.). This occurs at a range of 300 to 600 km, and is often detected in a southerly direction when $1E_s$ echoes are present. It usually shows fairly regular fading, but faster than that of sea echoes.

7.3 Skip Distance Focusing

In F region propagation, strong focusing of energy occurs at the skip distance, and in 1F backscatter echoes this occurs in both ionospheric reflections (out and back), giving considerable enhancement of echo power. The skip ray returns to the sounder just after the minimum time delay ray and persists for a time $1/2\ \delta t$, where δt is the pulse length. For 600 microsecond pulses, this corresponds to a range interval of 90 km. The echo power tends to fall off rapidly beyond this range. The effect is most pronoun-

ced in short range echoes (p'_{min} about 1200 km) and is an aid in distinguishing between $1E_s$ and 1F echoes, as $1E_s$ echoes show negligible focusing. Some $1E_s$ echoes, however, are limited in range by the size of the E_s cloud, and may appear to be focused. Fig. 28 illustrates the effect of skip distance focusing, for a 1F echo (28/3/63, 1556 hours, 80^o mag. az.). Fig. 29 shows a multiple-hop E_s echo (23/11/62, 1500 hours, 80^o mag. az.), when the E_s cloud was fairly large; focusing is not apparent.

7.4 Ionospheric Irregularities

(a) Tilts: The iso-ionic contours in the F region are often tilted from the horizontal by 1 or 2 degrees, causing an increase or decrease in the range of backscatter echoes. This effect is important for long range echoes, corresponding to low angle rays which are most sensitive to tilts. For a quiet ionosphere, the amount of tilting can be gauged from the rate of change of h'F measured at Brisbane as the ionosphere passes overhead. The tilts can be taken into account in the calculations (See 8.3 (a)), but normally it was found preferable to select data from days on which tilting was negligible.

(b) Ripples: If the ionosphere is disturbed by large-scale ripples such as travelling ionospheric disturbances, the leading edge of the ripple becomes a second region of focusing in addition to the focusing of the skip ray. Such

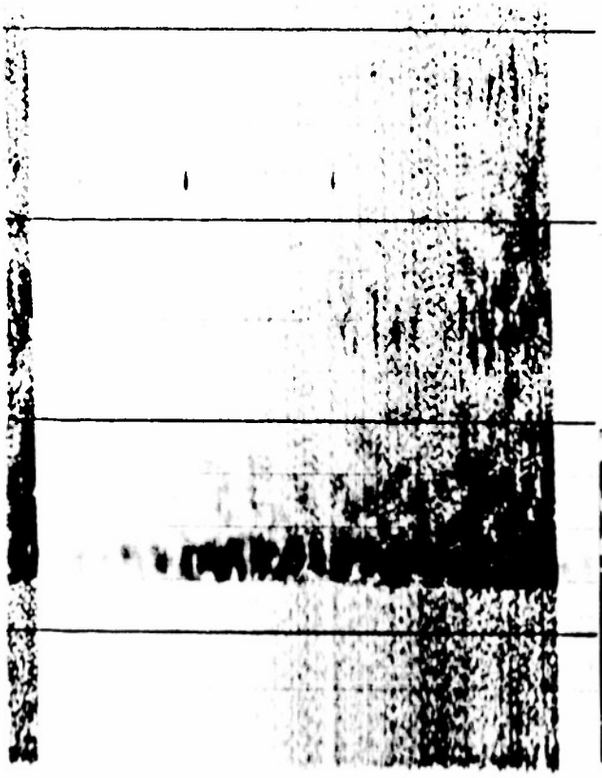

Fig. 28. Skip distance focusing in a 1F echo. 28/3/63, 1556 hours, 80° mag. az. One minute sweep.

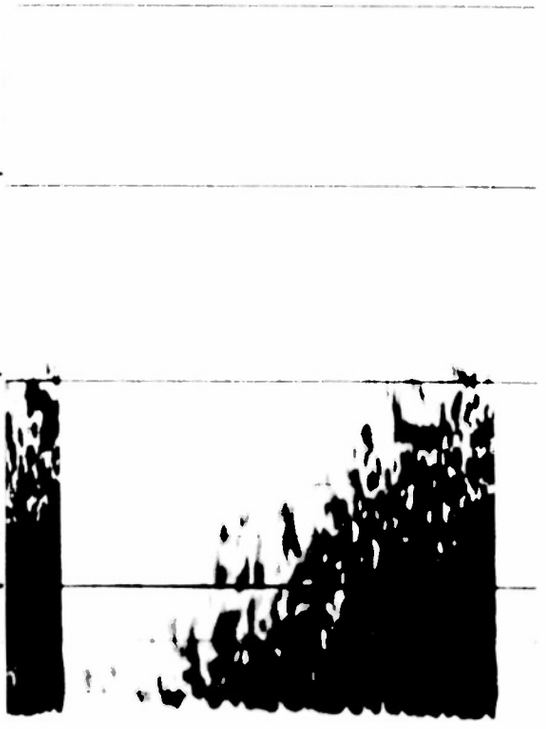

Fig. 29. Multiple-hop E_s echoes. 23/11/62, 1500 hours, 80° mag. az. One minute sweep.

ripples may be 500 km in extent and may move at about 600 km per hour, so that the secondary focused echo may move at twice this speed. Fig. 30 is a range——time record taken at slow film speed (22/7/60, 1100 hours, 180° mag. az.). The secondary focused echo moved towards the sounder until it coalesced with the skip region and temporarily reduced its range. A true height analysis of vertical incidence data at Brisbane and Canberra on 22/7/60 was performed, using the method of SCHMERLING and VENTRICE (1959). Fig. 30a shows the result. The two disturbances which passed over Brisbane at 1050 and 1210 hours are probably the same that passed over Canberra at 0930 and 1050 hours respectively. Each disturbance moved at the rate of about 600 km per hour, and can probably be identified with the disturbances on Fig. 30 which reached their minimum recorded ranges at 1040 and 1120 hours respectively. In routine swept-gain records taken at ½ inch per minute, the presence of such ripples is not always obvious, and care must be taken to detect them. The secondary focusing appears on swept-gain records as in Fig. 31 (22/3/63, 1800 hours, 80° mag. az.). Most ripples move from south or south-east to north or north-west, so for records of echoes from east or west, the ripples were usually observed end-on, and their influence on the range and power of echoes was not serious in this case.

Small-scale ripples have a focusing effect similar to travelling disturbances, but as a large number are illumin-

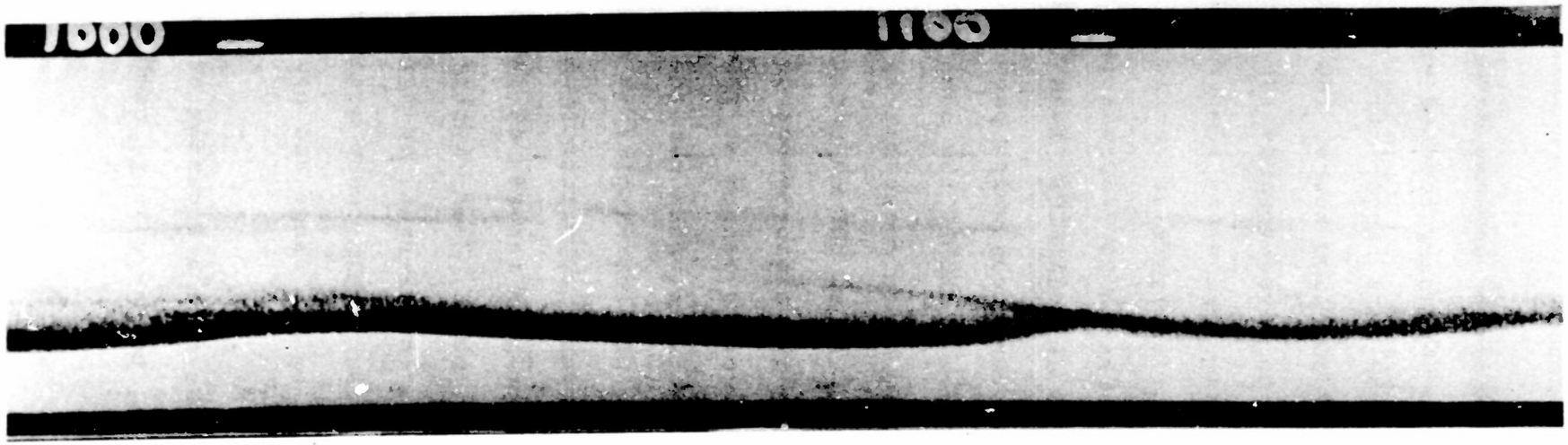

Fig. 30. Large ripples advancing from the south, observed by ground backscatter. 22/7/60, 1000 to 1130 hours, 180° mag. az. No gain sweep. Slow film speed. Film exposed from 300 to 4700 km.

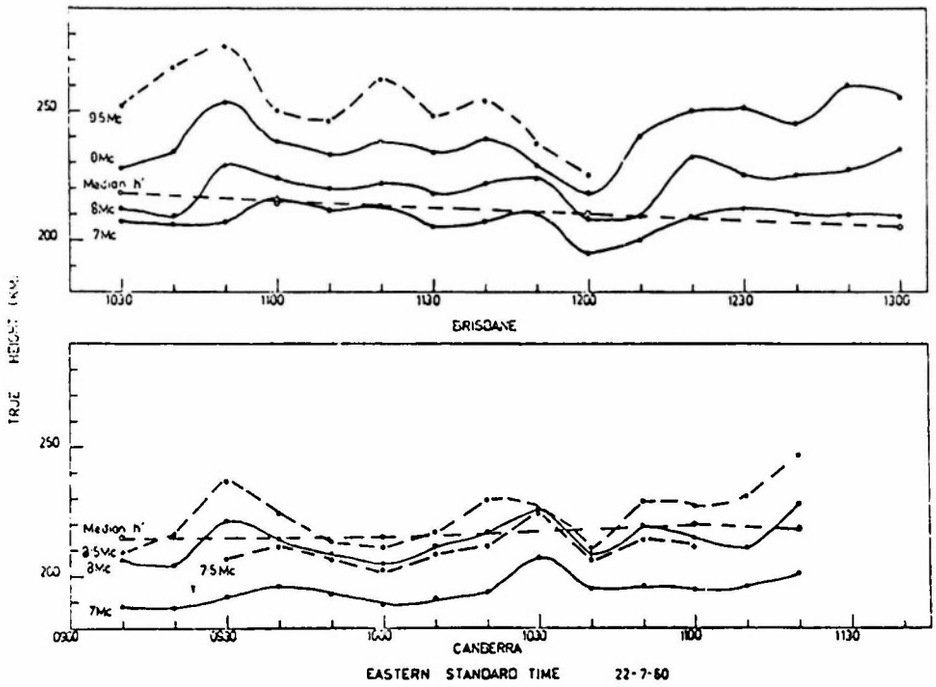

Fig. 30a. True heights at which various frequencies were reflected, 22/7/60. Brisbane and Canberra results are compared, to illustrate travelling disturbances.

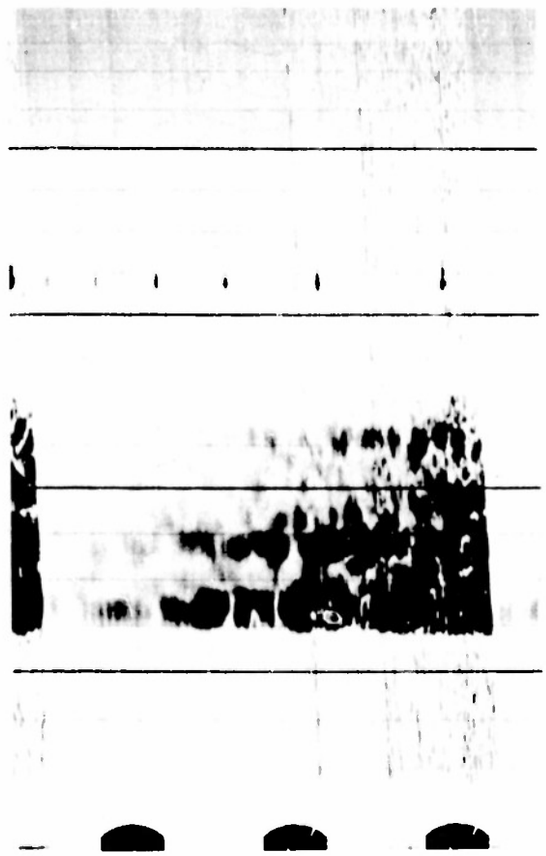

Fig. 31. Effect of ripples on swept-gain records. 22/3/63, 1800 hours, 30° mag. az. One minute sweep.

ated at one time by the sounder, their effect on the backscatter echoes is averaged out, and the result is "range spreading", similar to that observed on vertical incidence ionograms.

(c) Sporadic-E: E_s clouds are usually classed as irregularities. $1E_s$ echoes at 16 Mc/s occur between 500 and 1500 km, the lower limit depending on f_oE_s, and the upper limit being determined by the backscatter coefficient and the amount of range spreading. Either of these limits may be modified by the size of the cloud. Complete E_s blanketing is rare; a small cloud or one with low f_oE_s allows F-propagated backscatter to occur as well as E_s, provided 1F propagation conditions are suitable, but there is always some doubt as to how much the 1F echoes have been attenuated and such cases are best avoided in deriving the backscatter coefficient.

7.5 Summary

For the present purpose, swept-gain records are preferred to A-scan. They allow the echo power to be read more easily. They enable fading rates to be recorded, and facilitate the identification of propagation modes such as 1F, $1E_s$ or direct backscatter from field-aligned E_s. The distinctive types of fading allow the source of the scatter to be identified, whether sea, land or field-aligned E_s. The fading rates give support to the idea that backscatter arises from trees and wave crests.

Irregularities such as ripples in the F region can be recognized on swept-gain records.

8. CALCULATION OF BACKSCATTER ECHO POWER

8.1 Introduction

The method of calculation is similar to that given in SHEARMAN (1956b). There are three main stages.

(i) The Appleton and Beynon equations (APPLETON and BEYNON, 1940) are used to calculate the equivalent free-space path p' and the ground range D for a single-hop F-propagated ray, for given ionospheric parameters and a given angle of elevation Δ of the ray at the transmitter. The equations assume that the ionospheric profile is parabolic and that it is constant with range throughout the region traversed by the rays, that is, tilts and ripples are absent. The earth's magnetic field is neglected. The ionospheric parameters required are the base height h_o, the critical frequency f_o and the semi-thickness y_m of the layer (assumed parabolic) at the ionospheric control point of the ray. For the skip ray, the control point is at range $\frac{1}{2} D_s$, where D_s is the skip distance.

(ii) The focusing factor F is calculated, involving the first and second differentials of D with respect to Δ.

(iii) The radar equation is integrated to give the relative echo power received at the transmitter.

The data available include the virtual base height

h_o', the ordinary ray critical frequency f_o and the M(3000) factor (scaled from vertical incidence soundings at Brisbane every 10 minutes), and the 16 Mc/s minimum equivalent path p'_{min}, scaled from backscatter records taken every minute.

The true height h_o is normally about 20 km less than h_o' for h_o' about 200 km. This was ascertained from true height analysis of typical cases. This empirical adjustment of h_o' to obtain h_o may be in error by as much as 10 km, but this does not affect the result by more than about 0.6 dB (See Section 8.3), and in any case h_o' is only accurate to $\pm$ 5 km.

Two methods are available to find y_m. These will be discussed later (Section 8.3).

8.2 Matching Vertical Incidence and Backscatter Data

It is assumed that the ionosphere is quiet, and that the ionospheric configuration at any place in the ionosphere remains constant as the ionosphere passes over Brisbane from east to west. The ionospheric parameters at Brisbane at a given time will therefore apply at the control point of the skip ray at an earlier time if the backscatter sounder is pointing east, or at a later time if the sounder is pointing west. It is required to find the appropriate time lag between Brisbane and the control point, and hence to match the given ionospheric parameters at Brisbane with the appropriate backscatter record, taking into account the variation of

p'_{min} in the backscatter records; and finally to obtain the desired value of p'_{min} from the appropriate record.

A graphical method was devised to perform this matching process. A set of curves was prepared, plotting calculated p'_{min} against time lag for different values of h_o and y_m. These curves are shown in Fig. 32, designated (a), (b) and (c). They correspond to h_o = 190, 220 and 250 km, and y_m = 80, 90 and 100 km respectively. They were constructed by taking SHEARMAN's curves of $p'_{min} - D_s$ against p'_{min} (SHEARMAN, 1956b, Fig 11), and replotting them as p'_{min} against D_s, and then changing the D_s axis to a time lag axis by considering that at Brisbane ($27\frac{1}{2}^o$ south latitude) the earth rotates at about 1476 km per hour relative to the subsolar meridian, so that the ionosphere moves overhead at this rate with respect to Brisbane. Therefore if D_s = 1476 km, for example, the time lag to the skip zone will be 1 hour and the time lag to the control point of the skip ray will be 1/2 hour. The curves (a), (b) and (c) are referred to here as the overlay.

The observed p'_{min} on any day was plotted against the time of day on the same scale as the overlay, and the intersection of this curve with the appropriate curve of the overlay gave the backscatter frame appropriate to the given ionospheric parameters, and also the value of p'_{min} at that time.

For example, Fig. 32 shows the time lag curves super-

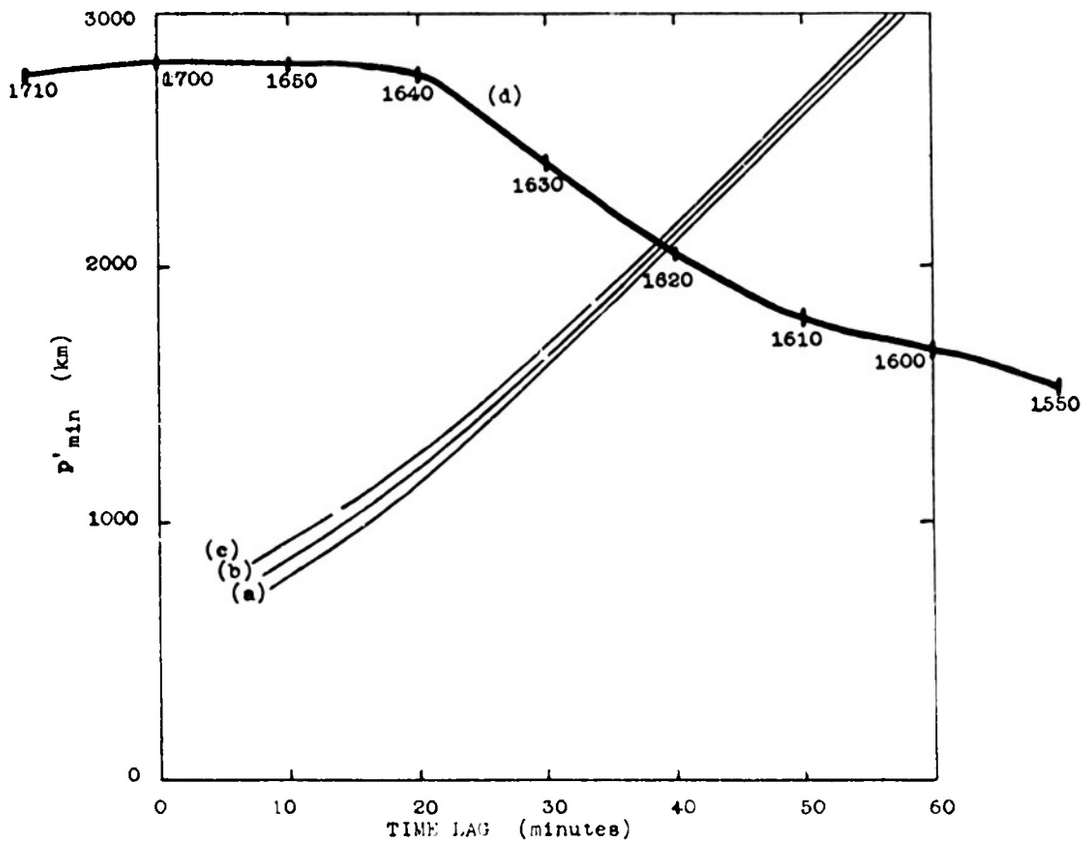

Fig. 32. Matching vertical incidence and backscatter data.

(a) h_o = 190 km, y_m = 80 km.

(b) h_o = 220 km, y_m = 90 km.

(c) h_o = 250 km, y_m =100 km.

(d) p'_{min} for 3/5/63, 80° mag. az.

imposed on part of the p'_{min} curve for 3/5/63 (80^{o} mag. az.) (Curve (d)). Suppose it is desired to find the swept-gain frame corresponding to a control point having vertical incidence parameters measured at Brisbane at 1700 hours. The overlay is placed with its zero time lag over 1700 hours on curve (d). The height h_o' at Brisbane at 1700 hours was 220 km, so h_o was taken to be 200 km, and curve (a) was chosen. The intersection of curves (a) and (d) occurred at a time delay of $39\frac{1}{2}$ minutes, when p'_{min} was 2075 km. The time of the backscatter frame required was 1700 - $39\frac{1}{2}$ or $1620\frac{1}{2}$, which could be read directly from the time scale of curve (d). Similarly, the vertical incidence data at 1710 hours at Brisbane (say) could be matched with another swept-gain frame.

It is to be noted that curve (d), representing eastern backscatter, is plotted with time progressing from right to left. For western backscatter echoes, the time is plotted from left to right, as in Fig. 33 for 14/4/63 (260^{o} mag. az.) (Curve (e)). At 1700 hours, h_o was about 200 km, so when the zero of the overlay was placed over 1700 hours, the result was given by the intersection of curves (a) and (e). The time lag was 32 minutes, p'_{min} was 1730 km, and the appropriate backscatter frame was 1732 hours.

If the estimated value of h_o is in error by 10 km (as is likely), the value of p'_{min} derived will be in error by about 10 km, and the backscatter swept-gain frame chosen may

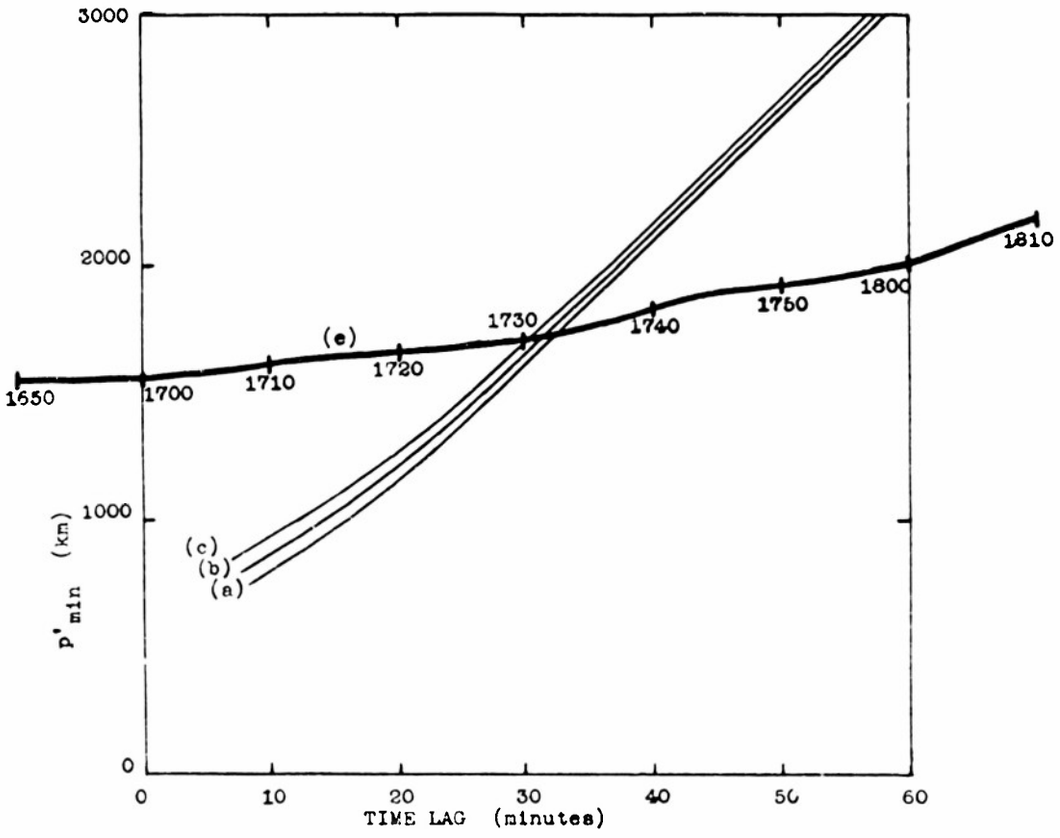

Fig. 33. As for Fig. 32, except:
(e) p'_{min} for 14/4/63, 260° mag. az.

be 1/2 minute in error, which is less than the probable error in recording and scaling the backscatter echoes.

8.3 Estimation of y_m

The next step in obtaining data for calculation was to find y_m. Two methods were used, and the second was found to be more satisfactory than the first.

(a) First Method, using M(3000)

TAIEB (1962) published a set of curves parametric in h_o, relating y_m to M(3000). His simple theory neglects the earth's magnetic field, and his more developed theory has not been produced in graphs except for a few examples of particular cases. To see if his method could be profitably employed in the present work, values of h_o' and M(3000) scaled from vertical incidence soundings at Brisbane were used in conjunction with the simple theory, neglecting the Earth's field and the correction for h_o, and corresponding values of y_m were read from the curves. The Appleton and Beynon equations were used to calculate p' for a range of values of Δ , and p'_{min} calculated in this way was found to disagree with the observed value of p'_{min} recorded on the corresponding backscatter record. A discrepancy of 20% or more was common, and the average calculated p'_{min} was systematically about 10% too large. Several possible explanations were considered.

(i) The true height h_o should have been used instead of

h_o'. But when this was done, TAIEB's curves yielded higher values of y_m which compensated for the lower values of h_o', and the resulting calculated p'_{min} was still in error by the same amount.

(ii) The earth's field should have been taken into account. In a few cases when this was considered, y_m was slightly reduced, thereby reducing the calculated p'_{min} and the systematic error, but the random discrepancies were still quite large.

(iii) The ionospheric parameters were assumed to be constant over a large area of the ionosphere from range $\frac{1}{2} D_s$ to infinity, or at least to the range of the control point of the tangent ray. This means that any tilts in the iso-ionic contours were neglected, and this neglect could have produced the discrepancies. A computer program due to B. A. Mc Innes was used, taking into account the ionospheric parameters at every 200 km along the propagation path. The results for 44 cases are shown in Fig. 34, where the calculated values of p'_{min} are plotted against the observed values. The full line represents the agreement desired, and the broken lines indicate $\pm$ 10% discrepancy. The scatter of points is still serious, and there is still a systematic disagreement of 10%.

(iv) The M(3000) values may be in error. SHEARMAN (1956a) found a systematic difference of 10-15% between observed and calculated values of p'_{min} which agrees with the present

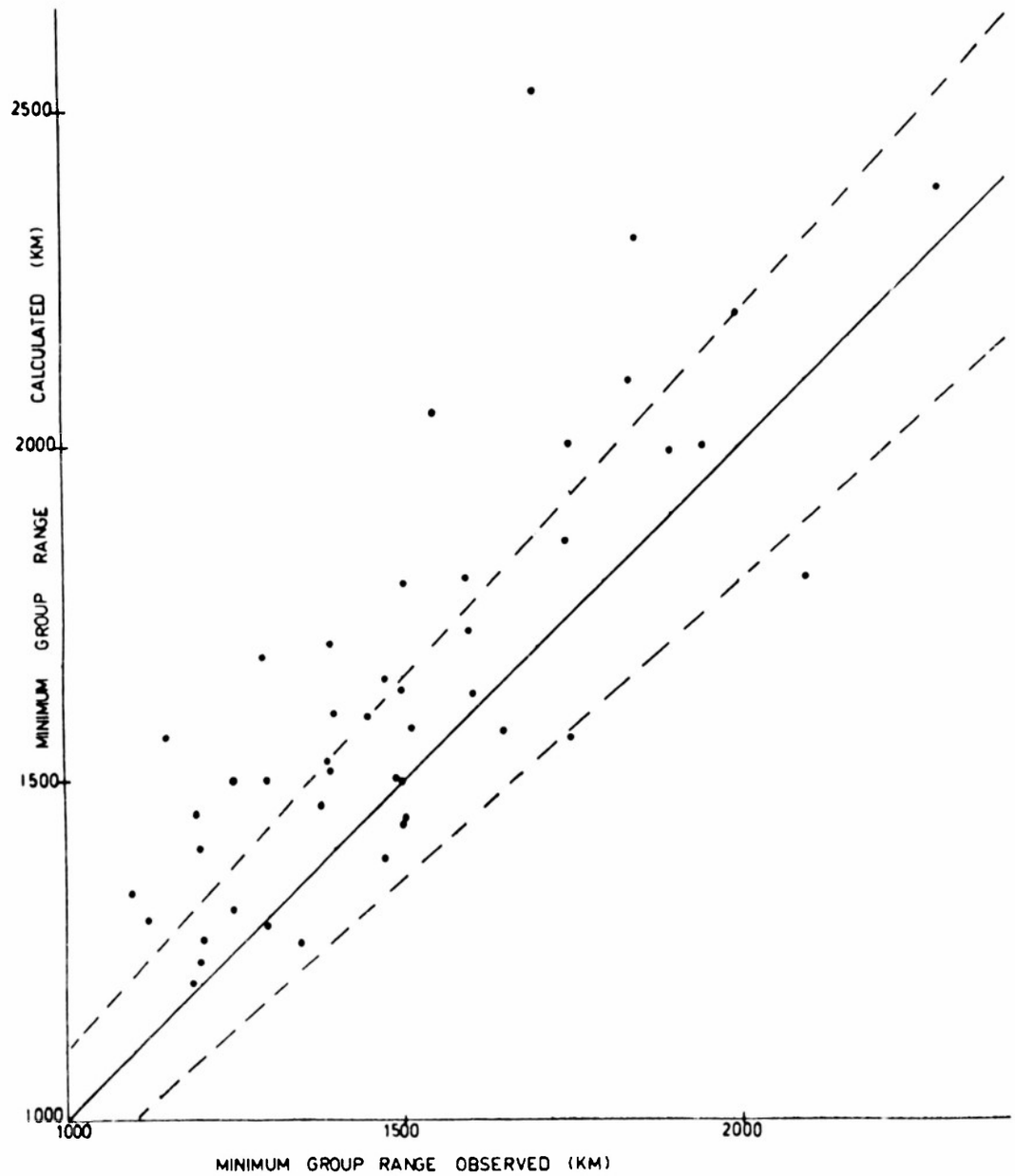

Fig. 34. Comparison of calculated and observed values of p'_{min}.

findings. He was inclined to attribute this discrepancy to the presence of echoes from azimuths other than the centre of the main antenna lobe, but such an explanation will not suffice for the narrow beam in use in the present work. In the discussion following SHEARMAN's paper it was suggested by W. R. Piggott that all conventional ionosondes give values of h' which are systematically too high by 5-15 km, and this introduces a significant consistent error in the M factor deduced.

(v) The extraordinary ray should be considered. The extraordinary ray critical frequency for vertical incidence is larger than f_o by an amount equal to 1/2 f_H, where f_H is the gyrofrequency at the particular locality considered (provided $f_H \ll f_o$). At Brisbane, 1/2 f_H is approximately 0.7 Mc/s, and when f_o + 1/2 f_H was used in place of f_o in the calculations, the calculated value of p'_{min} was reduced, and the average systematic error was virtually eliminated. However, this approach is not valid at oblique incidence, and in fact for east-west propagation the difference between the ordinary and extraordinary ray critical frequencies is negligible, amounting to only about 1/20 of the difference for north-south propagation.

The most likely sources of error are in explanations (ii) and (iv). As it is not easy to apply TAIEB's method when the earth's field is considered, and as there seems to be some doubt about the accuracy of M(3000), and as in any

case there would still be large random errors even if the systematic error could be eliminated, it seemed preferable to seek an alternative method of estimating y_m.

(b) Second Method, using observed p'_{min}

As explained in Section 8.2, for every set of values of h_o and f_o obtained at vertical incidence, the corresponding value of p'_{min} can be obtained from backscatter records. The parameter y_m can be obtained by calculating back from p'_{min}.

With the aid of a computer, p'_{min} was calculated for a wide range of values of h_o, f_o and y_m, and the results are plotted in Figures 35 to 40. Each chart applies for a single value of h_o, and f_o is plotted against p'_{min} for a range of y_m values, giving a set of curves parametric in y_m. y_m was obtained from the observed p'_{min} by means of these charts, and then used in subsequent calculations.

In this procedure it is assumed that the ionosphere is not tilted, so care was taken to reject data in which h_o was varying rapidly. However, a slight tilt of about 0.5^o would give rise to an error of 1^o in Δ_s, the elevation angle of the skip ray, and an error of this magnitude is acceptable. On the other hand an error in p'_{min} such as commonly arises when the first method above is used, could have a large effect on the calculated power returned.

The second method also tends to cancel out any errors

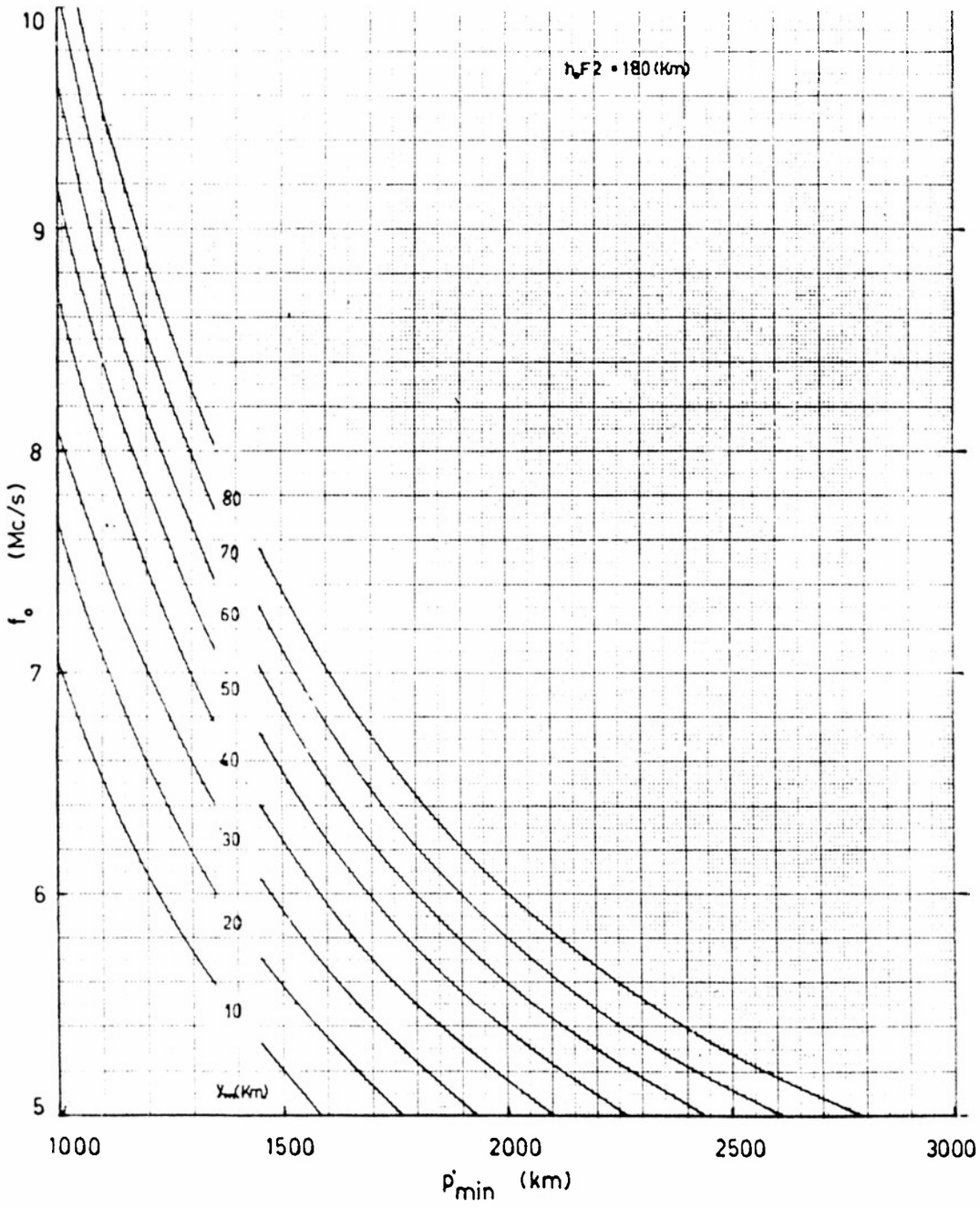

Fig. 35. Chart for deducing y_m.

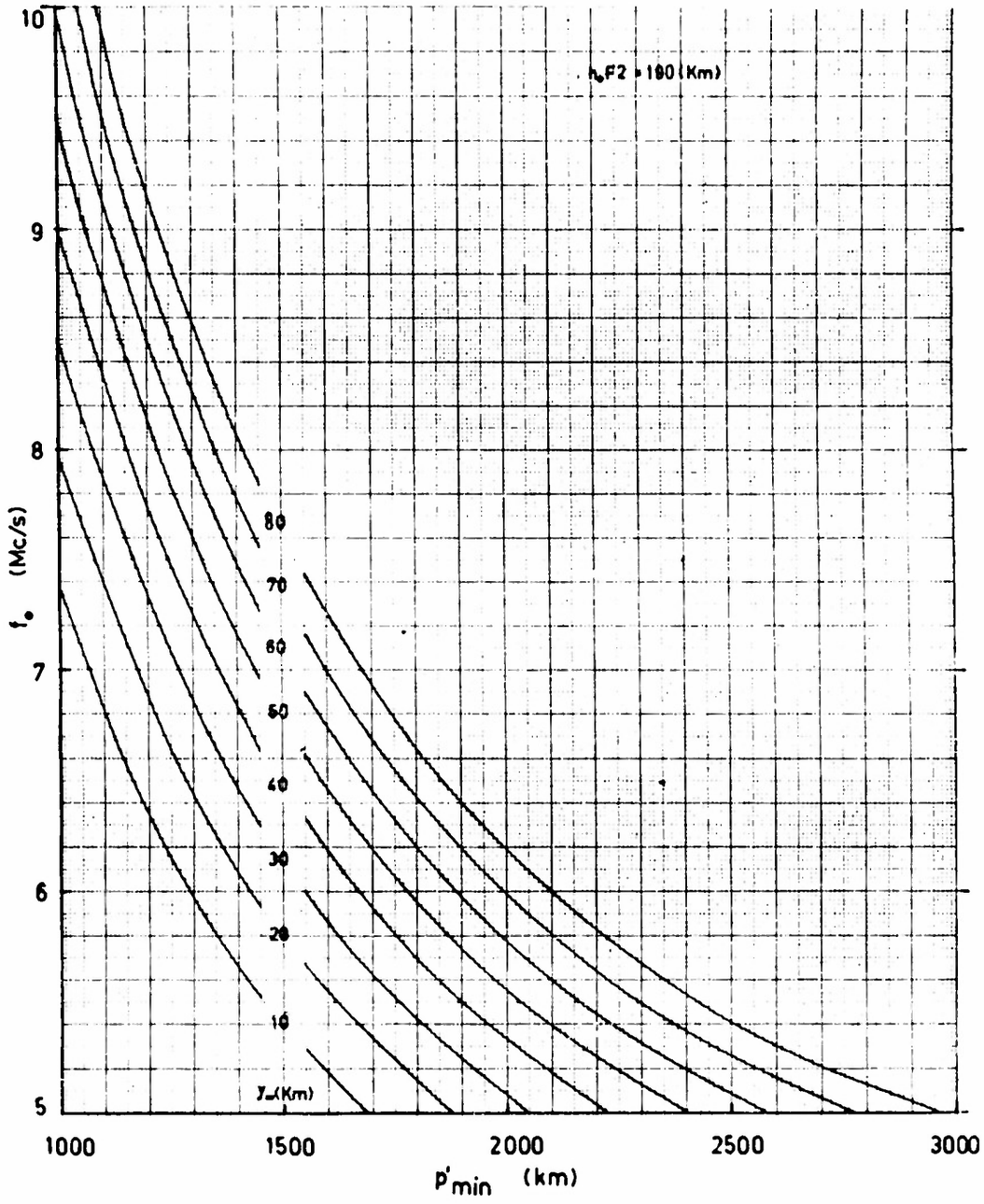

Fig. 36. Chart for deducing y_m.

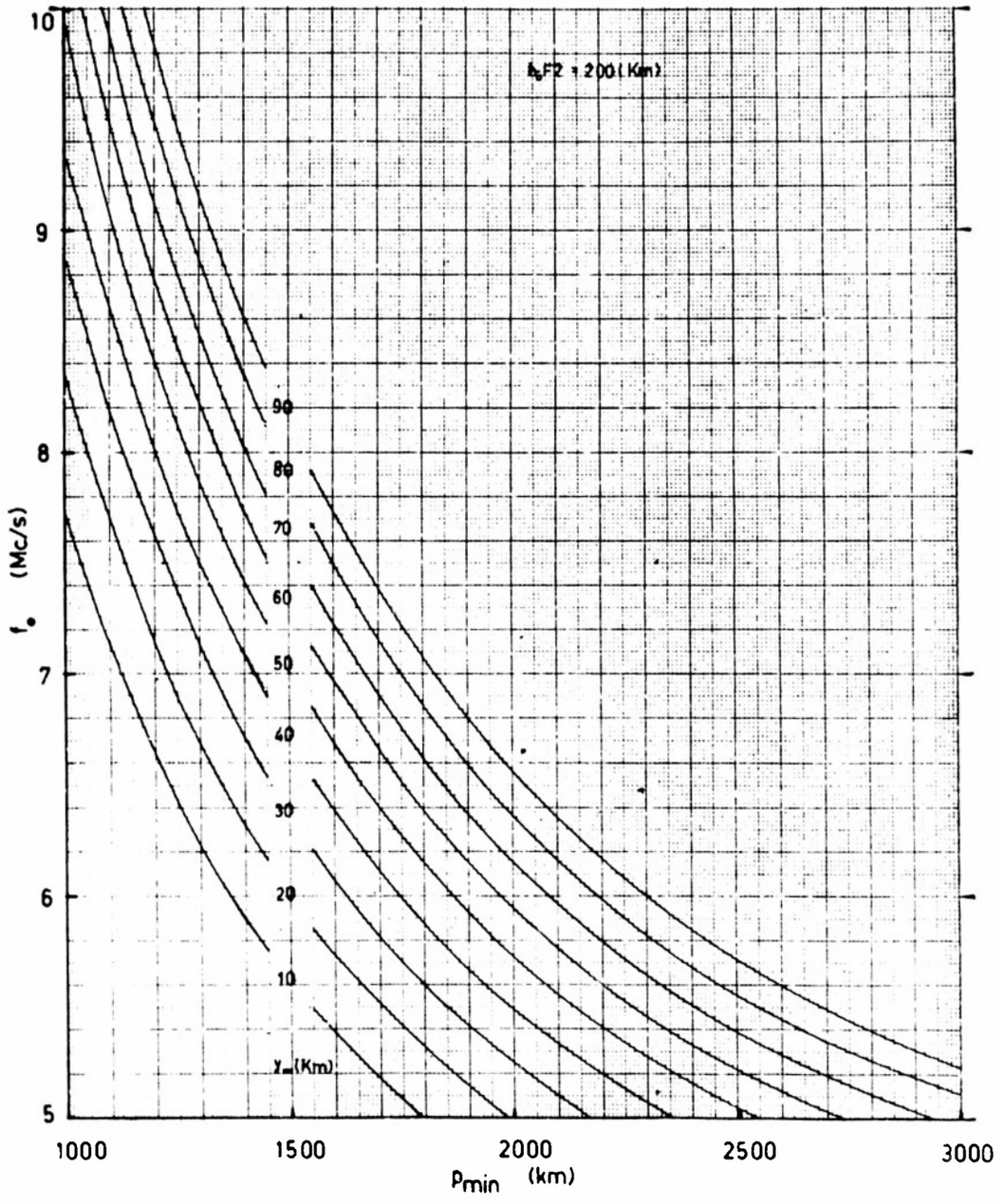

Fig. 37. Chart for deducing y_m.

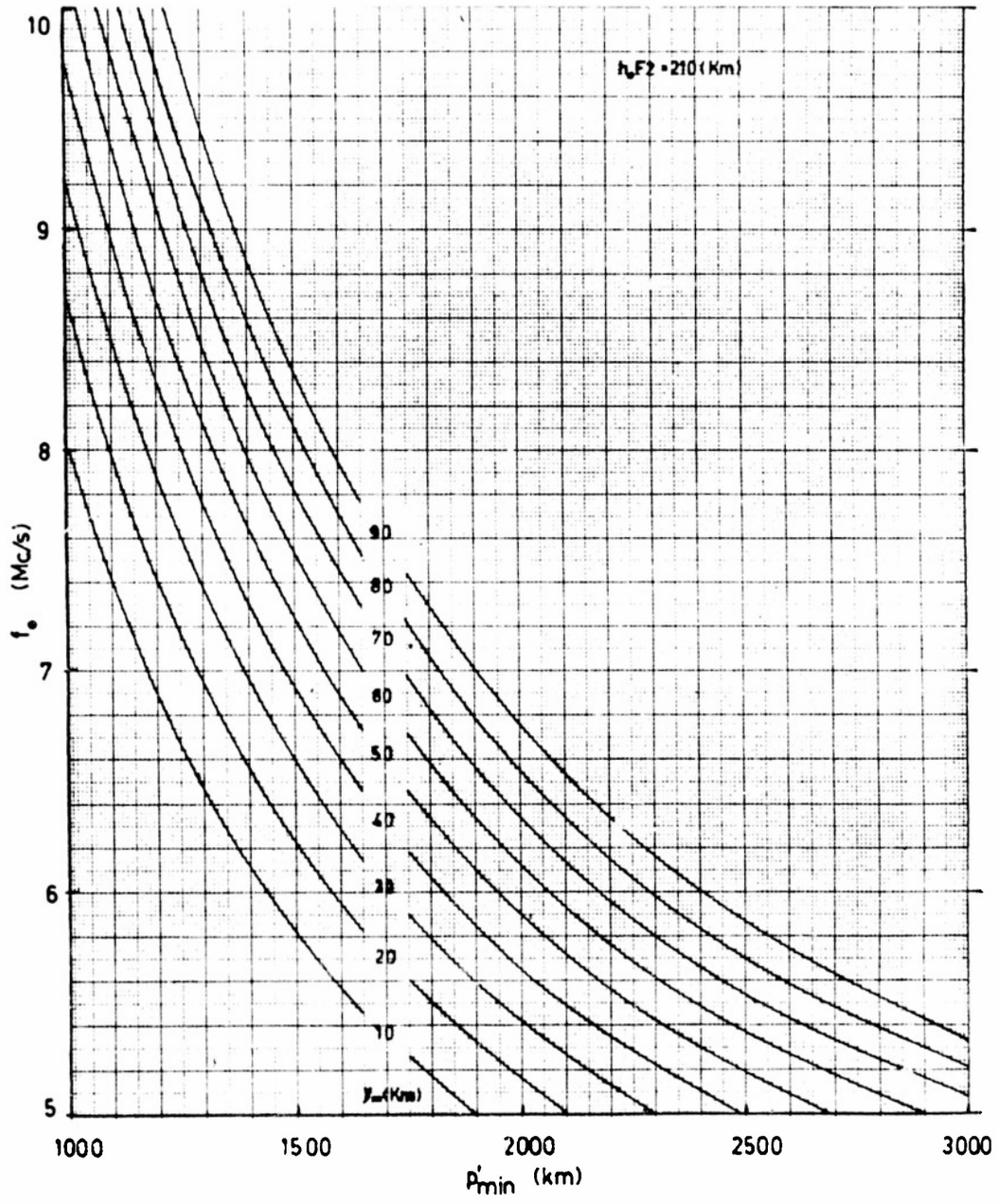

Fig. 38. Chart for deducing y_m.

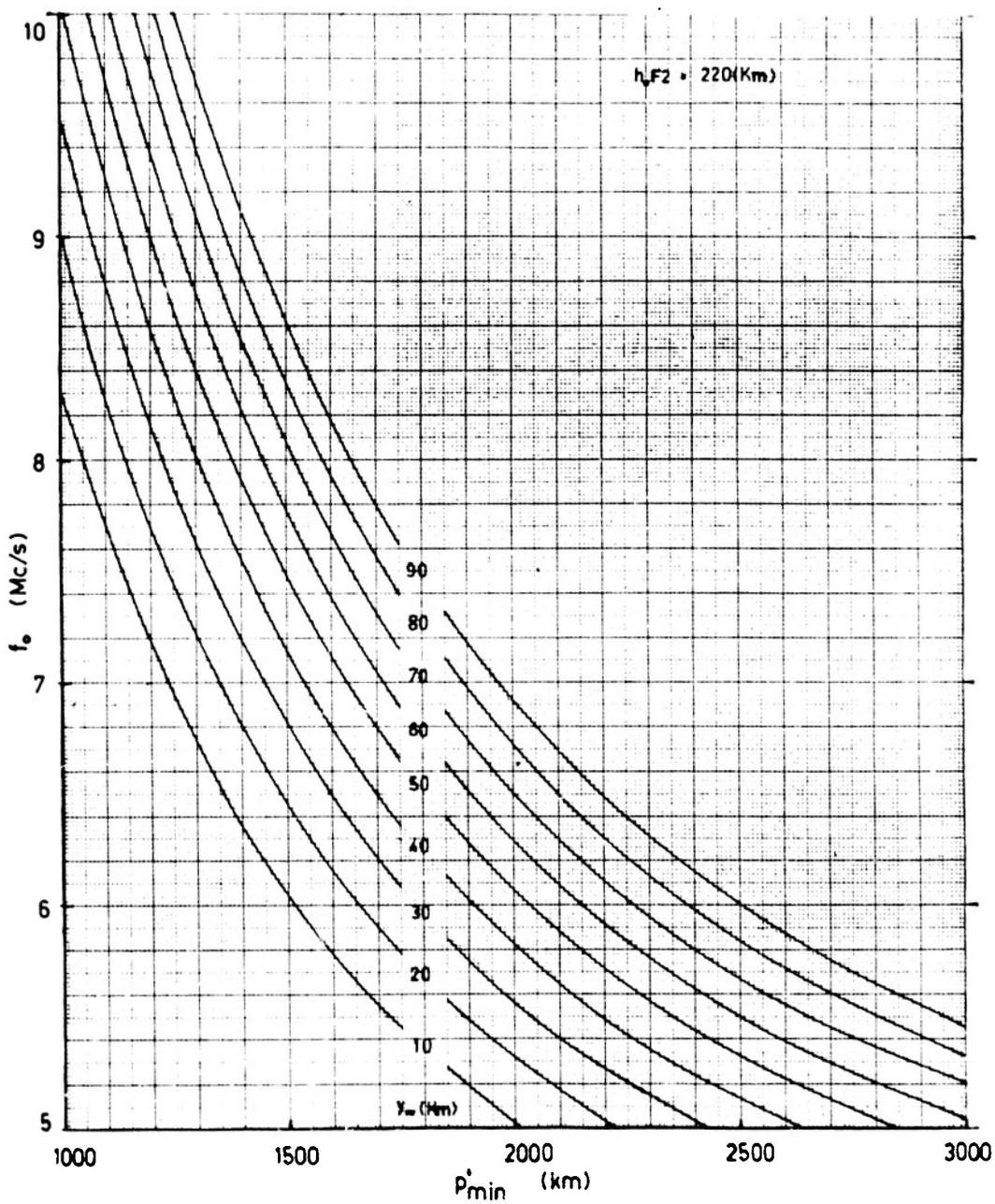

Fig. 39. Chart for deducing y_m.

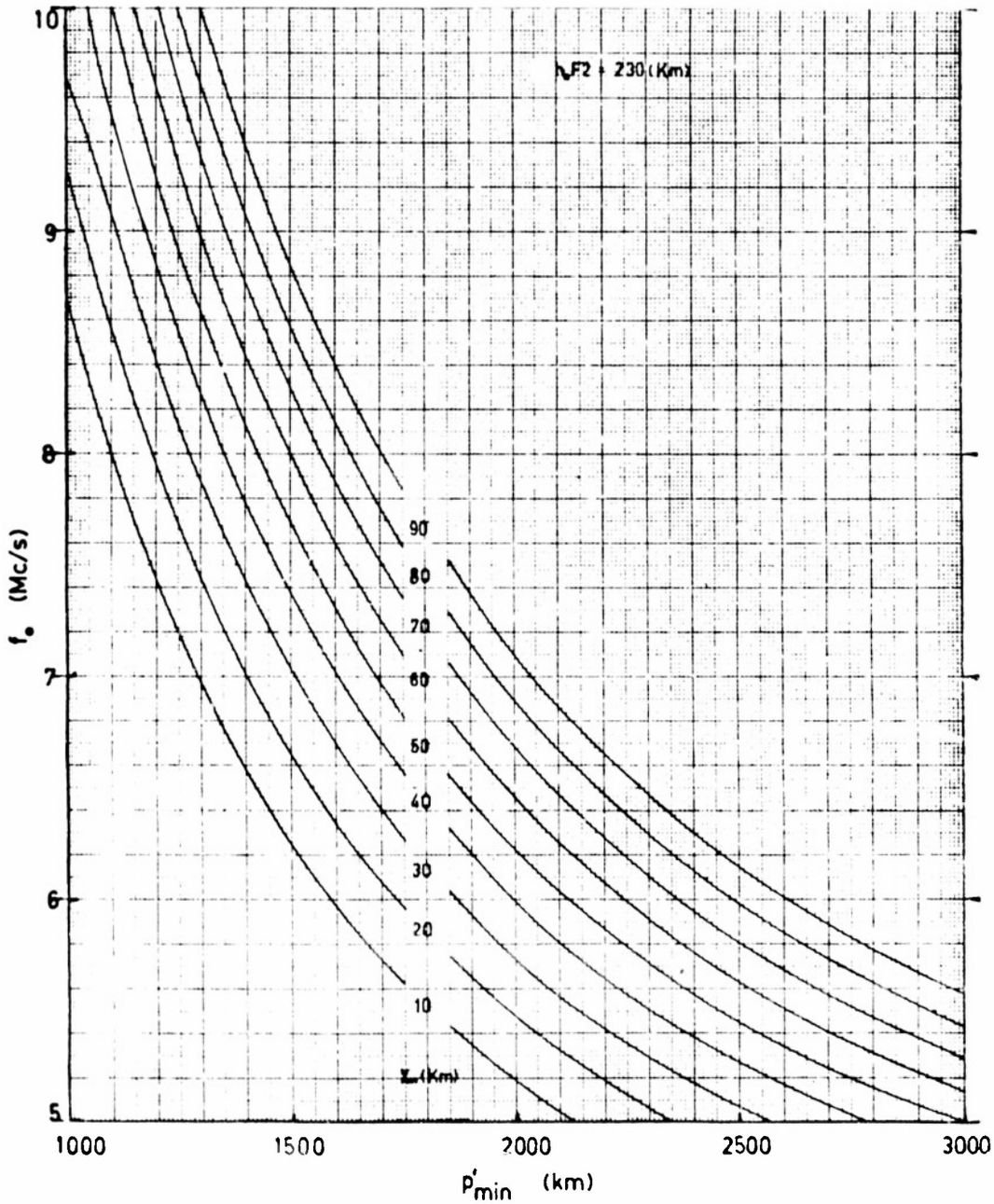

Fig. 40. Chart for deducing y_m.

in h_o. If h_o is 10 km too small, then y_m read from charts will be typically 7 km too large, in order to satisfy the correct p'_{min}. In consequence, the computed value of Δ_s will be 0.25^o too small, and P_c, the calculated peak power, will be 0.6 dB too large. All these errors are tolerable. Fig. 41 illustrates the consequences of errors in h_o for a typical case in which f_o = 7 Mc/s and p'_{min} = 1500 km. P_c is given in dB relative to its value at h_o= 200 km, for constant G and γ , which in any case do not vary much over the range of Δ represented.

In practice, the accepted variation in h_o was 5 km in 10 minutes, that is, in a range interval of 245 km on the east-west ionospheric height contours. Even 10 km was accepted if it was an isolated variation. A tilt of this magnitude could be due to a travelling ionospheric disturbance, as illustrated in Fig. 30a. But such a disturbance advancing from the south would not have much effect on east-west propagation, so the 10 km variation in h_o can be regarded as an error as far as the east-west contours are concerned. This error would be partially offset by the method of calculating y_m, and would be virtually eliminated by averaging adjacent points in the curve of γ against Δ . An estimate of the actual magnitude of east-west tilts may be gained from the result that the knee angle for land is fairly constant ($13^o \pm 1^o$), which suggests that tilts were effectively about $\pm 0.5^o$.

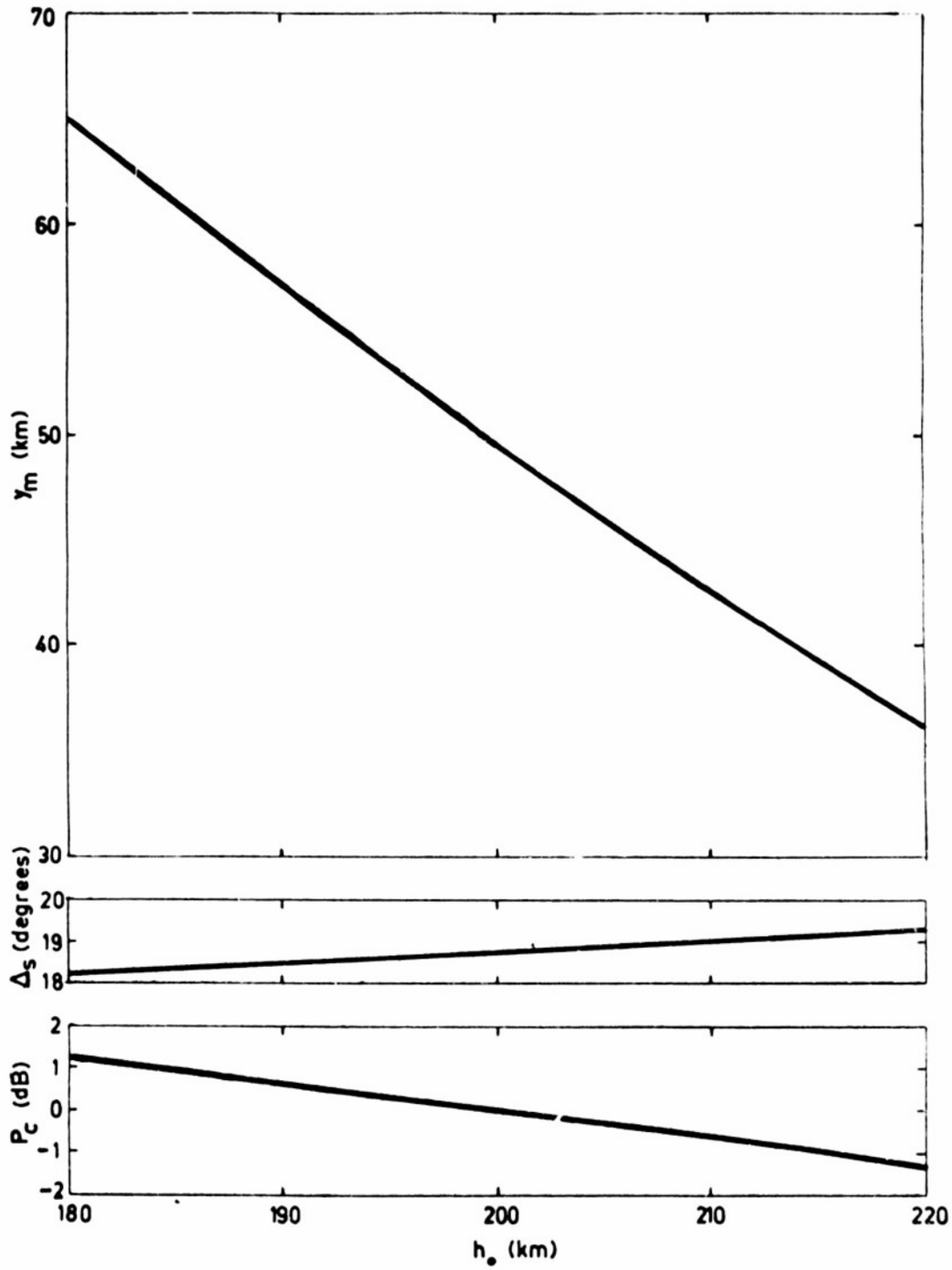

Fig. 41. Effect of errors in h_o on y_m, Δ_s and P_c, when f_o= 7 Mc/s, p'_{min}= 1500 km, and G and γ are constant.

In later versions of the main computer program, the use of the charts to find y_m was obviated by computing y_m from p'_{min} by successive approximations, before proceeding to find P_c and Δ_s. But in general the charts were preferred, as they enabled one to recognize and eliminate absurd results, such as negative y_m, more effectively, and also because the use of the charts involved a large saving in computer time.

A third method of finding y_m would be by calculation from p'f curves by the method of SCHMERLING and VENTRICE (1959). But the true height of the maximum ionization obtained in this way is subject to large errors, as the ruled overlay must be placed in line with the f_o value, and any error in judging this is greatly magnified by the concentration of rulings on the overlay near this frequency, that is, the concentration of h' values to be read from the curve where h' is large and rapidly varying. Probably y_m could be obtained to within about $\pm$ 10 km, but this would lead to large errors in the calculation of p'_{min}.

8.4 Calculation of P_c and Δ_s

The complete formulas are given in Appendix II. The method is summarized here.

The input data were h_o, f_o and y_m, and the antenna gain G, tabulated for every degree of Δ from 5^o to 40^o. The Appleton and Beynon equations were stored in a subrout-

ine for very frequent use; also in this subroutine was the formula to calculate $dD/d\Delta$.

The skip distance D_s and the skip angle Δ_s were found by calculating the penetration angle and then decreasing Δ in steps until $dD/d\Delta$ was zero, when the corresponding value of D was D_s, and the value of Δ was Δ_s. The second differential $d^2D/d\Delta^2$ at D_s was then calculated numerically from the gradient of the $dD/d\Delta$ vs Δ curve, and was used to calculate the focusing factor at the skip distance. The elevation angle Δ was decreased in further steps, and at each stage the first differential $dD/d\Delta$ was calculated and used to find the focusing factor.

Let δD be an interval of ground range from which the echo is being simultaneously received.

Then the actual power received back,

$$P_R \propto \int_{D-\delta D}^{D} G^2 F^2 \gamma \sin \Delta D \, dD$$ (See Appendix II).

The interval δD depends on the pulse width δt. If focusing is neglected,

$$\delta D = \frac{\frac{1}{2} c \, \delta t}{\cos \Delta} = \frac{90}{\cos \Delta} \text{ km for } \delta t = 600 \text{ microseconds.}$$

For a thick ionosphere, δD is considerably increased near D_s, an effect known as time focusing.

The data was chosen for the control point of the skip ray, because it is desired to calculate the peak value of the echo power, and owing to skip distance focusing this

power travels via the skip ray and adjacent rays, provided the antenna gain is reasonably constant over the range of angles involved. To illustrate this focusing for a typical case where h_o = 200 km, f_o = 7 Mc/s and y_m = 50 km, the variation of F with D was calculated and plotted in Fig. 42. The elevation angles corresponding to various points on the F——D curve are indicated on the graph. At D_s, F may be ten times its value at $D_s + \delta D$, and therefore the echo, which depends on F^2, may be enhanced a hundred times at D_s. At long ranges, F increases again (horizon focusing), but at the ranges and elevation angles concerned this effect is not important in the present work.

The value of F at D_s has to be calculated by a more rigorous method than at longer ranges, and involves $d^2D/d\Delta^2$, as mentioned before. This is because the ordinary formula is an approximation which results in F going to infinity as D approaches D_s. The curve of Fig. 42 shows that there is a smooth transition between the rigorous and approximate formulas as applied in this program.

The value of δD in this example is derived in the course of the calculations, and turns out to be 130 km for a 600 microsecond pulse and the given ionospheric configuration.

The calculated relative peak power, taking γ as constant, is given by

$$P_c = \int_{D_s}^{D_s + \delta D} G^2 F^2 \sin \Delta \, D \, dD.$$

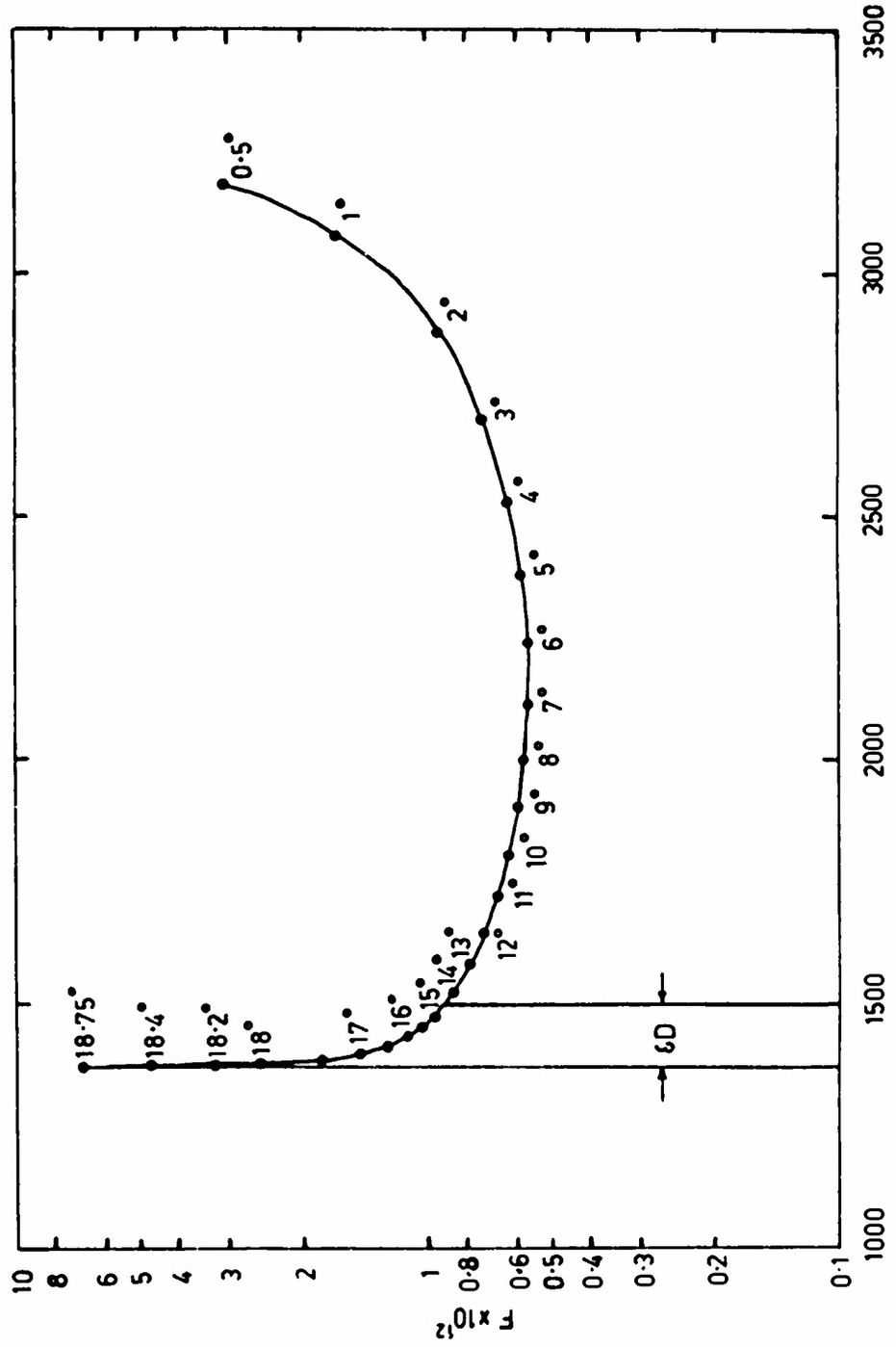

Fig. 42. Focusing factor at various ranges, for h_o = 200 km, f_o = 7 Mc/s and y_m = 50 km.

The integration was performed by calculating the area of the strip $G^2F^2 \sin \Delta \, D \, dD$ each time Δ was incremented until such time as $p' = p'_{min} + \frac{1}{2}c \, \delta t$ (that is, when $D = D_s + \delta D$). The sum of the strips then gave the total integral P_c for subsequent comparison with the observed P_R.

The optimum size of the steps $d\Delta$ was chosen by trial and error so that P_c varied by less than 0.1 dB from its value when $d\Delta$ was very small. The values finally chosen for $d\Delta$ were 0.2^o for Δ between the penetration angle and Δ_s, and also until p' reached p'_{min}, and then 0.5^o for p' between p'_{min} and $p'_{min} + \frac{1}{2}c \, \delta t$.

It might be thought that it would be profitable to calculate the complete P_c——p' echo pulse shape for comparison with range——amplitude (swept-gain) records, to give a γ——Δ curve for a wide range of Δ and not just for Δ_s. This was attempted for $1E_s$ echoes, assuming that the layer was at a height of 110 km and of negligible thickness, but results so obtained for the backscatter coefficient were very inconsistent. This was attributed to the fact that an E_s cloud does not usually cover the whole area of the E region illuminated by the sounder, and the echo varies in shape as the cloud passes through the illuminated area. Ideally it should be possible to select $1E_s$ echoes at times of complete E_s blanketing. The leading edge of the echo then depends only on the E_s critical frequency (assumed constant throughout the cloud), and the trailing edge should provide

data useful for deriving γ , but unfortunately the tail of the echo is often lengthened due to range spreading due to small irregularities in the E_s cloud, which can no longer be considered to act as a smooth mirror. For oblique reflection, the irregularities have their greatest influence at low elevation angles (long ranges), although it might be possible to overlook them at the leading edge. These considerations make it very hazardous to draw conclusions about the backscatter coefficient from the shape of the complete range —amplitude records.

For 1F records, what is said about range spreading of $1E_s$ echoes applies even more, although the F layer can normally be assumed to extend across the entire illuminated F region. The F region irregularities that cause spreading can be much larger than E_s irregularities. Not only may the irregularities cause confusion at long ranges, but also the tail of the 1F echo is reflected in the ionosphere at a much greater range than $1E_s$, and the Brisbane vertical incidence data appropriate to the control point of the skip ray cannot confidently be assumed at the longer ranges. Therefore the ordinary ionospheric parameters are known with less certainty, and there is no way of checking the assumed parameters such as is afforded by the observations of p'_{min} at the leading edge.

It seems preferable, therefore, to concentrate on the peak observed value of P_R, and to observe its variations

with the time of day, as h_o, f_o and y_m vary, and hence as Δ_s varies. By plotting $P_R - P_c$ against Δ_s it should be possible to obtain the relative backscatter coefficient at the angles represented.

Every 10 minutes h_o and f_o were available from vertical incidence soundings, and when these were matched with backscatter records, it was possible to draw up a table giving time of vertical incidence sounding, h_o, f_o, corresponding backscatter record time, p'_{min}, P_R and y_m. Calculations then gave P_c and Δ_s, hence $P_R - P_c$ could be plotted against Δ_s. Table 4 is an actual example (14/4/63, 260° mag. az.). The computer time involved was about 3 minutes.

P_R, the peak power scaled from the backscatter records, is given in dB relative to the highest gain stage of the swept-gain unit. Thus if an echo is just discernable on the swept-gain frame, P_R = 0 dB, and if it extends right across the frame, P_R is about 40 dB. P_C is relative to an equally arbitrary zero, but $P_R - P_C$ suffices to describe the relative backscatter coefficient.

The calibration of the swept-gain unit appropriate to the period 22/10/62 to 16/5/63 is shown in Fig. 43. Gain stage 12 represents the lowest receiver gain, and therefore echoes discernable in section 12 of the swept-gain frame are the strongest. The errors shown on the calibration chart are cumulative errors relative to stage 12. Comparison with the dotted line shows that the gain steps are

TABLE 4

EXAMPLE OF CALCULATIONS

14/4/63, 260° mag. az.

TIME (hr)	h_o (km)	f_o (Mc)	TIME (hr)	p'_{min} (km)	P_R (dB)	y_m (km)	P_C (dB)	Δ_s (°)	P_R-P_C (dB)
1500	220	8.4	1523	1370	31.0	61	-127.3	24.6	158.3
1510	210	8.2	1533	1360	31.0	61	-127.7	23.7	158.7
1520	210	8.2	1543	1390	31.0	66	-128.0	23.4	159.0
1530	210	8.2	1553	1370	31.0	63	-127.4	23.6	158.4
1540	210	7.8	1603	1370	30.6	50	-129.2	22.4	159.8
1550	210	7.7	1615	1450	30.3	59	-129.8	21.4	160.1
1600	200	7.4	1626	1500	29.6	49	-130.2	20.7	159.8
1610	200	6.7	1636	1500	29.3	40	-134.3	17.9	163.6
1620	200	6.7	1647	1550	29.0	46	-134.8	17.6	163.8
1630	200	6.4	1657	1550	28.6	36	-136.1	16.7	164.7
1640	200	6.5	1708	1600	28.0	44	-135.7	16.7	163.7
1650	200	6.4	1719	1650	27.3	46	-136.6	16.1	163.9
1700	200	6.3	1730	1700	26.3	47	-137.4	15.5	163.7
1710	200	6.3	1744	1900	24.4	67	-137.4	14.5	161.8
1720	200	6.3	1755	1950	12.0	72	-137.8	14.2	149.8
1730	190	5.9	1810	2200	3.0	82	-138.8	11.8	141.8
1740	190	5.4	1822	2300	3.0	65	-141.0	10.0	144.0

approximately 3 dB each, except for steps 1 to 2 and 2 to 3, which in any case could not be calibrated as accurately

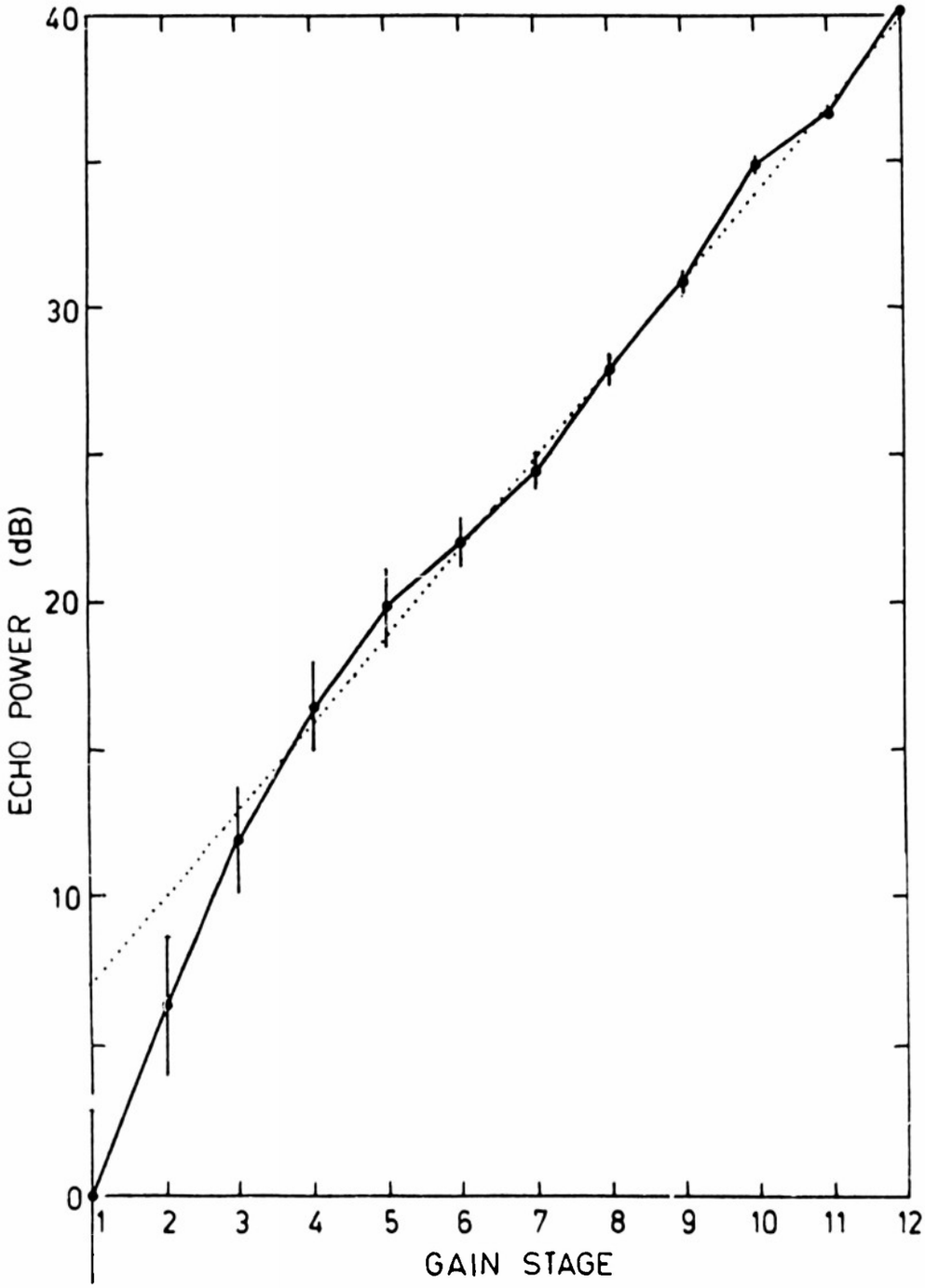

Fig. 43. Calibration chart for swept-gain unit. Error bars indicate the cumulative error in the gain steps relative to stage 12.

as the others, owing to receiver noise. The peak echo power is normally recorded in stages 3 to 12, thereby minimizing receiver noise. (Note that this would not be so in A-scan records taken with maximum receiver gain).

8.5 Selection of Data

The following principles governed the selection of data.

(a) Both backscatter and vertical incidence data should be simultaneously available and clearly recorded. This condition was sometimes not fulfilled, owing to breakdownsin either sounder or use of the backscatter sounder for other work.

(b) Radio interference should be at a minimum. Interference sometimes rendered the vertical incidence records useless, even when good backscatter records were available.

(c) No large ripples should be present in the ionosphere. Large ionospheric disturbances are most frequent in the winter, therefore other seasons were preferred.

(d) Sporadic-E should not be present. E_s is most prevalent in summer. In view of (c) and (d), the most useful data was obtained in the autumn.

(e) D region absorption should be negligible. This condition was satisfied by confining attention to the early morning or late afternoon.

(f) The F region should approximate to a simple parabolic layer. This is most nearly so in the afternoon, after the F1 layer has merged with the F2 layer, normally after 1600

hours.

(g) The swept-gain unit calibration should be known. The most reliable calibration, described in Section 8.4, was performed in April, 1963.

Attention was therefore concentrated on afternoon data taken during the period from 19/3/63 to 16/5/63, when back-scatter data to the east or west was taken on 38 days. Of these days, 20 were capable of yielding results in conjunction with vertical incidence data and calculations.

8.6 Discussion of Calculations

To find the way in which P_C and Δ_s might be expected to behave as f_o decreases at sunset, a sample calculation was performed for h_o= 200 km, y_m= 50 km and f_o varying from 10 Mc/s to 5 Mc/s; G and γ were assumed constant. The results for P_C and Δ_s were plotted against the results for p'_{min}, and the f_o values were indicated on the P_C curve. Fig. 44 shows these results. If p'_{min} increases at a constant rate, then the P_C curve is a measure of the rate of change of P_C with time. The curve suggests that P_C varies slowly and is fairly constant at long ranges. This is fortunate, as it means that provided Δ_s is greater than zero, any sudden changes in P_R will be due almost entirely to changes in G and γ .

G and γ are both functions of Δ , so it is interesting to note the range of values of Δ_s that may be expected

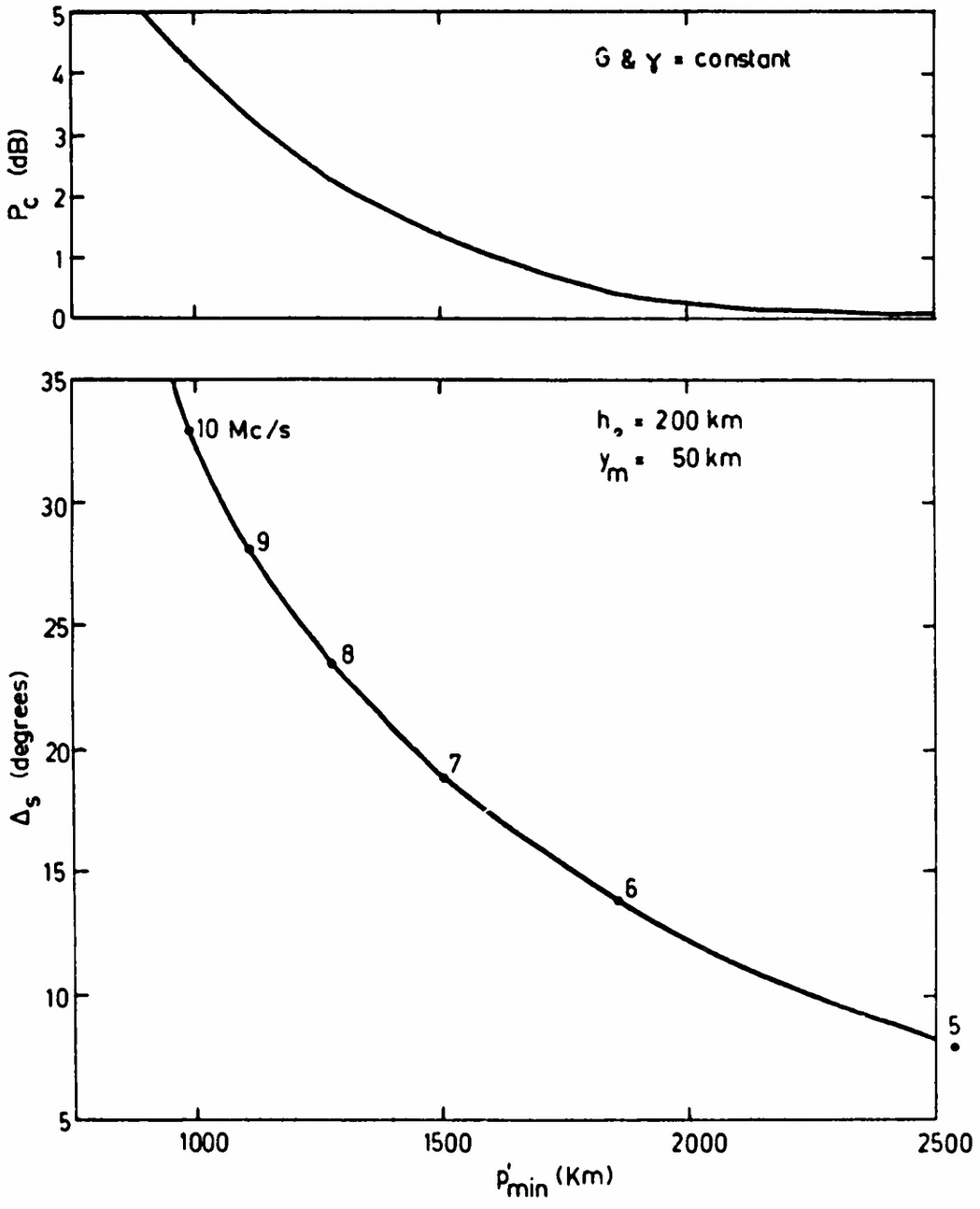

Fig. 44. Variation in P_c and Δ_s with p'_{min} as f_o varies, assuming G, γ, h_o and y_m to be constant.

for typical data. When f_o = 10 Mc/s, $\Delta_s = 33^o$, and as f_o decreases, Δ_s approaches zero at the rate of about 5^o/Mc (Fig. 45). On many days when records were suitable for scaling, f_o was below 8 Mc/s, and therefore Δ_s was less than about 23^o. At about 4 Mc/s, $\Delta_s = 0$, although even at 5 Mc/s the computer program may fail, as after Δ_s has been computed, it may not be possible to compute the integral for P_C as Δ becomes smaller. To avoid wastage of computer time, the work was programmed to reject data whenever it required Δ to become less than 5^o. The inability of the computer to cope with low values of Δ appears to manifest itself in the Appleton and Beynon equations. Three programs containing these equations failed to cope with the very low angles, including programs written in both GAP and WIZ source languages.

The program used to find the curves giving y_m from h_o, f_o and p'_{min} also yielded the value of Δ for the p'_{min} ray. When Δ_s is 30^o, this angle is 1^o or 2^o less than Δ_s. When Δ_s is small, this angle is very slightly less. The values of Δ for p'_{min} have been plotted against f_o for h_o = 180, 220 and 260 km, and various values of y_m, in Figures 46 to 48. In all these cases it can be seen that Δ becomes zero between about 4 and 5 Mc/s. The rate at which Δ approaches zero increases at low angles, so that a very small decrease in f_o may cause the p'_{min} ray to fall to zero elevation. It is expected therefore that the disappearance

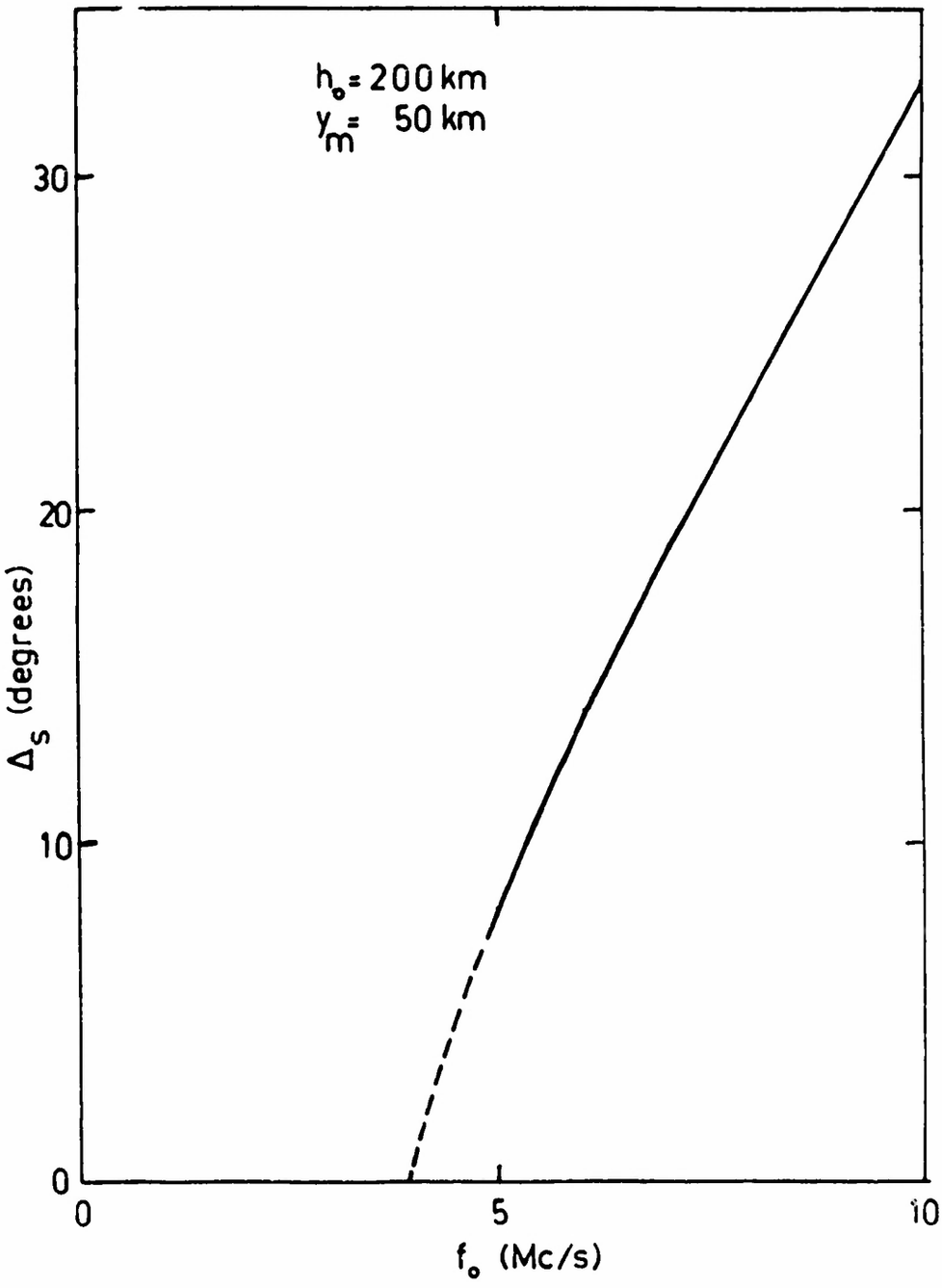

Fig. 45. Variation in Δ_s with f_o, assuming h_o and y_m to be constant.

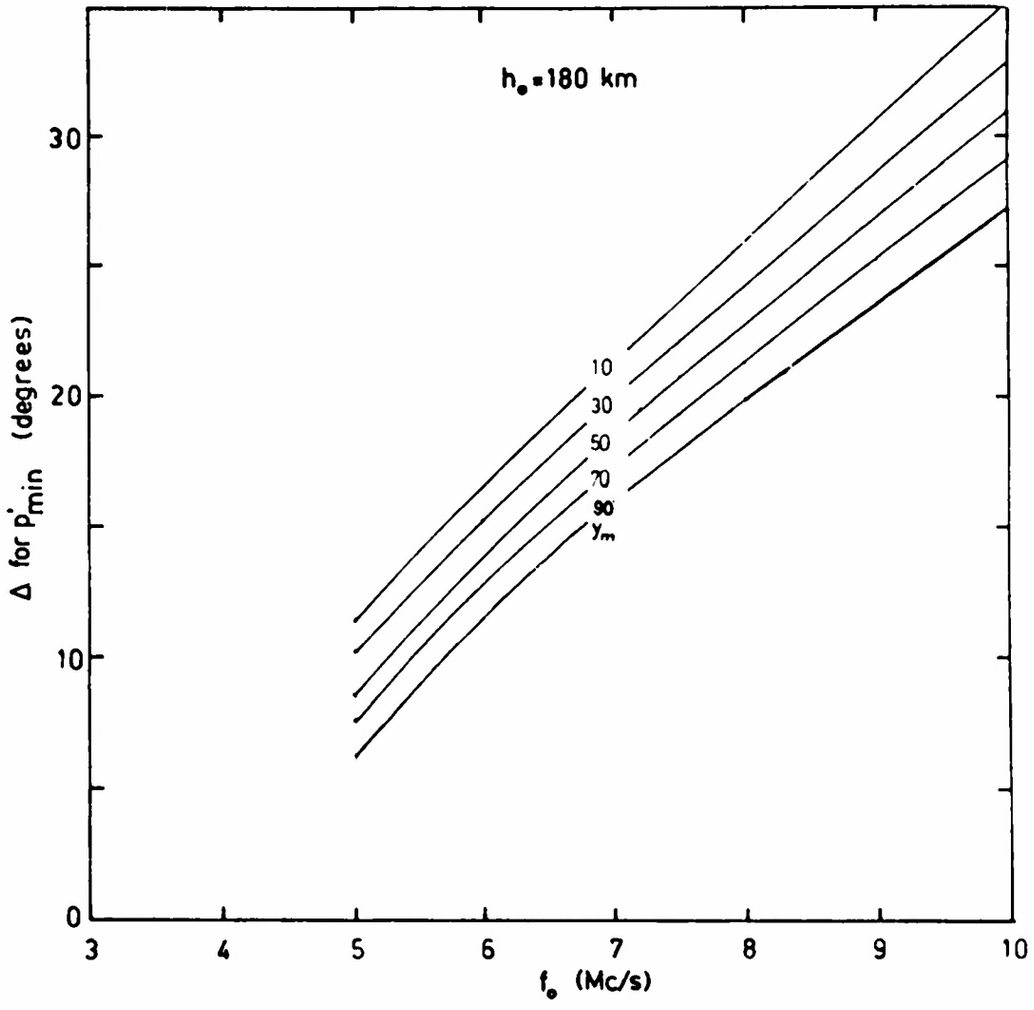

Fig. 46. Variation in elevation angle of the minimum path-length ray as f_o varies.

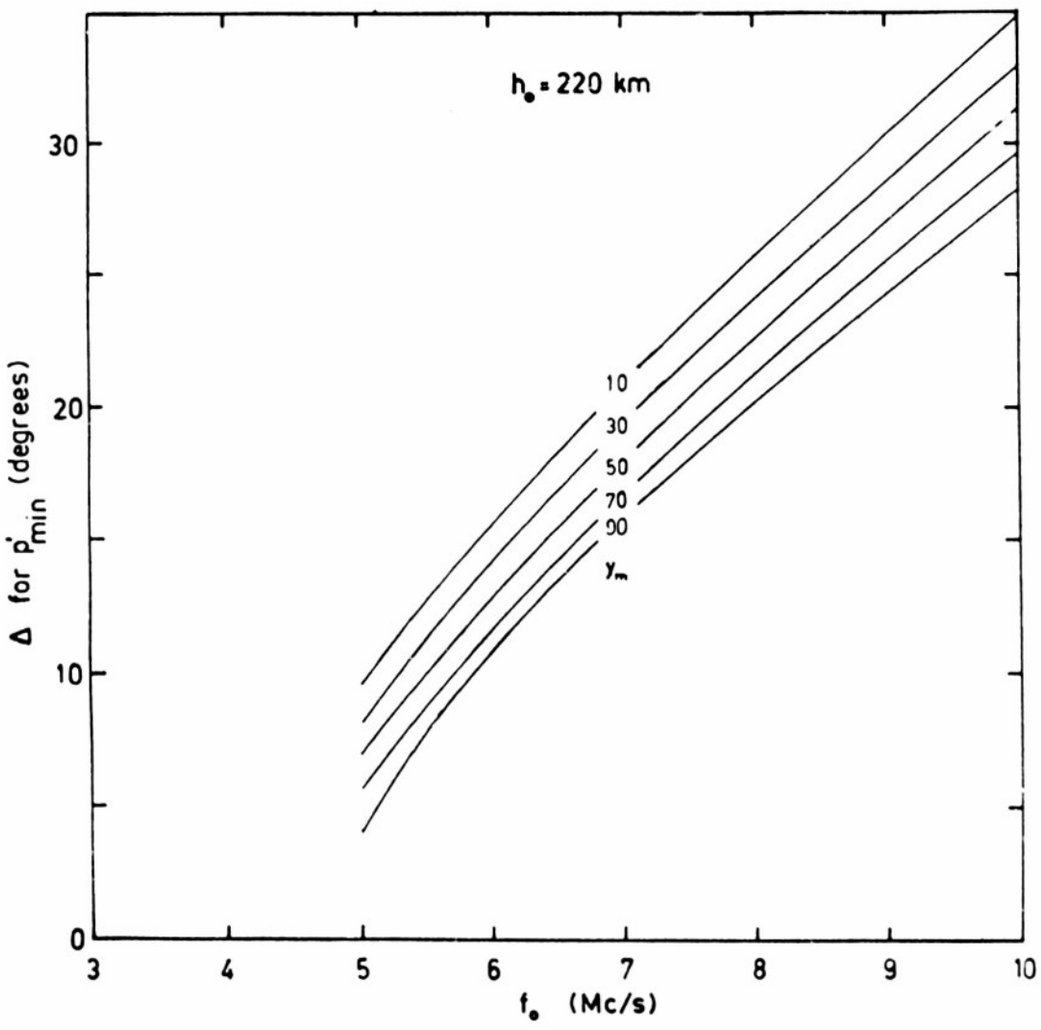

Fig. 47. Variation in elevation angle of the minimum path-length ray as f_o varies.

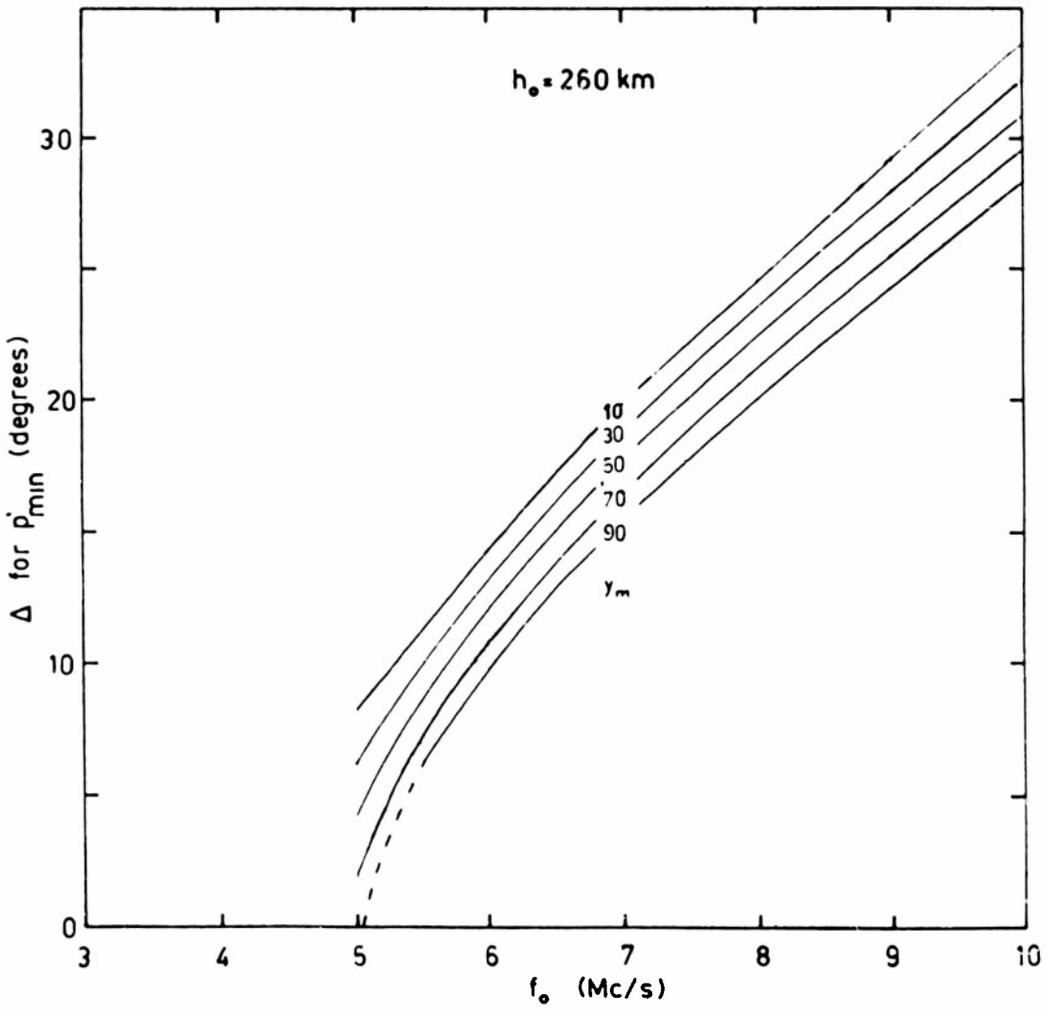

Fig. 48. Variation in elevation angle of the minimum path-length ray as f_o varies.

of the echo as Δ approaches zero after sunset should occur rapidly, even if G and γ are constant. Any sudden decrease in P_R when Δ is small is probably due to this, as an error of only 0.1 Mc/s could give rise to an error of 3^o in Δ ; but a sudden decrease in P_R when Δ is, say, 14^o, can only be due to G or γ .

Fig. 49 (6/4/63, 80^o mag. az.) is a graph of echo power against time of day. Each gain stage represents about 3 dB. The echo power is almost constant for several hours, then drops off rapidly near sunset. Within half an hour, the echo has disappeared from the record. Investigation shows that in that time the critical frequency dropped from 7 Mc/s to 5.3 Mc/s, p'_{min} increased from 1550 km to 2250 km and Δ_s dropped from 17^o to about 10^o. It is that short space of time (not quite as short for western echoes) which can reveal most about the variation of γ with Δ .

8.7 High angle rays

The present calculations, in common with SHEARMAN (1956b), have neglected the high angle rays, that is, those with angles of elevation greater than Δ_s. Actually at ranges beyond D_s the high angle and low angle rays interfere, producing a pattern of fringes about 1 km per fringe in width (BREMMER, 1948, Fig. 72). At ranges considerably beyond D_s, the fringes virtually disappear, owing to geometrical considerations which cause the intensity of the high angle rays to fall away (BREMMER, 1948, Fig. 69). At a

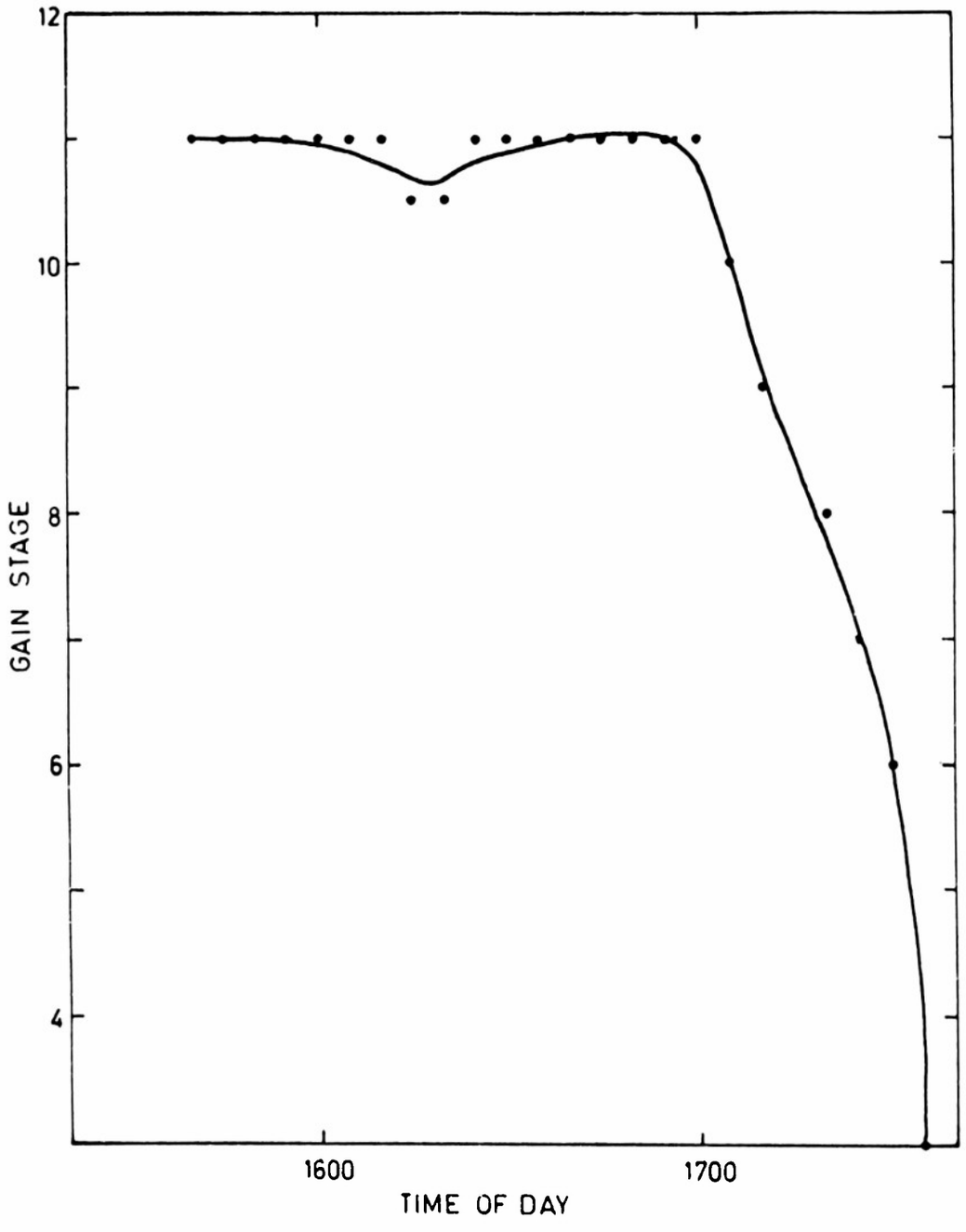

Fig. 49. Variation in echo power with time of day, 6/4/63, 80° mag. az.

range 100 km beyond D_s, a high angle ray is typically 3 dB weaker than the low angle ray, and at D_s + 1000 km it is 20 dB weaker. In addition, the deviative absorption of the high angle rays is comparatively very large (BIXBY, 1953, Fig. 28).

As the present work is concerned with echoes from near the skip distance, it may be assumed that high and low angle rays are equally strong, and that well-defined fringes will be formed, although the width of the transmitted pulse prevents any resolution of the individual fringes. The maxima are about twice as strong as the low angle contribution alone, that is, about 3 dB stronger than the calculated intensity. As the results are only relative, this 3 dB error is of no consequence. Even if the size of this error varies slightly as Δ varies, neglect of the high angle rays does not give rise to significant errors in the results.

Therefore the high angle rays have been neglected but not overlooked. Further, in the curves of γ against Δ, the high angle rays have been taken into account as follows: γ was plotted against Δ_s, but in any echo of finite pulse-width, the echo from the skip distance is combined with echoes from beyond the skip distance propagated by both high and low angle rays. The value of Δ_s plotted is therefore not only the angle of the most powerful ray, but also the approximate mean of all the angles represented.

8.8 Magneto-ionic splitting

In the calculations, only the ordinary ray has been considered. The neglect of the extraordinary ray is justified in the case of east-west propagation. This Section gives a summary of the theory leading to estimates of the errors to be expected if magneto-ionic splitting is neglected.

The formulas are expressed in the form given by RATCLIFFE (1959), and the relevant symbols are as follows:

f = wave frequency = 16 Mc/s

f_c = critical frequency, neglecting the earth's field

f_o = ordinary ray critical frequency

f_E = extraordinary ray critical frequency

f_H = gyrofrequency = 1.4 Mc/s at Brisbane in the F region

θ = angle between ray and geomagnetic field

$X = f_c^2/f^2$

$Y = f_H/f$ = 0.0875 here

Y_T, Y_L = components of Y transverse and longitudinal to the ray

The treatment here is consistent with BIXBY (1953) and C.R.P.L. (1948). Collisions are neglected.

(a) No magnetic field

$$n^2 = 1-X$$
$$= 1- f_c^2/f^2 \qquad (1)$$

(b) Quasi-transverse approximation

(i) Ordinary (O) ray $n^2 = 1 - \dfrac{X}{1 + (1-X)\cot^2\theta}$

$= (1-X)\,\mathrm{cosec}^2\theta$ approx.

$= 1 - X$ approx., for θ near 90°.

This approximates to the "no field" case, so $f_o = f_c$.

(ii) Extraordinary (E) ray $n^2 = 1 - \dfrac{X}{1 - \dfrac{Y_T^2}{1 - X}}$

$= 1 - \dfrac{X}{1 - Y^2}$ if $X \ll 1$.

Then if f_E is the critical frequency of a fictitious ionosphere in which the E ray propagates as if there were no magnetic field, that is, f_E replaces f_c in (1),

$$f_E^2 = \frac{1}{1 - Y^2} f_c^2$$

$= (1+Y^2) f_o^2$ approx., since $Y \ll 1$ and $f_o = f_c$.

Hence, $f_E = \sqrt{1+Y^2}\, f_o$

$= 1.004\, f_o$.

(c) Quasi-longitudinal approximation

$n^2 = 1 - \dfrac{X}{1 \pm Y_L}$ where $Y_L = Y$ approx., for θ near 0°.

Reflection occurs at two levels, where $X = 1+Y$ and $X = 1-Y$. The ray reflected at the upper level $(1+Y)$ is designated as the O ray; for this,

$$f_o^2 = \frac{1}{1 + Y} f_c^2 \qquad (2)$$

The lower level ray is the E ray, for which

$$f_E^2 = \frac{1}{1 - Y} f_c^2$$

$$= (1+Y) f_c^2, \text{ since } Y \ll 1. \qquad (3)$$

Also, we have

$$\frac{f_E^2}{f_O^2} = (1+Y)^2$$

hence, $f_E = (1+Y) f_o$

$$= 1.09 f_o.$$

(d) Conditions intermediate bet between (b) and (c)

O ray: $f_o = f_c$

E ray: Most of the E ray reflection takes place at the lower level, where $X = 1-Y$, hence from (3),

$$f_E = \sqrt{1+Y} f_c$$

$$= 1.043 f_o \text{ since } f_o = f_c.$$

(e) Effect of neglecting splitting

Suppose $f_c = 7$ Mc/s, $h_o = 200$ km, $y_m = 50$ km.

(i) Quasi-transverse: $f_E = 1.004 f_o = 7.028$ Mc/s.

Fig.37 shows that for the assumed configuration,

$p'_{min}(O) = 1500$ km, and $p'_{min}(E) = 1490$ km.

(ii) Quasi-longitudinal: $f_o = \frac{1}{\sqrt{1+Y}} f_c = 6.7$ Mc/s (from (2))

$f_E = \sqrt{1+Y} f_c = 7.3$ Mc/s (from (3))

Then from Fig.37 , $p'_{min}(O) = 1610$ km and $p'_{min}(E) = 1430$ km.

In the present work, the pulse width contributes to the echo an interval $\delta p'$ of 90 km, so for east-west propagation (quasi-transverse) the two parts of the echo cannot be resolved. The only effect of neglecting the E ray is an error of about 10 km in p'_{min}, which is smaller than the accuracy of reading p' from the films.

For north-south propagation, however, the rays approach the quasi-longitudinal condition. The E ray echo may be resolved from the O ray echo, especially if the skip distance focusing is strong and if the O and E rays are of equal intensity; in any case, p'_{min} observed is that for the E ray. Magneto-ionic splitting should not be neglected in north-south propagation. Fig. 27 probably illustrates splitting in a 1F echo.

8.9 Deviative absorption

The calculations neglect any correction for deviative absorption, that is, the absorption that takes place within the F layer and causes the F layer reflection coefficient to be less than unity.

The amount of deviative absorption is believed to be negligible in the present work. An estimate of its magnitude can be gained from the relation

$$-\ln \rho = \frac{\nu}{2c} (p'-p),$$

where ρ = reflection coefficient

ν = collision frequency = 10^3 sec^{-1} approx., for the

F region.

p' = group path

p = phase path.

This formula is given by RATCLIFFE (1959, pp 116 and 132) and applies when there is no magnetic field, and approximates to the case for east-west (quasi-transverse) propagation. The loss of power (in dB) for a ray from the bottom of the F layer to the top of its path is

$$L = -\frac{10}{2.3} \ln \rho$$

$$= -4.35 \ln \rho \quad .$$

For propagation up and down, the total loss will be

$$L = -8.7 \ln \rho$$

$$= \frac{8.7 \nu}{2c} (p' - p)$$

$$= 1.45 \cdot 10^{-5} (p'-p), \text{ if } (p'-p) \text{ is in metres.}$$

For a rough estimate of $p'-p$, let us assume a flat earth and flat ionosphere. In the usual notation (the subscript 1 denoting the ionospheric portion of the path),

$$p'-p = p_1' - p_1.$$

p_1' is simply $D_1 \sec \Delta$. To estimate p_1, we note that

$$\sqrt{D_1^2 - (2y_m)^2} > p_1 > D_1.$$

Taking p_1 as the r.m.s. value of these limits,

$$p_1 = \sqrt{D_1^2 + 2y_m^2} \quad .$$

The curves in THOMAS and McINNES (1962, Fig.3) show

D_1 for various values of Δ , given h_o = 200 km and y_m = 150 km.

For $\Delta_s = 25^o$, the penetration angle is about 29^o, so the 9 Mc/s curve is appropriate. For this, D_1= 650 km.

Then p'-p = 33 km approximately, for which L=0.5 dB.

For $\Delta_s = 12^o$, D_1= 1000 km, p'-p = 0 approx., and L = 0 approx.

For the echo, the losses would be twice as large. Actually, in the present work y_m is nearer to 50 km than 150 km, therefore the absorption is less than estimated here.

We may conclude that the loss of echo power due to deviative absorption is no greater than 1 dB in the present work.

8.10 Summary

The method of calculating the maximum power returned in 1F echoes takes into account all known influences, including antenna, ionospheric, geomagnetic and ground effects. Skip distance focusing is of great importance, while for the data chosen it was possible to neglect D region absorption, E and F1 layer effects, deviative absorption, high angle rays and magneto-ionic splitting.

A graphical method of matching oblique backscatter data with vertical incidence data extrapolated to the control point has been developed, as well as a satisfactory way to estimate the semi-thickness of the assumed parabolic

layer. The theoretical behaviour of the echo power at sunrise or sunset has been discussed on the assumption that backscattering is isotropic.

9. RELATIVE BACKSCATTER COEFFICIENT——RESULTS

Figures 50 to 61 show P_R-P_C (relat .e backscatter coefficient γ) plotted against Δ for most of the days for which calculations were done. To save space, results for sea (80^o mag. az., crosses) were sometimes plotted with other results for land (260^o mag. az., circles). Three notable features emerge.

9.1 Comparison of land and sea

Backscatter from the land is much weaker than from the sea. The γ —— Δ curves above 15^o are approximately parallel, but there is a 10 dB difference between land and sea. This difference is much greater than any likely errors in the antenna patterns or in the choice of the ionospheric parameters, and is therefore largely due to a difference in γ . The asymmetry of east and west propagation at sunset could conceivably have affected the result, so a sample calculation was done for both east and west in the morning, when the asymmetry was reversed. Fig. 59 shows these results; sea scatter is still stronger than land by about 10 dB. Morning calculations were not as reliable as those of the evening, owing to the presence of the morning F1 layer, which rendered the Appleton and Beynon formulae not strictly

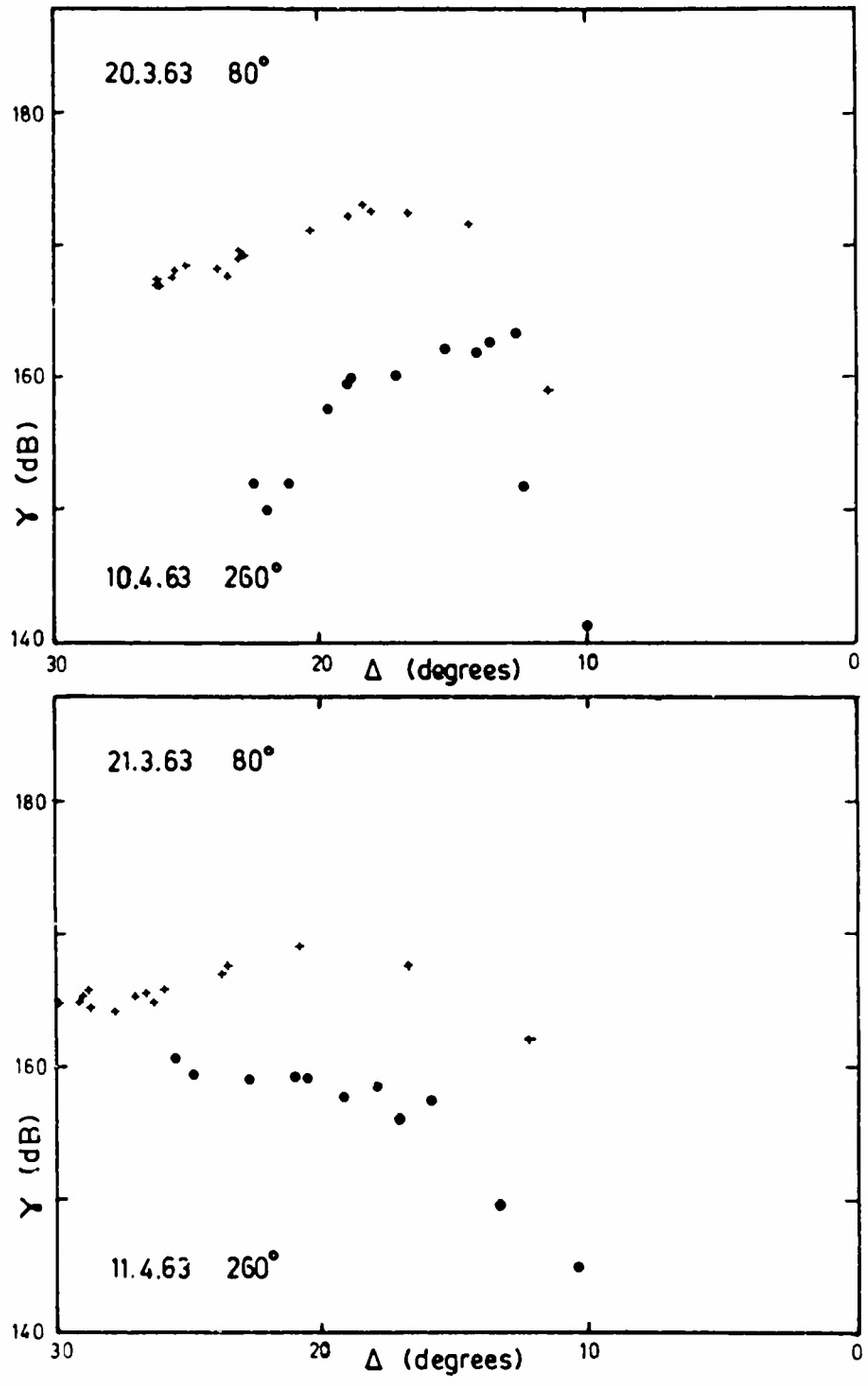

Figures 50 and 51. Relative backscatter coefficient.

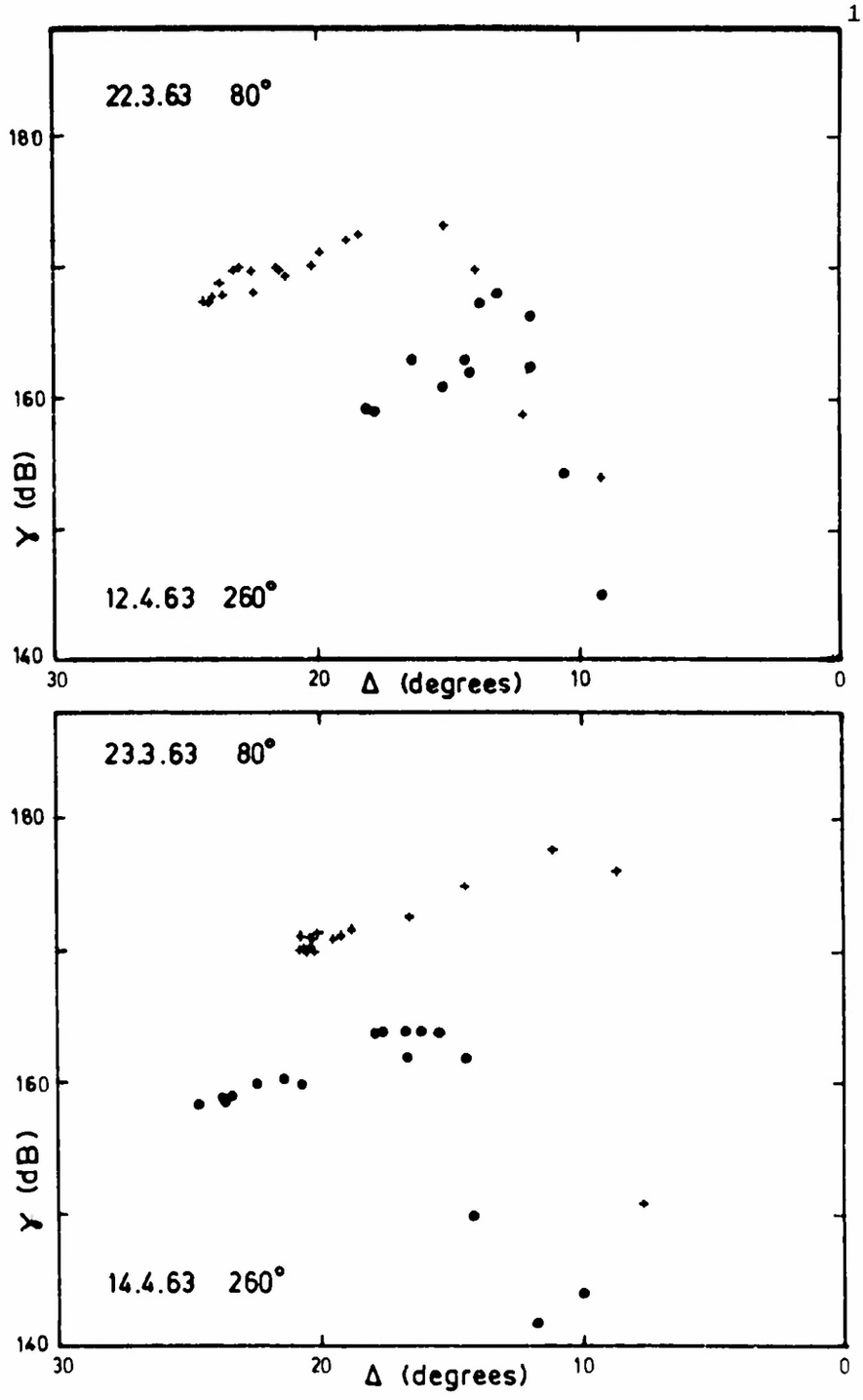

Figures 52 and 53. Relative backscatter coefficient.

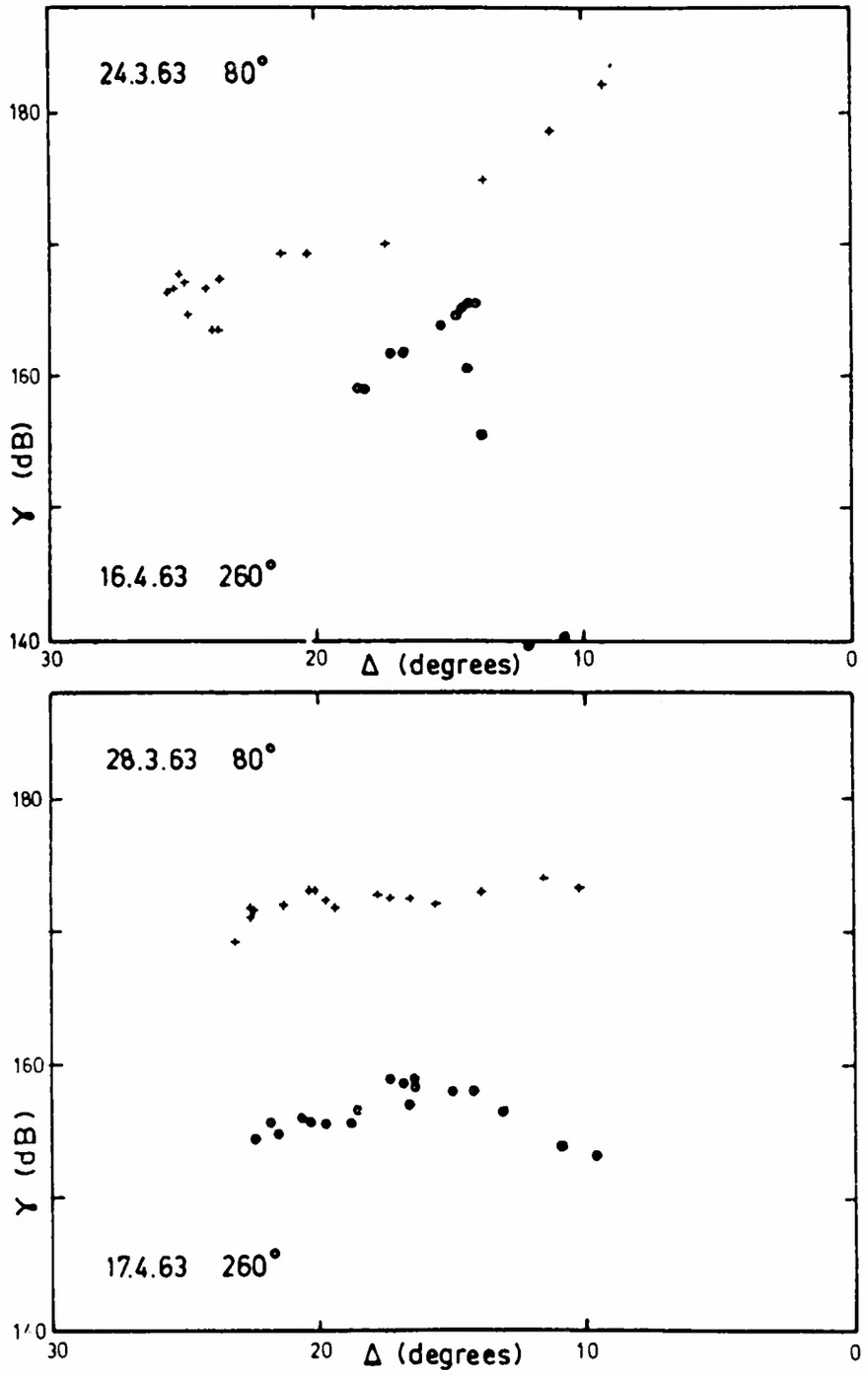

Figures 54 and 55. Relative backscatter coefficient.

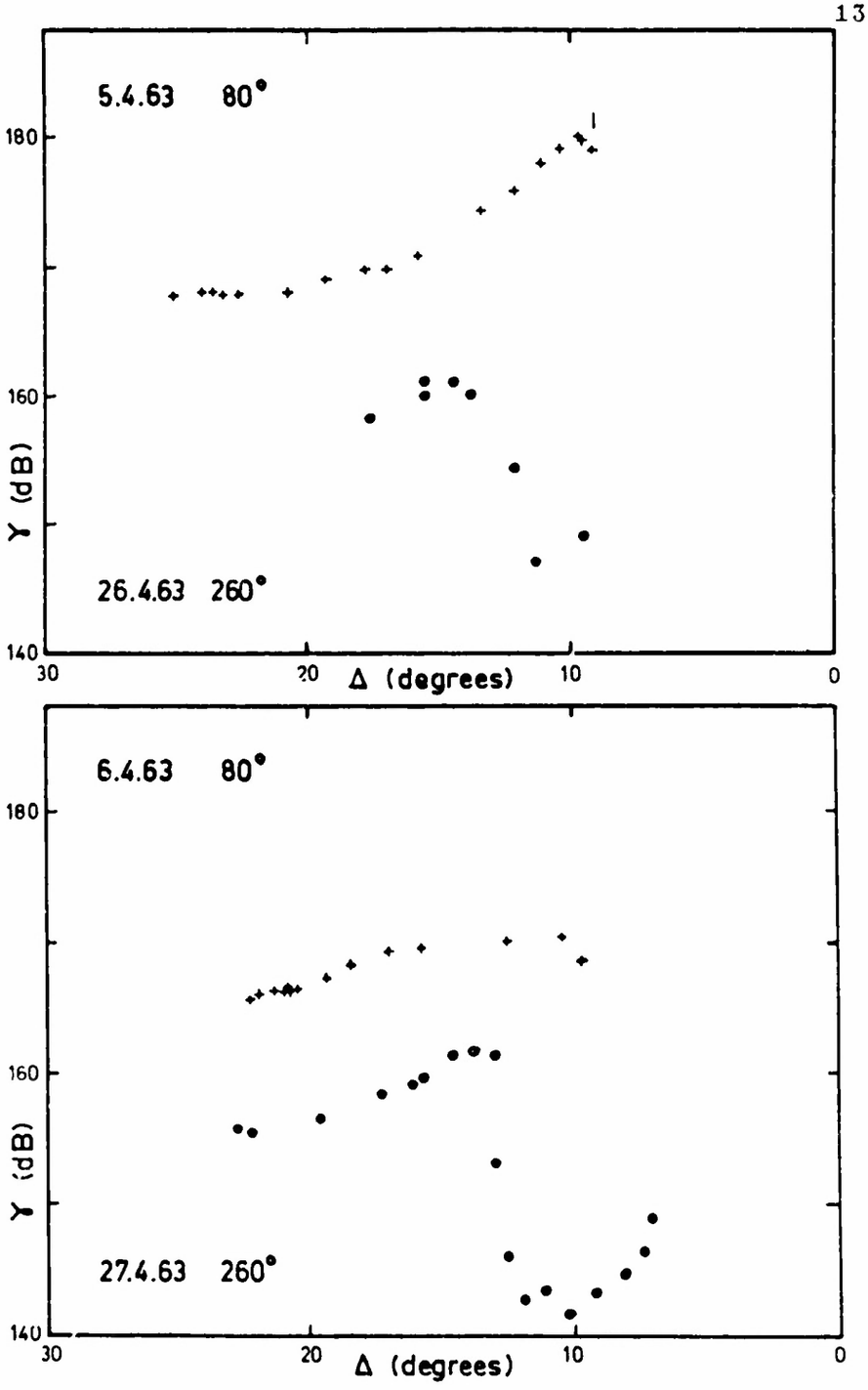

Figures 56 and 57. Relative backscatter coefficient.

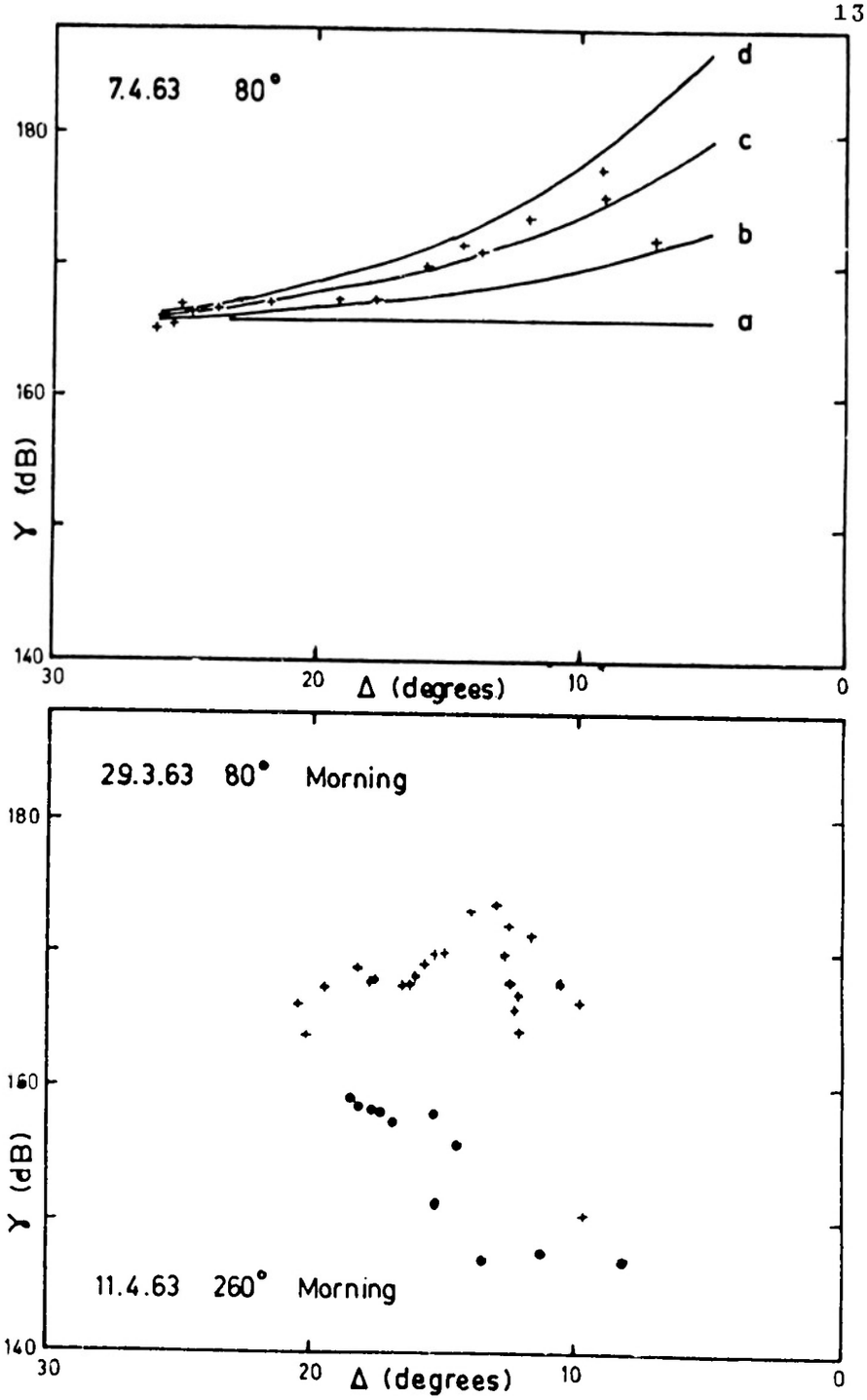

Figures 58 and 59. Relative backscatter coefficient.

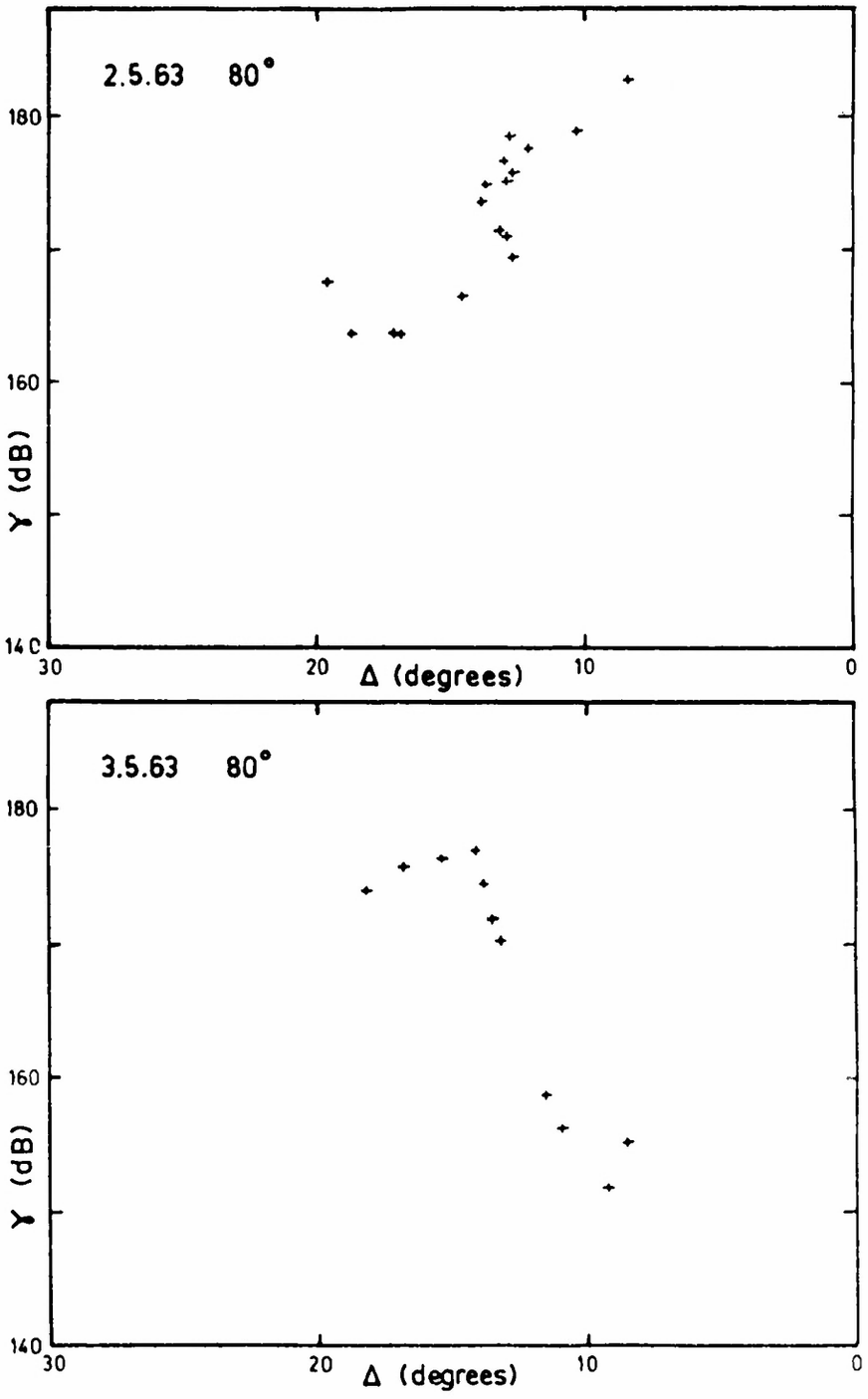

Figures 60 and 61. Relative backscatter coefficient.

applicable. Nevertheless the morning results were sufficiently accurate to show that the 10 dB difference between sea and land scatter is independent of ionospheric asymmetry.

This difference agrees with the observations of RANZI and DOMINICI (1959), although their estimate was a very rough one based only on a visual inspection of B-scan records, and was subject to serious doubts as the behaviour of the vertical radiation pattern of their antenna varied markedly with azimuth, and this had not been taken into account.

The present result also agrees qualitatively with HAGN (1962), who found land backscatter to be about 20 dB weaker than sea, for comparatively smooth land surfaces. In the present work, it is possible that mountains and other large features contributed to the higher backscatter coefficient than that given by HAGN.

The difference between sea and land backscatter has important implications which will be dealt with in Chapters 10 and 11.

9.2 The knee effect

For most of the cases calculated, as Δ decreases, γ declines suddenly at some angle. This effect, also described by HAGN (1962), is called the knee effect. According to HAGN, the angle at which the knee occurs is not constant, even for similar types of terrain. For example, in HAGN, the knee occurred at angles between 0° and 25° for dry land of apparently the same type.

Here we are concerned with only two terrains, land and sea, and it is probable that these terrains are fairly constant in type, as the location of the sounder does not change, and as in the directions chosen the land or the sea extends to long ranges, without any conspicuous change in type.

For land, the angle at which the knee occurs is usually between 14^{o} and 12^{o}; in view of the closeness of these limits, the variation is likely to be due to experimental errors, and 13^{o} may be taken as the true and virtually invariant knee angle for the given terrain.

The constancy of this angle may be ascribed to the fact that in the present experiment, the terrain was the same for all measurements (apart from very small amounts of scattered rainfall, of the order of 10 points on some days) whereas in HAGN's work, the terrain types investigated were quite different samples which were only apparently similar.

Two possible doubts arise concerning the reality of the knee.

(a) It may be due to failure of the transmission path; as f_o falls, so that Δ_s approaches 0^{o}, P_R vanishes as virtually all rays penetrate the ionosphere. This might appear to be a knee if the calculations erroneously give values of Δ_s that are too large. But the discussion in Section 8.6 shows that Δ_s would not be in error by so much; a sudden decrease in P_R when Δ_s is over 10^{o} can only be due to G or γ.

(b) The terrain may not be uniform to long ranges. Perhaps at some range there is an abrupt change in the terrain, and γ becomes very small at long ranges (corresponding to low angles of elevation). But reference to a map of the region from Charleville to Alice Springs and beyond (LEWIS and CAMPBELL, 1951) shows that whereas there are large patches of sandy or rocky desert interspersed with "tall grass savana" and "tropical desert shrub", there is no range at which the terrain in the illuminated region changes abruptly; at every range, the azimuthal beamwidth of the antenna is wide enough to include a fair mixture of these types. As far as large features are concerned, the only one of note that corresponds in range to the knee angle is the Macdonnel Ranges west of Alice Springs, which would be more likely to cause an increase in γ than a decrease.

For sea, the knee angle is less constant than for land and in half the cases plotted the knee (if it existed) was at an angle below those at which data was available. When the knee was observed, it occurred at angles ranging from 14^{o} to 9^{o}. The presence of a knee at 14^{o} shows that in some cases at least the knee is a real effect, although at angles below 10^{o} it could possibly be due to errors as mentioned in 9.2 (a) above. But the problem is not to explain away a knee observed at low angles, but to explain its apparent absence in some cases. Probably the knee is always present, even if it exists below the angles investigated. The knee

angle can probably vary from about 13^{o} down to almost 0^{o}. This variation could be due to the state of the sea surface, which, unlike the land to the west of Brisbane, is subject to quite large variations. The number of cases considered is not large enough to show any correlation between knee angle and sea roughness. Dr D. F. Martyn (private conversation) is convinced that the sea state does have an effect. The effect known to exist at u.h.f. is discussed in Section 9.4.

The presence of the knee (especially when the knee angle is known) is an aid in distinguishing between different types of echoes such as $1E_s$ and 1F. In the west, owing to the knee, backscatter is negligible below 10^{o}. E_s at a height of 110 km therefore gives $1E_s$ echoes with a limiting range of about 1000 km. In fact, western $1E_s$ echoes observed do show a sharp cut-off at about this range. Incidentally, this observation gives support to the conclusion that the knee is not due to a change in ground type at Alice Springs, since for $1E_s$ echoes, the knee angle corresponds to a quite different value of D.

For echoes from the sea, the variation of the knee angle means that the maximum range of $1E_s$ cannot be as easily predicted, but observations show that $1E_s$ echoes do not usually extend beyond 1500 km, which corresponds to an elevation angle of about 6^{o}. In both east and west, range spreading may increase the maximum range of the echoes. E_s

echoes are discussed further in Chapter 10.

9.3 The shape of the γ —— Δ curve above the knee

The points shown on Figures 50 to 61 were collected on Fig. 62, the ones above the broken line being for sea, and those below for land. Points which definitely fell below the knee were omitted. Points on Fig. 59 were not used (morning data), nor on Figures 60 and 61, when ripples were known to be disturbing the ionosphere. Also omitted were some points which were due to P_R = 40 dB, the maximum value capable of being read from a swept-gain frame, and which could possibly have been due to even stronger signals.

The curves superimposed on the points of the figure represent the relation $\gamma \propto 1/\cos^2\varphi$ ($= 1/\sin^2\Delta$). For both eastern and western echoes, this fitted better than $1/\cos\varphi$ or $1/\cos^3\varphi$, although on individual days one of the latter sometimes fitted better. In any case, the results are consistent with the relationship given by KATZ and SPETNER (1958) (See Section 4.3). The curves for $\gamma \propto$ 1, $1/\cos\varphi$, $1/\cos^2\varphi$ and $1/\cos^3\varphi$ are illustrated in Fig. 58 as curves (a), (b), (c) and (d) respectively, and the best fit in this case is for $1/\cos^2\varphi$.

In Fig. 62, the scatter of the points about their respective means is not as bad as may appear, as the γ scale is merely relative. Owing to day-to-day changes in transmitter output, sea roughness, receiver gain and CRO bright-

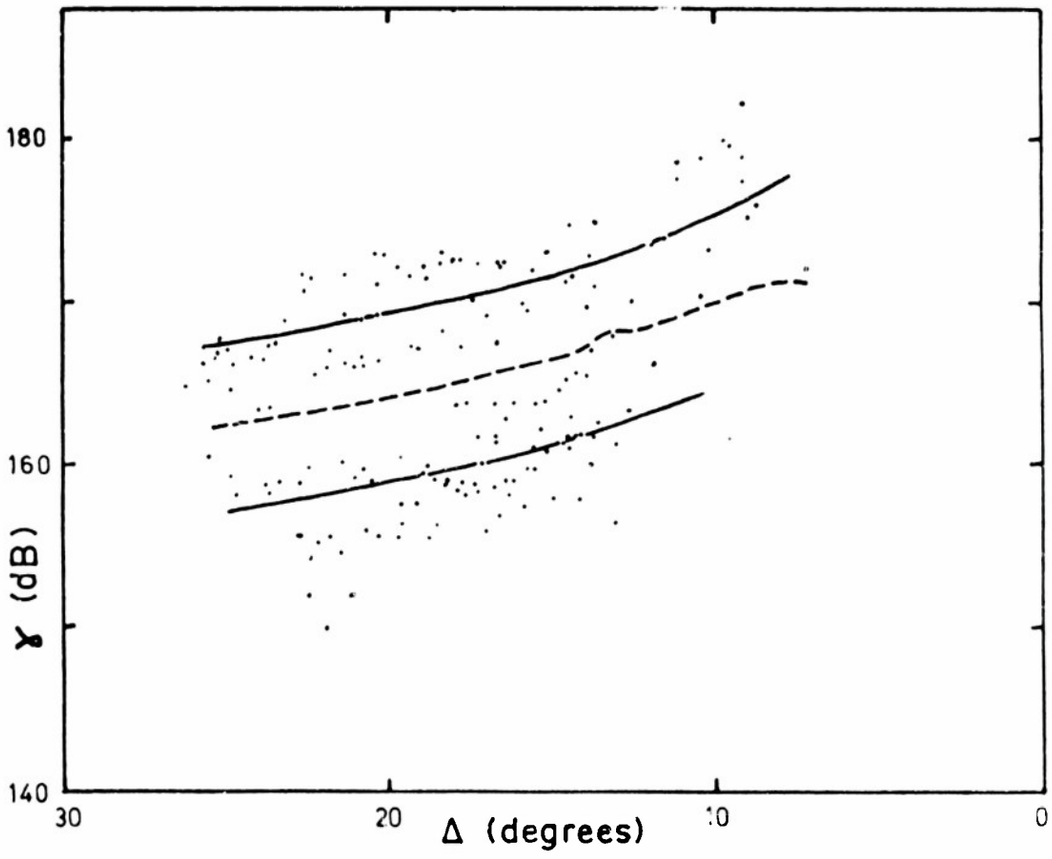

Fig. 62. Curves for $\gamma \propto 1/\cos^2\phi$ superimposed on data selected from Figures 50 to 61. Points above broken line are for sea, and those below are for land.

ness, the points for various days probably have slight zero errors differing from one day to the next, and therefore can legitimately be moved up or down the γ axis relative to one another for better agreement. This has been done in Fig.63, where the points shown in Fig. 62 have been replotted to give a better fit to the two curves. It should be emphasized that this procedure cannot be used to find γ (Δ) more accurately, but is merely used to illustrate what the scatter of points would be <u>if</u> $\gamma \propto 1/\cos^2 \varphi$. The scatter of points is 3 dB on either side of the curve, and this is about the accuracy to be expected if the probable errors are 2 dB in reading P_R and 1 dB in calculating P_C.

9.4 Discussion on the knee angle

The relation $\gamma \propto 1/\cos^2 \varphi$ which seems to fit the results between 25° and 10° is not true at all angles. KATZ and SPETNER (1958), who derived such a relation theoretically for low angles, derived other relations for higher angles. Further, at $\Delta = 0^\circ$, $1/\sin^2 \Delta$ becomes infinite, so there must be yet another relation for γ (Δ) as Δ approaches zero; the knee effect is evidence of this. The variable behaviour of the knee in the present work does not permit any conclusions to be drawn concerning γ (Δ) below the knee but in some cases γ decreases at the rate of at least 10 dB per degree.

KERR (1951, p. 508) reported a knee effect for sea return at u.h.f. He found a relationship such as $\sigma_0 \propto \Delta^3$

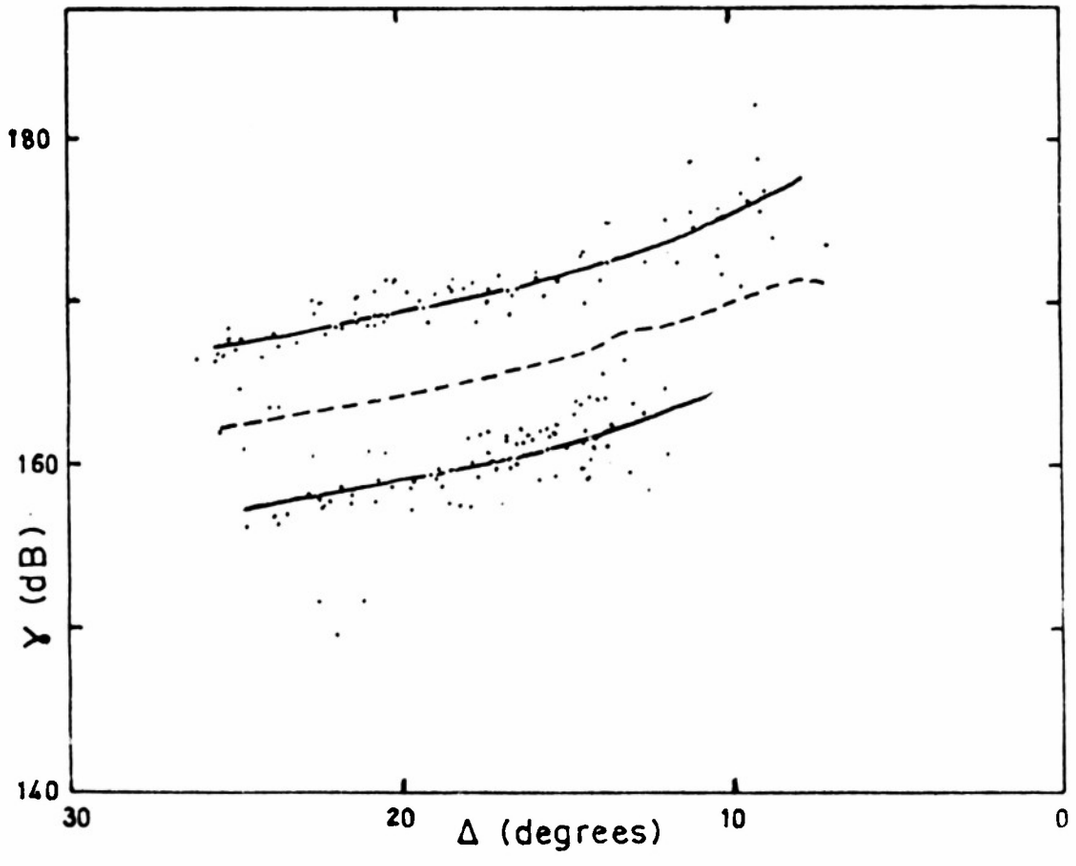

Fig. 63. Data from Fig. 62 normalized to fit the curves.

below the knee, which is the same as $\gamma \propto \Delta^2$ if Δ is small.

It may be possible to describe $\gamma(\Delta)$ both above and below the knee by a single function. For example, let

$$1/\gamma \propto A/\Delta^2 + B \sin^2 \Delta \ .$$

This reduces to $\gamma \propto 1/\sin^2 \Delta$ when Δ is large, and $\gamma \propto \Delta^2$ when Δ is small. At the knee angle, neither term is predominant, so let

$$A/\Delta^2 = B \sin^2 \Delta \quad \text{for } \Delta = \Delta_k,$$

that is, $A = B \Delta_k^4$ approximately (Δ_k in radians).

Then $$1/\gamma \propto \Delta_k^4/\Delta^2 + \sin^2 \Delta \ .$$

This function is plotted in Fig. 63a, for $\Delta_k^4 = 10^{-3}$ radians^4, that is, $\Delta_k = 10^\circ 12'$. The slopes above and below the knee agree with observations, but the observed sharpness of the knee is not reproduced. There appears to be a discontinuity associated with the knee. It seems that no single function will suffice to describe $\gamma(\Delta)$ at all angles.

HAGN (1962) suggested two possible causes for the knee effect — absorption of the signal by the ground, or scatter at an angle other than back. He suggested that for vertical polarization, absorption could be due to a Brewster angle effect.

In the present work, the echo is probably due to the vertical component of the outgoing wave at the point of scatter (See Section 5.4), so it is relevant to consider the Brewster angle. On land, the Brewster angle occurs at about $\Delta = 17^\circ$ for dry land or rocky soil, and on sea the pseudo-

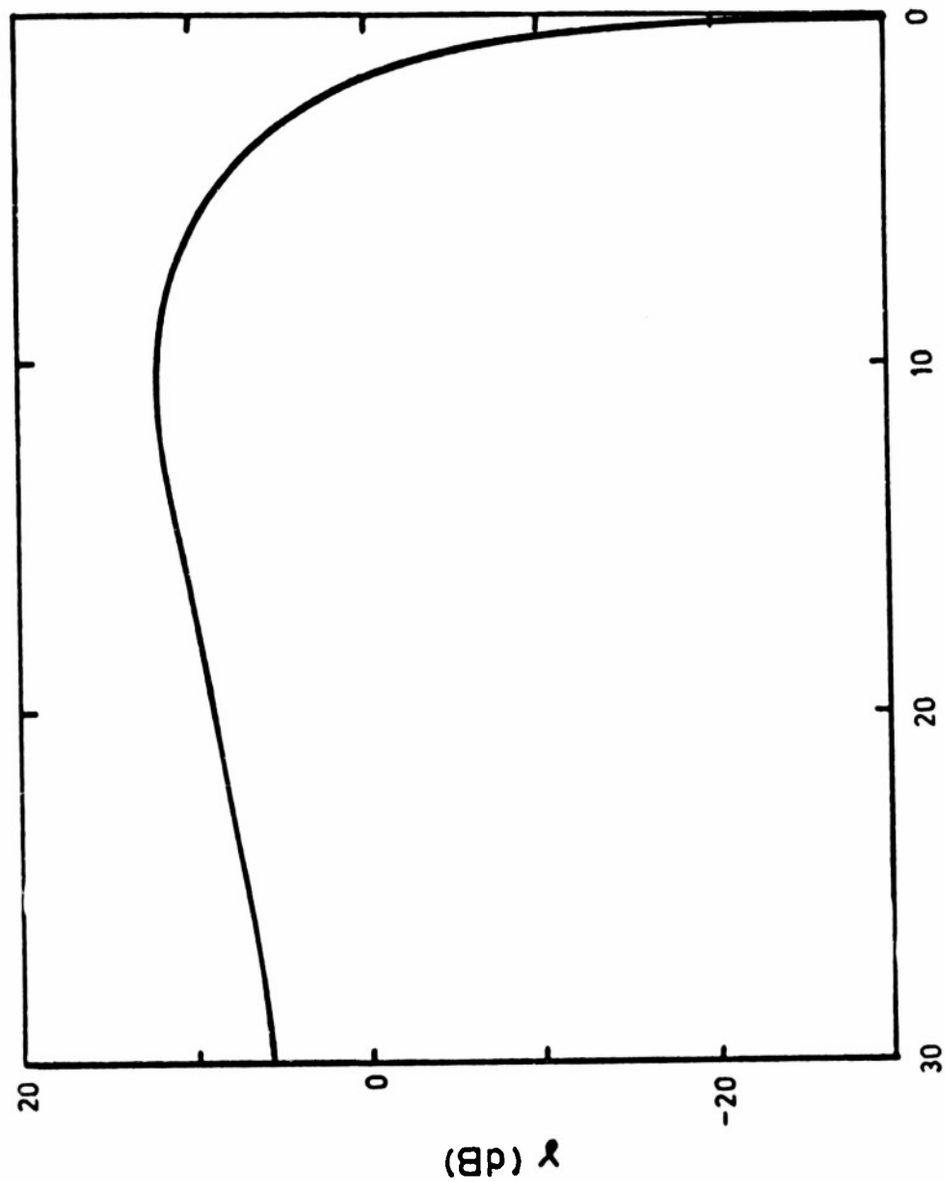

Fig. 63a. The function $1/(\Delta_k^4/\Delta^2 + \sin^2\Delta)$ for $\Delta_k = 10^\circ 12'$.

Brewster angle is about 0.5^{o}. At the Brewster angle, all the energy is absorbed, and the reflection coefficient is zero (or nearly zero in the case of the pseudo-Brewster angle). But this applies for smooth surfaces, whereas it is considered that the backscatter observed here is due to rough surfaces with specular type scatterers, so that echoes are received even when the value of Δ is nominally equal to the Brewster angle. This explains why the knee does not occur at the Brewster angle, and suggests that the knee is not primarily a Brewster angle effect, at least in the present investigation.

The second suggestion by HAGN (1962) which is preferred by him, is that the energy at low angles is practically all reflected in the forward direction, and so is not observed in the back direction. He suggests that there is some critical angle at which the surface looks very smooth. This approach is certainly better than the Brewster angle treatment. The behaviour of γ must depend on the surface roughness rather than on the dielectric nature of the surface. In fact, at u.h.f. there is some evidence that the knee angle depends on the roughness of the sea. Goldstein (KERR, 1951, pp. 505 ff), working at 10 cm wavelength, found that as the sea becomes more rough, the knee angle decreases from 4^{o} to 1^{o}. KATZIN (1957) suggested that if the knee angle $\Delta_k = \lambda/4H$, where H is the height of the scattering irregularities above a horizontal plane, then for Δ less

than Δ_k there will always be destructive interference between the direct field and that scattered by the sea surface. This is true even for vertically polarized waves (SHEARMAN, 1956b), which at low angles can exhibit phase reversal on reflection. A sudden reversal of phase could explain the discontinuity at the knee. In the present work, however, if wave heights are typically about 3m, which is the rms wave height expected for a wind of 30 knots (KATZ and SPETNER, 1960), the corresponding value of Δ_k would be about 90°, which does not agree with experiment. To make Δ_k less than 10°, we would need to assume a wave height of at least 30 m, which is very improbable. KATZIN's theory therefore fails to predict the knee angle at 16 Mc/s, and according to KATZ and SPETNER (1960) it also fails at u.h.f.

For centimetric radar, it has been found that Δ_k is proportional to λ (BECKMANN and SPIZZICHINO, 1963, pp. 414 and 417; KATZIN, 1957). This means that whereas at 10 cm, Δ_k is between 1° and 4°, at 18.5 m (16 Mc/s), Δ_k would be at least 190°, which does not agree with experiment. The proportionality therefore does not hold over the range of wavelengths considered, but it is nevertheless true that Δ_k is larger at h.f. than at u.h.f. for similar sea states.

It seems that no existing theory will suffice to describe the knee, although effects noted at u.h.f. seem to be qualitatively true even at 16 Mc/s. All that can be said with confidence is that the knee angle does vary according

to the roughness of the sea, and it seems to take higher values at h.f. than at u.h.f.

9.5 Dependence of γ on sea roughness

Although there was insufficient data to establish any correlation between Δ_k and the roughness of the sea, it was possible to consider the values of γ above the knee, say at 20^o, and compare these with sea states.

The Commonwealth Bureau of Meteorology at Brisbane was able to supply data on windspeeds at sea level at Norfolk Island and New Caledonia. These islands are at a range of about 1500 km from Brisbane, and in the present work sea backscatter was obtained chiefly from the area between these places. The windspeeds W were averaged to give a measure of the average sea roughness at the scattering area. At u.h.f. it has been found that γ is proportional to W or W^2 (BECKMANN and SPIZZICHINO, 1963, p. 413), so it is to be expected that γ will be some increasing function of W even at 16 Mc/s.

Before proceeding to a comparison of γ and W, we should note the difference between "sea" and "swell". Sea refers to waves which are still in the process of development, with sharp crests. Swell consists of waves propagating some distance from the region where they were generated, and these have rounded crests. Sea and swell normally exist simultaneously and may move in different directions.

Table 5 gives wave heights and percentage occurrences appropriate to an area 1500 km east of Brisbane, compiled from U.S.A.F. (1960, p.12-44). The corresponding windspeeds have been estimated from the percentage occurrences and from the fact that a wind of 30 knots generates waves about 10 feet high (KATZ and SPETNER, 1960).

TABLE 5

SEA STATES

State	height (ft)	occurrence (%)	windspeed (knots)
Low seas	1-3	40	0-10
Medium seas	3-8	50	10-20
High seas	over 8	10	over 20
Low swell	1-6	40	
Medium swell	6-12	40	
High swell	over 12	20	

As it is considered that the backscatter comes from the sharp wave crests of the sea, and not from the swell, the backscatter coefficient should correlate with the sea and hence with windspeed. On the other hand, the knee angle probably depends on the total wave height H (Section 9.4), which depends mainly on the swell; therefore the knee angle would not be expected to correlate with the windspeed.

Table 6 lists wind data at 1800 hours, Brisbane time, along with backscatter results from Figures 50 to 58.

TABLE 6

WINDSPEEDS AND BACKSCATTER RESULTS

Date	Windspeed (knots)			Backscatter Results	
	Norfolk Island	New Caledonia	Average	γ at 20° (dB)	Δ k (degrees)
20/3/63	10 E	10 E	10 (10)	171.2	13
21/3/63	15 N	20 E	17.5 (10)	168.9	13
22/3/63	5 NE	5 E	5 (4)	170.4	14
23/3/63	15 NE	15 E	15 (12.5)	170.4	8
24/3/63	10 NE	15 E	12.5 (11)	168.7	< 9
28/3/63	20 E	20 E	20 (20)	172	<10
5/4/63	5 W	10 SE	7.5 (5)	168.7	< 9
6/4/63	10 SW	10 SE	10 (5)	167	<10
7/4/63	10 SE	10 S	10 (3.5)	167.4	< 7

The average values in the table were calculated initially without regard to the direction of the winds. The bracketed figures in the table are the "effective" windspeeds in an east-west direction. These effective speeds were obtained by weighting the absolute windspeeds according to direction, and then averaging. The weights were based on information concerning the dependence of γ on the direction of the wind, given by MACDONALD (1956, quoted in BECKMANN and SPIZZICHINO, 1963, p. 413). If u, d and c denote upwind, downwind and crosswind values, then for ver-

tical polarization MACDONALD found that $\gamma_u > \gamma_d > \gamma_c$, and for horizontal polarization $\gamma_u > \gamma_c > \gamma_d$, the differences involved in the inequalities being 0 to 5 dB. It is assumed that in the present project the polarization is effectively vertical and that $\gamma_d = \frac{1}{2}\ \gamma_u$ and $\gamma_c = 0$. Then if γ is approximately proportional to W, W can be weighted thus:

$W = W_u$ or $\frac{1}{2}\ W_d$ or $0.W_c$. For directions oblique to the east-west direction, projected values are used.

Fig. 64 is a plot of relative backscatter coefficient against windspeed regardless of wind direction. Allowing for errors of $\pm$ 3 dB in γ (Section 9.3), we find that while a smooth curve can be drawn through the error bars, its slope could be positive, zero or negative.

If, however, the effective east-west windspeeds are used, as in Fig. 65, there may be some correlation. Even if the error bars are reduced to $\pm$ 2 dB, it is still possible to draw a smooth curve through them. This curve has a definite positive gradient, averaging 0.2 dB per knot. The better result obtained for the effective windspeeds justifies weighting them according to wind direction, and not only supports the hypothesis that the scatter arises from the sea wave crests, but also suggests that scatter is most effective on the sharper down-wind sides of the crests.

If, then, the backscatter coefficient depends on the sea rather than on the swell, γ should approach zero as W

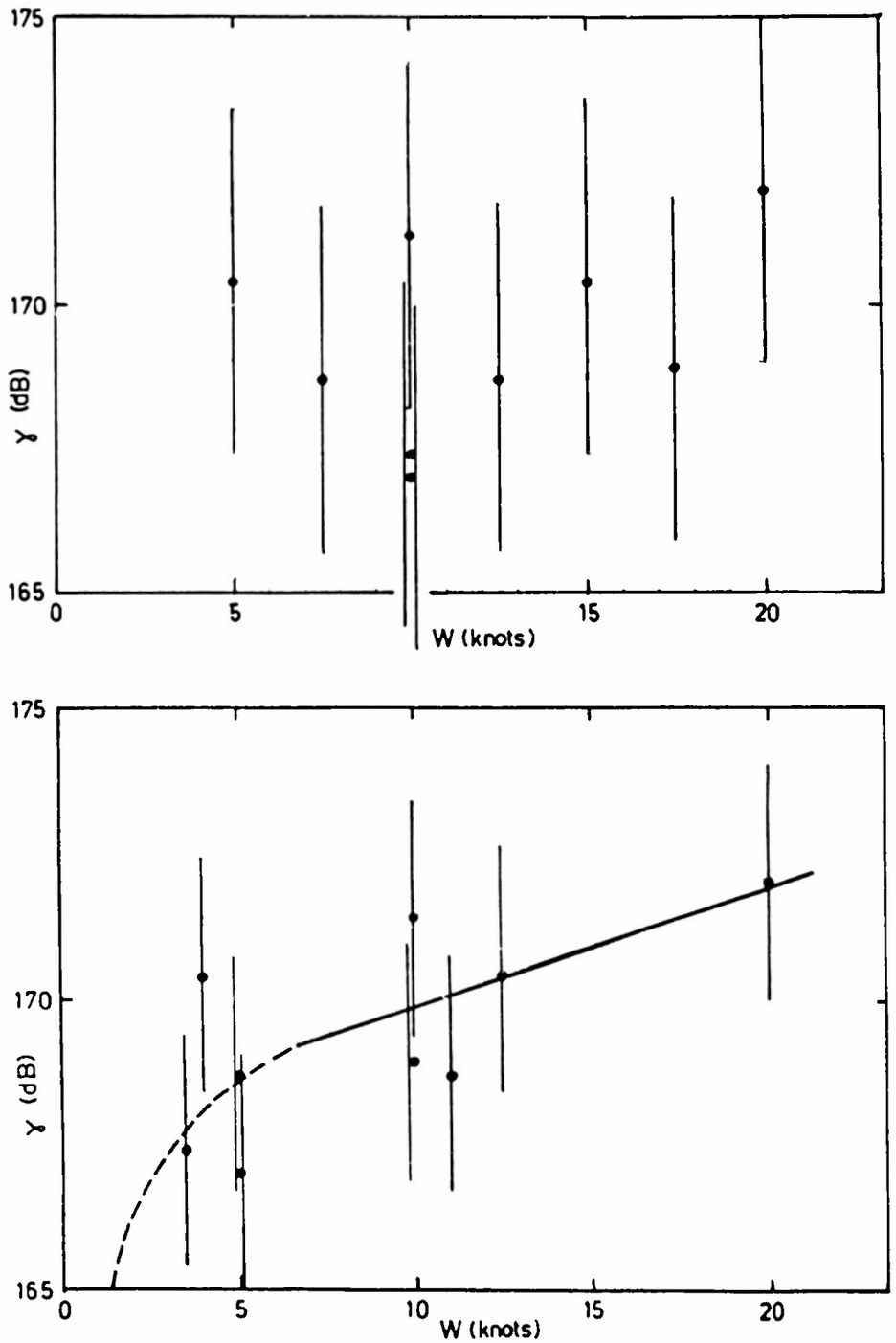

Figures 64 and 65. Variation of backscatter coefficient with windspeed (weighted according to direction in Fig. 65).

approaches zero. On Fig. 65, γ in dB should approach $-\infty$, and the curve as drawn is capable of such an interpretation. Probably for effective windspeeds below 3 knots the backscatter coefficient changes rapidly with sea roughness, but above 6 knots is not much influenced by the state of the sea. A sea sufficiently calm to suppress all backscatter would be very rare.

Experiments at n.h.f. by DAVIES and MACFARLANE (1946, reported by BECKMANN and SPIZZICHINO, 1963, p. 412) are in general agreement with this hypothesis. They found that γ increased rapidly with wave height until it reached a saturation value, when it remained constant. At 16 Mc/s, it seems that saturation is virtually complete for W = 10 knots, that is, for wave heights of about 3 feet.

9.6 Summary

There are three important results, namely, that the sea scatter is stronger than land scatter by about 10 dB; that at some angle (13° for land and lower for sea) there is a knee effect below which backscatter is much reduced; and that above the knee the curves for both sea and land are consistent with a theory of quasi-specular scatter from upright objects such as trees and wave crests.

The knee is probably due to destructive interference between the direct ray and the ground-reflected ray at the point of scatter, due to phase reversal of the reflected

ray at low angles. The knee angle may therefore depend on the height of the scatterers above the reflecting plane, and in the case of sea scatter this height would depend on the swell rather than on the sea.

In contrast, the backscatter coefficient at a given angle above the knee should depend on the wave crests, that is, on the sea rather than the swell. The results are not inconsistent with a correlation between the backscatter coefficient and the windspeed.

10. OCCURRENCE OF SPORADIC-E

10.1 Comparison of E_s occurrences over land and sea

Backscatter sounding has been used to investigate the geographical distribution and movement of E_s clouds, and has yielded good results concerning the sizes and shapes of E_s clouds and their direction and speed of travel. One result of this investigation, however, is hard to explain: the apparent predominance of E_s over the sea compared to its occurrence over the land. The evidence for this apparent behaviour has been published by EGAN and PETERSON (1961, 1962). Centroids of $1E_s$ backscatter echo patches were plotted on maps, and in a given period the occurrence over the sea was significantly greater than over the land. This was true whether the data was taken at Stanford, U.S.A., or at Camden, N.S.W.; the $1E_s$ echoes were mainly in the west at Stanford and in the east at Camden, but in each case over the sea. The transmitted frequencies were 12, 18 and 30 Mc/s.

The results could be due to a difference in the occurrence of E_s, or to a difference in the backscatter coefficient. EGAN and PETERSON rejected the second explanation by referring to the results of NIELSON et al. (1960), which

indicated that the coefficients for sea and land were not markedly different, being in fact equal at 17^{o}, a typical elevation angle for E_s-propagated rays.

The present work, which shows that the backscatter coefficient for land is 10 dB less than for sea, does not support NIELSON et al. It now seems that the apparent difference in E_s occurrence may be ascribed entirely to the difference between the backscatter coefficients for sea and land. $1E_s$ echoes from the land are suppressed by two factors - the lower backscatter coefficient above the knee in the γ (Δ) curve, and the existence of the knee at the comparatively high elevation of 13^{o}; many E_s clouds have a low critical frequency, and will propagate 16 Mc/s waves only below 13^{o}.

The main features of this conclusion were published (STEELE, 1964) but it should be noted that in the figure the curves for Brisbane were obtained by a method less accurate than that reported in Chapter 8, and the sharpness of the knee in each curve has been lost, owing to excessive smoothing. It should also be remarked that the Stanford curves with which the Brisbane ones were compared are now obsolete, having been superseded by those of HAGN (1962), who in any case prefers not to compare sea and land scatter below 20^{o}.

The conclusion that there is no difference between the occurrences of E_s over land and sea agrees with the ob-

servations of HEISLER and WHITEHEAD (1964). They used data from vertical incidence sounders in many parts of the world, including both continental- and island-based stations. They found no predominance of E_s occurrence over the sea.

The conclusion arrived at here disagrees in part with the interpretation of DOMINICI (1962, 1963), who found that E_s observed at Rome by ground backscatter was most prominent in the north-west and least in the north-east. The echoes north-west of Rome are scattered at the Atlantic Ocean, and the north-east echoes on the land in European Russia, as illustrated in RANZI and DOMINICI (1959). DOMINICI was of the opinion that there was a real difference in E_s occurrence, although the observations were influenced to a greater or lesser extent by variations in the backscatter coefficient and variations in the antenna vertical pattern due to the topography at the antenna site. In the present work, the two last mentioned influences are not in doubt, and the backscatter coefficient is entirely sufficient to explain the difference.

The distribution of $1E_s$ echoes around Brisbane, scaled from range——azimuth records, was plotted in a similar way to the Stanford and Camden results given by EGAN and PETERSON. The Brisbane results are shown in Figures 66 to 68. Range circles are at 1000 km and 2000 km ground range. The points represent centroids of $1E_s$ echo patches, and their oblique range plotted on the figures differs from the

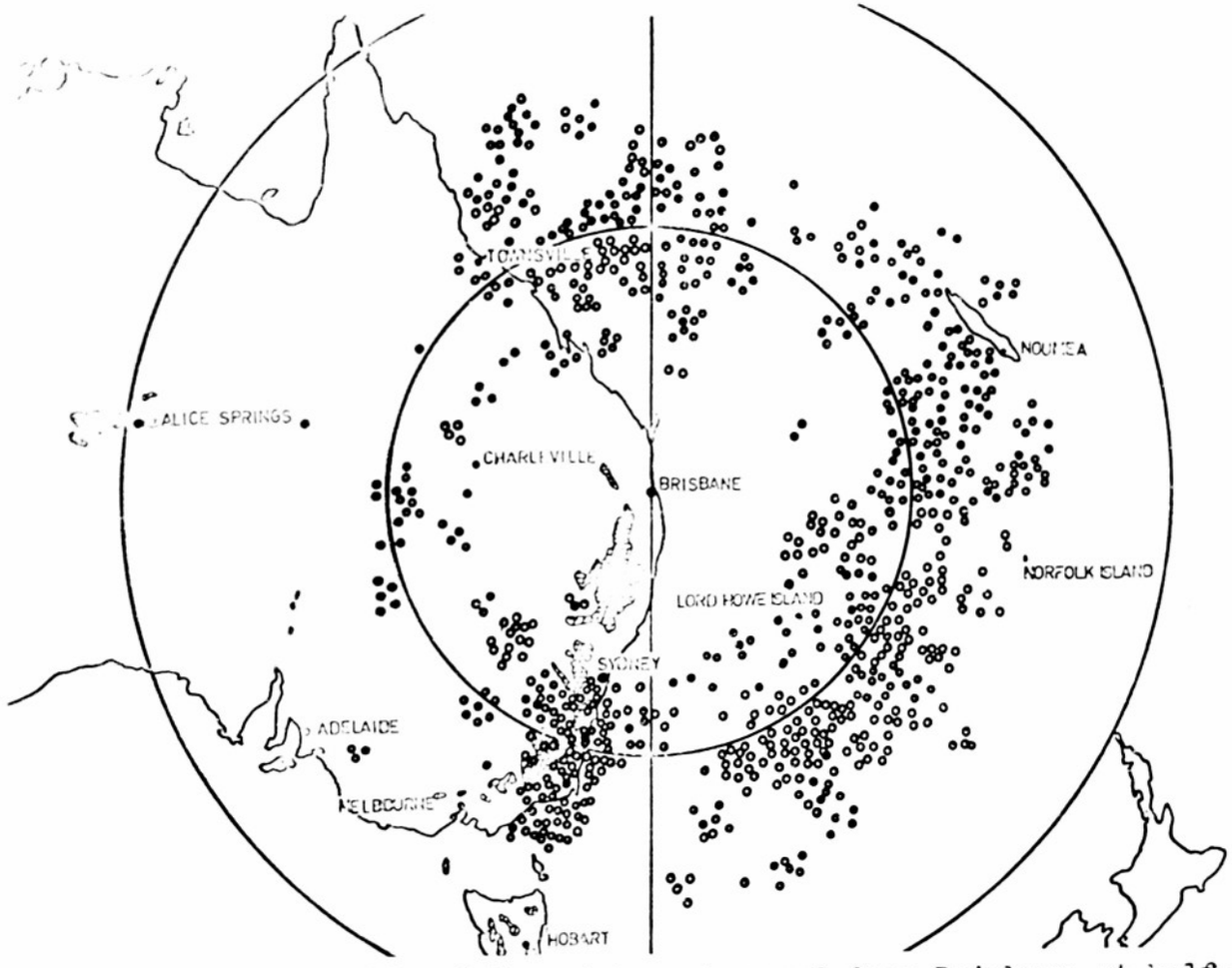

Fig. 66. Centroids of E_s patches observed from Brisbane at half-hourly intervals on 38 days between December, 1962, and March, 1963, and between October and December, 1963. Range circles are for 1000 and 2000 km.

Fig. 67. Centroids of Es patches observed from Brisbane at half-hourly intervals on 23 days during May, 1960.

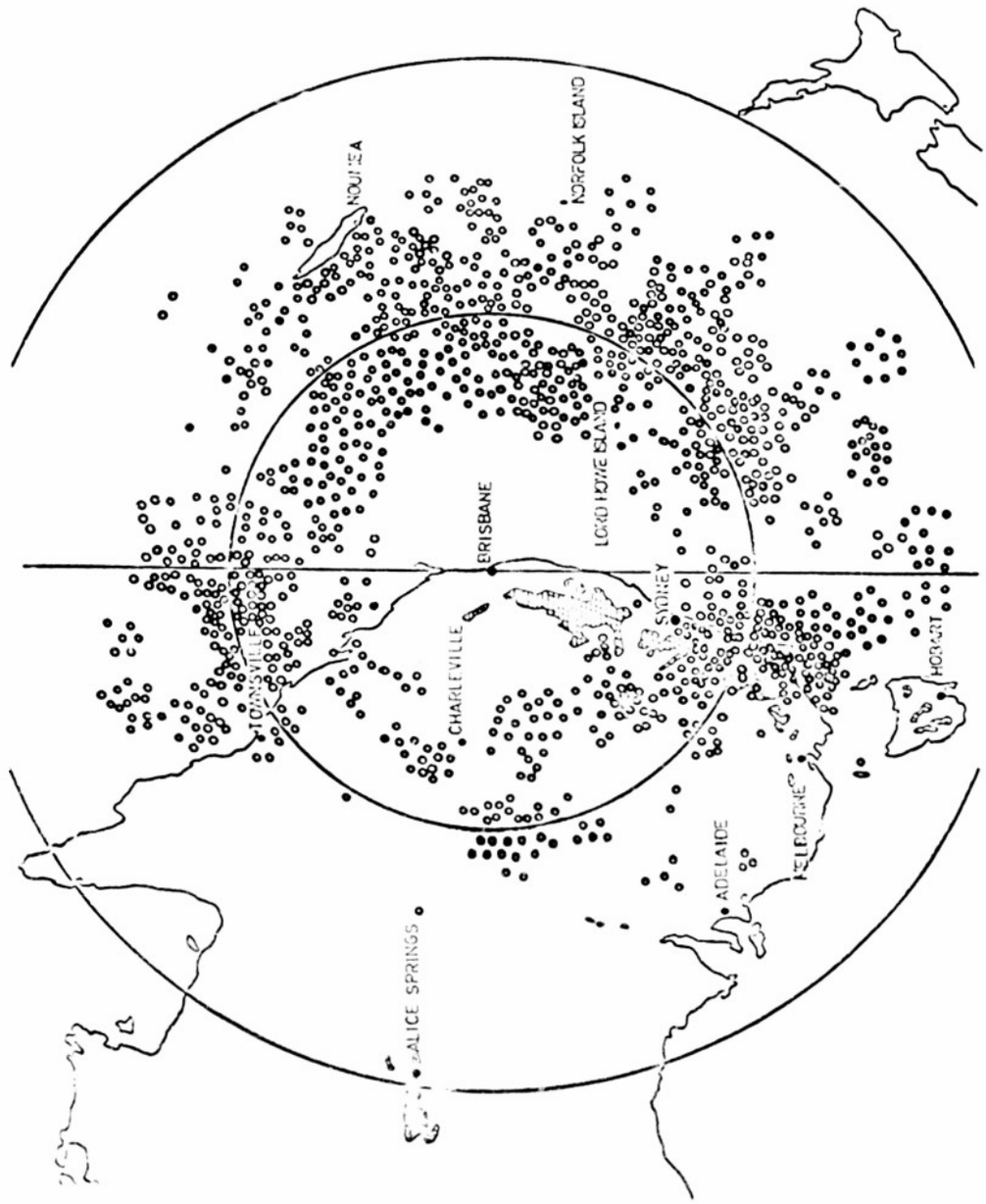

Fig. 68. Data of Figures 66 and 67 combined.

ground range by less than 60 km, provided the oblique range is greater than 500 km, assuming E_s at a height of 110 km. The transition from sea to land conditions is quite clear, especially along the Queensland coast. In Fig. 66 the large number of centroids of $1E_s$ patches near the New South Wales coast may be due to a high backscatter coefficient on the Australian Alps, but more probably to a bias towards this direction in scaling data from films, as the azimuth mark on the films was at 185° mag. az., and many centroids which were at $185^{\circ} \pm 10^{\circ}$ were ascribed to 185°. Also, there was probably a genuine predominance of E_s in the south, which often appeared additionally on the records as direct backscatter from field-aligned E_s at half the range of the E echo. For the data of Fig. 67, the azimuth mark was at 117°. Fig. 68 combines the results of Figures 66 and 67.

The main points of difference between the results for sea and land are that the land echoes are less frequent and extend to shorter maximum ranges than the sea echoes. Both these effects are consistent with what is now known about the backscatter coefficient.

10.2 Comparison of 1F echo strengths on range——azimuth records

The difference between sea and land scatter which is apparent in $1E_s$ records is just as pronounced for 1F echoes. Fig. 69 is a typical range——azimuth record with range marks every 250 km. Superimposed on this record is a range——

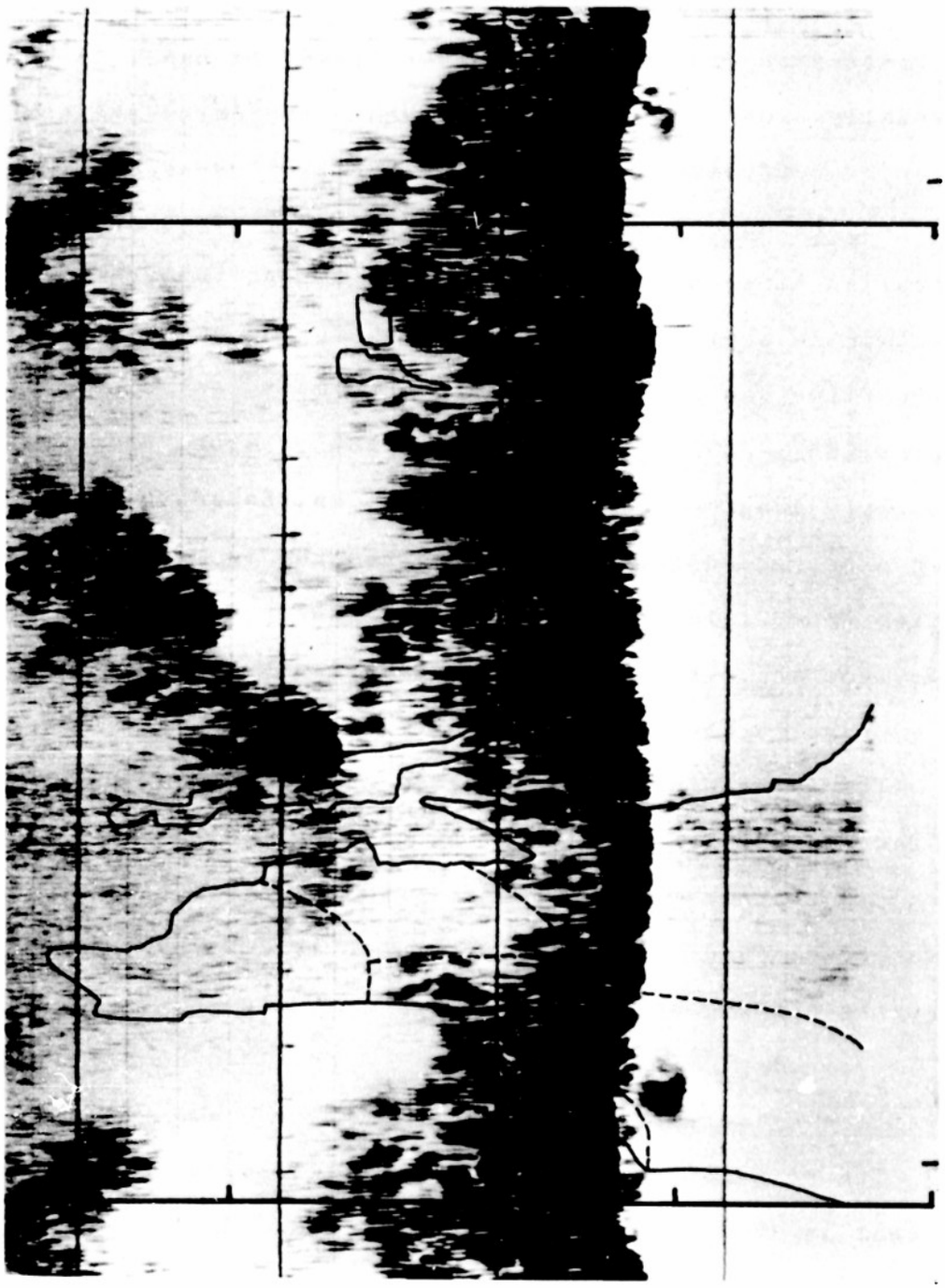

Fig. 69. Range-azimuth record with map superimposed.

azimuth map of Australia drawn to the same scale. This map is shown in greater detail in Fig. 70, where the azimuth scale is relative to geographic north at Brisbane. A short line drawn on the bottom of the record indicates the position of the azimuth mark (185° mag. az.). The record shows the oblique range, but the map is drawn in terms of ground range; this leads to a discrepancy of about 200 km, depending on the range. A rough correction has been made by moving the map 200 km up the page.

It may be seen that there is a thinning out of F region-propagated ground scatter coinciding with scatter from the Australian continent. The regular fading characteristic of sea echoes and the random fading of land echoes are also evident. Even though the antenna pattern varies slightly from east to west, there is such a strong correlation of backscatter strength with the sea that antenna differences are negligible.

This relative weakness of 1F echoes from the land was observed on range——azimuth records at Rome by RANZI and DOMINICI (1959), though with less azimuthal resolution, and with some misgivings about the vertical pattern of the antenna used (DOMINICI, 1962, 1963).

These results strengthen the case against any predominance of E_s over the sea, as the same reasoning which led to that theory would lead to a predominance of F region ionization over the sea, which is known to be untrue.

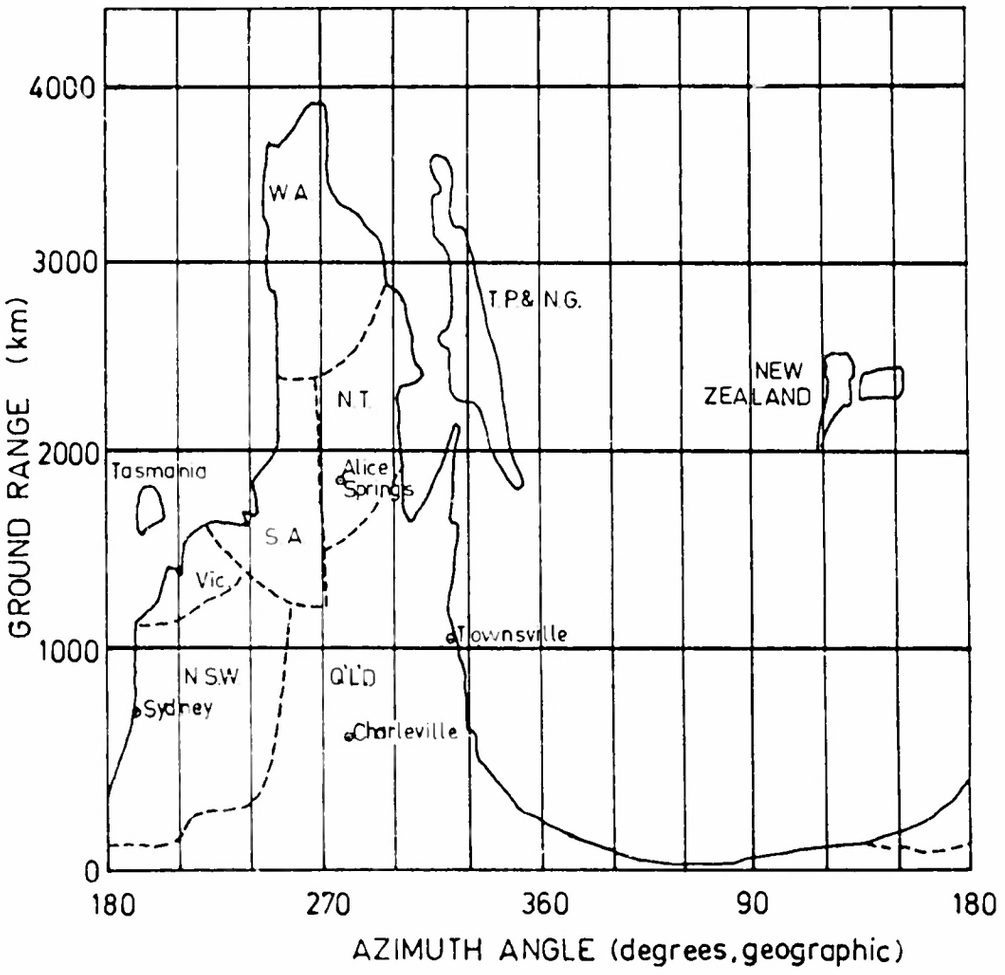

Fig. 70. Range—azimuth map used in Fig. 69.

10.3 Occurrence of E_s over mountains

EGAN and PETERSON (1961, 1962) also drew attention to the apparent predominance of E_s over mountainous regions. They admitted that this could well be due to a higher backscatter coefficient. Mountain ranges do not in general give rise to a stronger echo, unless they lie broadside on to the direction of propagation (See Section 2.2). In the present investigation, no such echoes are possible, as practically all mountain ranges are aligned radially with respect to Brisbane. The effect of the Great Dividing Range could not be investigated, as it is close to the coastlines and it is not possible to eliminate a certain amount of sea scatter from the results; by its strength, sea scatter would tend to obscure any effect due to the mountains. This was also true of New Zealand, where the high ranges of South Island might constitute a coherent echoing surface; beam and pulse width were not small enough to resolve the island.

In general, mountains may be expected to enhance the backscatter coefficient in two ways: by an average tilt which might effectively decrease the knee angle, and by an increase in the number of scatterers per unit area. The first way seems likely only at the near side of a range of mountains, preferably broadside-on. The second seems unlikely, as the main scatterers are believed to be objects such as trees, which are not necessarily more numerous on

mountains.

Insofar as it is possible to come to any conclusion about this, it may be noted that in Figures 66 to 68 the relative occurrence of $1E_s$ echoes seems to be associated with the coastlines and not with the mountains. If the mountains do increase the backscatter coefficient, the effect is small.

10.4 The "south-east patch"

In early work on field-aligned irregularities observed by backscatter, attention was drawn to an apparent predominance of ionization south-east from Brisbane, manifesting itself as a patch echo on range——azimuth records. Figures 66 to 68 were prepared partly to investigate the reality of this patch, and the result was negative. All patches which were not obviously 1F echoes or direct backscatter from field-aligned E_s were plotted, and no predominance of patches appeared in the south-east. There was, however, a larger number in the south-east than in the south-west, and as has been shown, this can be ascribed to the relative backscatter coefficients of the ground. It is now considered that the "south-east patch" is really the normal E_s occurrence, and that it only achieves prominence when attention is concentrated on southerly directions, as is done when scaling echoes from field-aligned irregularities. When the original records which suggested the patch were examined, there was nothing to suggest that this was

anything other than a normal $1E_s$ echo.

10.5 Summary

Although it has been thought that E_s occurs predominantly over the sea, the present work shows that this belief was largely unfounded. Backscatter records suggest an apparent predominance which may now be accounted for as due to the difference in the backscatter coefficient. A similar apparent predominance is observed in the case of 1F echoes.

There did not appear to be any predominance of E_s over mountainous regions, but resolution was insufficient for any certainty about this. From what is now believed about the behaviour of the backscatter coefficient, it may be predicted that the knee in the backscatter curve would be lower, and therefore echoes might be possible from longer ranges.

11. TRANSEQUATORIAL PROPAGATION

11.1 Introduction

Long-range one-hop propagation to the north of Brisbane has been described by THOMAS (1961, 1962a, 1962b, 1964) and by THOMAS and McINNES (1962, 1964). Backscatter paths between the directions 290° Mag. and 70° Mag. are considered. The typical transequatorial echo appears in the late afternoon towards the north-east, first as a weak echo at an azimuth of 60° to 70°, and at a range of 9000 to 10,000 km. It gradually extends towards the north at closer ranges, appearing as the right arm of a U on the range——azimuth plot. It may remain in position for 3 or 4 hours, lying roughly along the line of magnetic latitude 20° north, as shown in Fig. 71.

The predominance of the transequatorial echo in the north-east is stressed. Peak occurrence is at 10° to 30°, and very little of the echo is detected further west than about 320° (THOMAS, 1962a).

11.2 Interpretation

The reason for this east-west asymmetry is partly given by THOMAS (1962b). Analysis of ionospheric height contours shows that an upward bulge favourable to long range

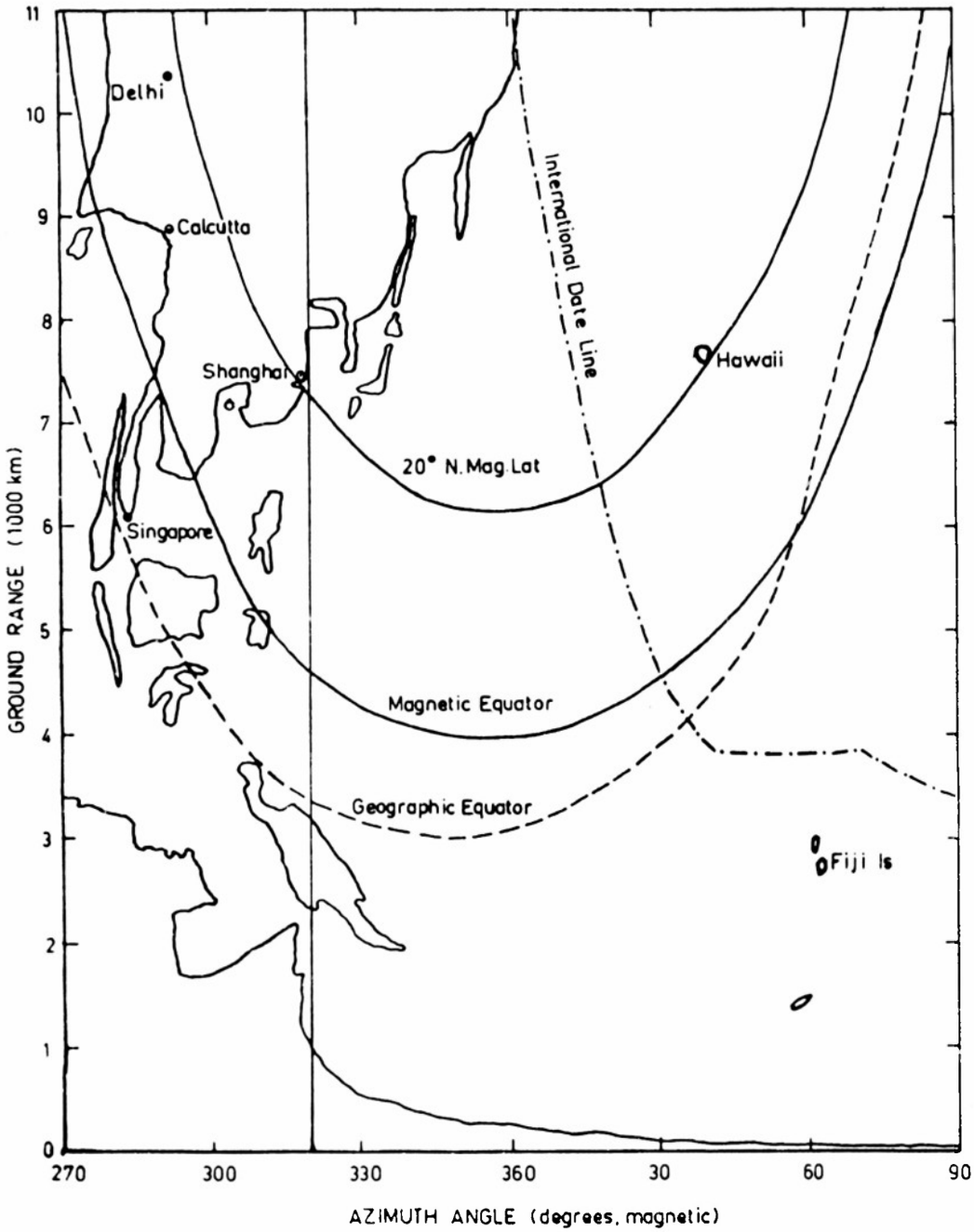

Fig. 71. Range—azimuth map showing the relation of transequatorial echo occurrence at 20° north magnetic latitude to the continent of Asia.

propagation occurs progressively between 70° and 310°, but not at 290°. According to THOMAS et al. (1962), the bulge finally disappeared at long ranges at about 300°. But this does not entirely explain the decrease in occurrence of transequatorial echoes at 320°.

It might be suggested that the layer tilts which permit transequatorial propagation have an east-west asymmetry that militates against propagation to the north-west at about 310°, even though the bulge is present. This suggestion seems unlikely, as in the late afternoon and evening very strong interference appears on the records at 310°. This has sometimes been identified as the Overseas Telecommunications Commission service, and the direction of arrival indicates that the signals come probably from London, or at least from Hongkong or Manila. This shows that long distance propagation from the north-west is particularly good by at least one mode, which must cross the equator in the tilted region of the ionosphere to the north-west of Brisbane. A tilted region which allows transequatorial propagation to the north-east and north, and later allows good propagation of some kind to the north-west, would surely be expected to allow transequatorial propagation to the north-west.

It might also be suggested that D region absorption is high near the scattering region in the north-west. But geographical symmetry suggests that this absorption would

be just as high in the vicinity of the sounder at the time of onset of transequatorial propagation to the north-east, so that the arms of the U should nevertheless be equal.

It is now suggested that the rarity of transequatorial echoes at about 310° is due, wholly or in part, to the low backscatter coefficient of the land to the north-west. Examination of Fig. 71 shows that at the range at which transequatorial echoes terminate (7000 km, 320° Mag.) lies the coast of China, and further west the line of 20° north magnetic latitude remains on the land, from Shanghai, across China and Tibet to Delhi at a range of 10,000 km from Brisbane. Even if the sea covered this region, we would expect transequatorial echoes to be weak, by comparison with equidistant echoes to the north-east. The 10 dB difference between land and sea backscatter is therefore sufficient to suppress practically all the transequatorial echo in the north-west. Even more significant, however, is the fact that the more important of the transequatorial paths occur at low elevation angles (THOMAS and McINNES, 1962, 1964), especially below 8°. This means that the most powerful transequatorial signals will arrive at the ground at an angle below the knee angle for land, and will not be returned to the sounder.

In further support of this explanation, it is observed that in the north-west not only are transequatorial echoes scarce, but also 1F, 2F and 3F (when they occur to the

north) (THOMAS, 1962). If the lack of echoes in the north-west were due to the shape of the equatorial bulge alone, this would not explain the shortage of 1F echoes, which occur at ranges short of the bulge. The 1F echoes are markedly scarce west of about 320° Mag., which coincides with the Queensland coastline. It seems that the geographical asymmetry in the occurrence of transequatorial echoes not only accompanies an asymmetry in 1F occurrence, but has the same explanation.

11.3 Summary

The comparative lack of one-hop transequatorial echoes to the north-west of Brisbane may be ascribed, wholly or in part, to the fact that the north-west echoes would be scattered on the land between Shanghai and New Delhi, and therefore would be much weaker than those returned from the sea to the north and north-east.

12. THE PROSPECTS OF OBTAINING DISTANT IONOSPHERIC DATA FROM BACKSCATTER SOUNDINGS

12.1 Historical background

The usefulness of backscatter sounding to find the maximum usable frequency for a given communication path (or conversely, the skip distance obtaining on a given frequency) was foreseen even before the backscattering range was definitely identified with the ground (SMITH, 1945; BENNER, 1949). Later, the backscatter P.P.I. display gave promise of a simple "communication zone indicator" (de BETTENCOURT, 1952) to give instantaneous information on possible communication zones and modes of transmission.

PETERSON (1951) and WILKINS and SHEARMAN (1957) pointed out the need for great care in deducing D_s from p'_{min}. In particular, the accuracy of the determination depends on the correct identification of modes (1F or $1E_s$) and the effect of off-beam echoes on the observed p'_{min}. With the antennas and techniques of the present project these problems are minimized, but they would be rather serious if inexpensive equipment were used. In SHEARMAN (1961, discussion) it was mentioned by P.A.C. Morris that backscatter sounding was successfully used to find the fade-out time of fixed-

frequency transmissions between Singapore and Hongkong, by pulsing the spare sideband of a normal multiplex telegraphic circuit. However, backscatter sounding has not been widely adopted as an operational tool for commercial services.

Even more ambitious is the proposal to obtain ionospheric parameters such as f_o, h_o and y_m from backscatter sounding. This would be very desirable, as routine vertical incidence sounding is possible over less than a quarter of the earth's surface. Oblique sounding could possibly be used to extend our measurements of the ionosphere into isolated regions.

SHEARMAN (1956b) pointed out that measurements of p'min do not give unique values of layer height and critical frequency. To supplement the p'_{min} observations, therefore, EGAN (1960) and SHEARMAN (1961) recorded echo pulse shapes (A-scan) and compared them with calculated pulse shapes. SHEARMAN calculated the echo pulse shapes using values of h_o, f_o and y_m given in ionospheric prediction maps, and correcting these values so that they agreed with actual vertical incidence measurements. Although he neglected ionospheric focusing, D layer absorption, magneto-ionic splitting and variations in the backscatter coefficient, he found good agreement with observations.

EGAN (1960) neglected splitting and variations in the backscatter coefficient, and assumed that h_o and y_m were the

same at the control point as measured above the backscatter sounder. He then calculated the echo shapes and ranges for various values of f_o, and selected the one which agreed best in range and shape with that observed by backscatter. The value of f_o obtained in this way agreed well with that deduced by interpolating vertical incidence data.

12.2 Comments on previous work

(a) For reasons given in earlier chapters of the present work, the calculation of the complete echo shape can only be done accurately by taking into account all known factors, including antenna, ionospheric, geomagnetic and ground effects. While this would be theoretically possible, the amount of data required would be prohibitive except in specially selected cases. The measure of success obtained by EGAN (1960) and SHEARMAN (1961) is thought to be largely fortuitous.

(b) Even if the calculation could be done accurately, it would still not be possible to deduce unique values of f_o, h_o and y_m. An accurate knowledge of p'_{min} could allow the deduction of one of these parameters provided the other two were known. Figures 35 to 40 could be used for this. The shape of the echo pulse might allow the deduction of two parameters if the third were known, but the shape is not very sensitive to changes in these parameters, so the results would be rather inaccurate.

12.3 Future possibilities

While the calculation of echo pulse shapes holds little promise for the deduction of ionospheric parameters, the measurement of angles of arrival of backscatter echoes at the receiver should make possible the deduction of two parameters if the third is known. Calculated values of Δ_s, or of Δ corresponding to the p'_{min} ray, could be marked along the curves of Figures 35 to 40. Then, for example, given h_o, we could use the observed values of p'_{min} and Δ_s to read off unique values of f_o (or f_E) and y_m.

Δ_s could be measured by strobing the echo pulse, and measuring the angle of arrival of the skip ray; the component of the echo pulse due to the skip ray is concentrated around the highly-focused region just beyond p'_{min}, but other angles will also contribute to this section of the echo. The angle of arrival of the p'_{min} ray might be more useful; it could be found by selecting the leading edge of the echo pulse and measuring its angle of arrival. Such a sample would be easier to isolate by strobing and would contain a narrower spread of angles. Unfortunately the power contained in this part of the echo is relatively weak.

The accuracy of this method may be estimated by considering typical data. Suppose $p'_{min} = 1500 \pm 20$ km and Δ for the p'_{min} ray $= 18^o \pm 1^o$. Then if we are given $h_o =$ 200 km, the values of f_o and y_m may be read from Fig. 72. The shaded area on the figure shows the limits of probable

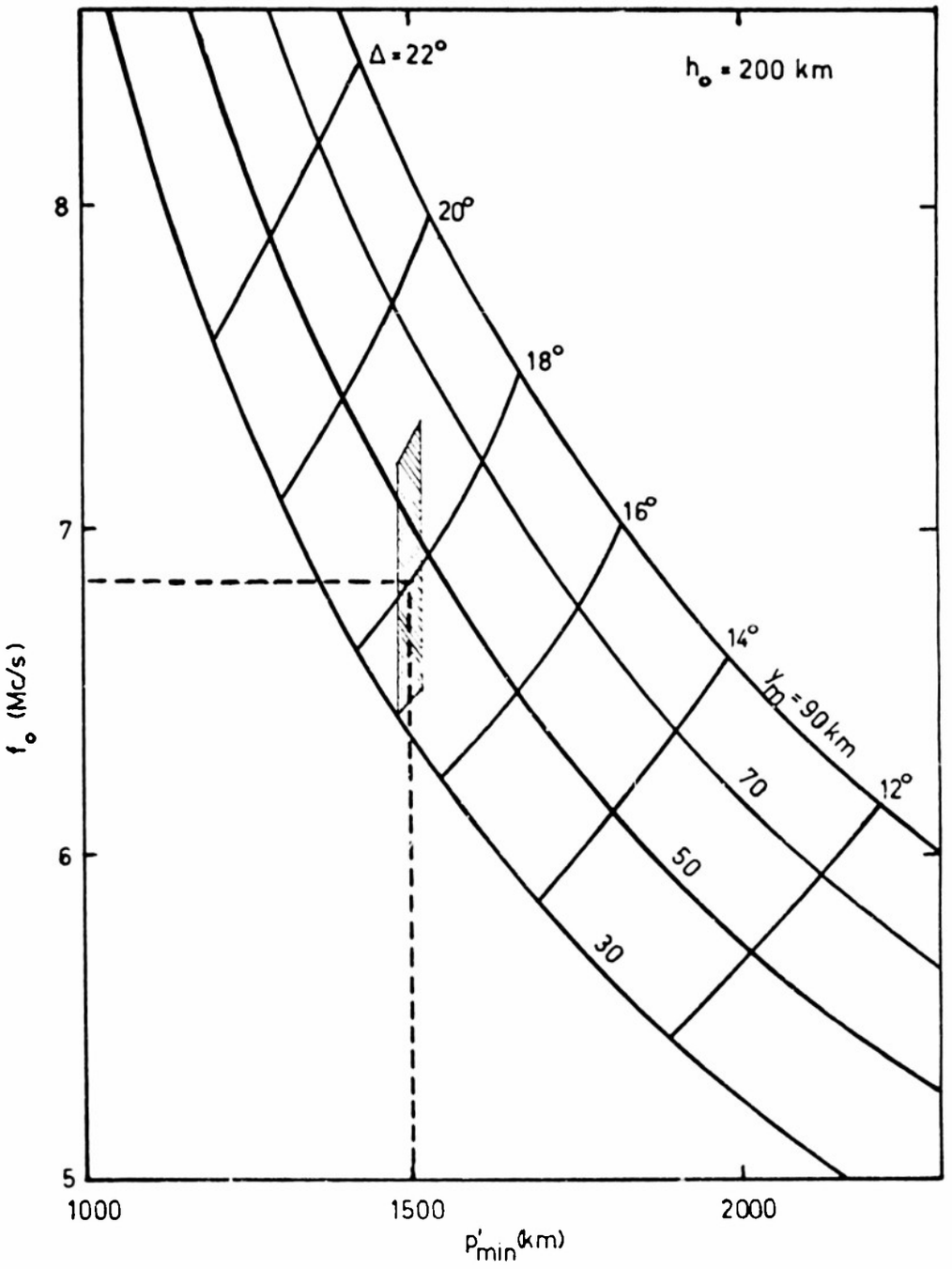

Fig. 72. Part of Fig. 37 with additional curves parametric in Δ appropriate to the minimum path-length ray, illustrating the deduction of f_o and y_m.

error in the data, and hence the limits of error of the result. We have, $f_o = 6.84 \pm 0.4$ Mc/s and $y_m = 45 \pm 15$ km.

If y_m were known, a similar method would permit the deduction of f_o and h_o. The error to be expected in h_o would be

$$\delta h_o = \frac{\delta y_m}{dy_m/dh_o} \text{ , for constant } f_o \text{ and } p'_{min}.$$

From Section 8.3 (b) and Fig. 41 it is seen that dy_m/dh_o typically equals -0.75, so $\delta h_o = \mp 20$ km.

More generally, if $\delta\Delta$ is the error in Δ, in degrees,

$\delta f_o = \pm 0.4 \ \delta\Delta$ Mc/s,

$\delta y_m = \pm 15 \ \delta\Delta$ km (given h_o),

$\delta h_o = \mp 20 \ \sigma\Delta$ km (given y_m).

Much depends on the accuracy with which Δ can be measured.

For sporadic-E, which may be assumed to exist in a thin layer, we can take $y_m = 0$. If the rays penetrate the layer at high angles, p'_{min} and Δ_s could give unique values of h_o and f_o, at the point of penetration. If the rays do not penetrate the cloud, as when the cloud is at a long range from the sounder and the rays meet its nearest edge at a small grazing angle, p'_{min} will then be a measure of the range of the cloud, and not of its critical frequency.

Fig. 73 is a set of curves parametric in h_o, with $y_m = 0$, for use with Sporadic-E data. For example, suppose

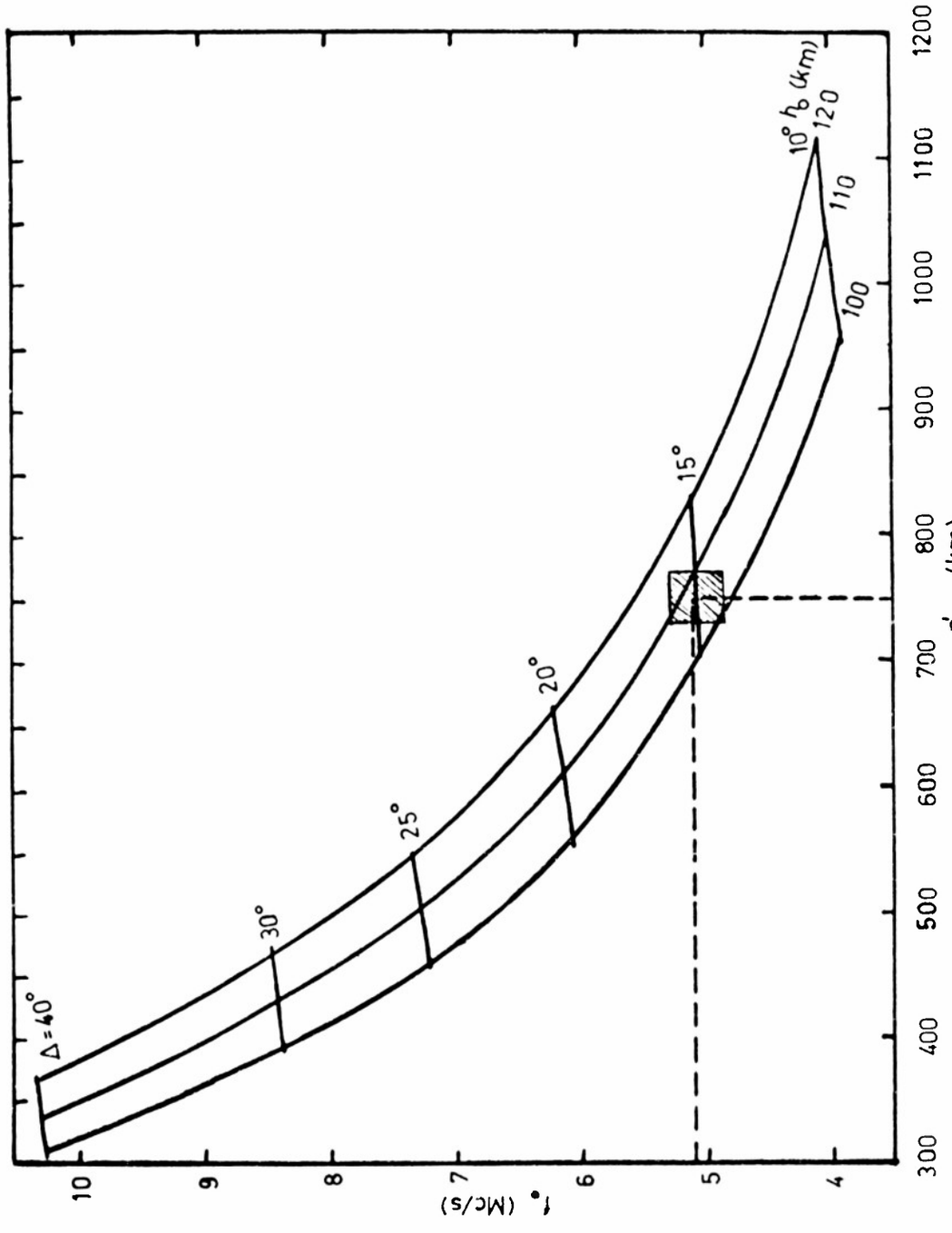

Fig. 75. Curves to find f_oE_s and h_oE_s from 16 Mc/s data.

$p'_{min} = 750 \pm 20$ km and $\Delta_s = 15^o \pm 1^o$. Then $f_o = 5.06 \pm 0.2$ Mc/s and $h_o = 107 \pm 8$ km.

More generally, the errors are

$$\delta f_o = \pm 0.2\, \delta\Delta \text{ Mc/s},$$

$$\delta h_o = \pm 8\, \delta\Delta \text{ km}.$$

If f is not 16 Mc/s, the curves of Fig. 73 may still be used if the values of f_o obtained are multiplied by f/16.

Swept-frequency sounding is necessary if the ionospheric parameters at particular ranges are to be measured continuously, since with fixed frequency sounding the control point range varies considerably as the ionospheric configuration varies. Angle of arrival measurements would be very difficult with swept-frequency backscatter, owing to the problem of keeping the angle of arrival equipment in tune with the sounder. A crude estimate of angle of arrival could, however, be obtained by noting that for 16 Mc/s backscatter from the land west of Brisbane the knee angle is remarkably constant at about 13^o. The maximum value of p'_{min} for the western echo (at its appearance or disappearance) would therefore correspond to an angle Δ_s approximately equal to 10^o.

12.4 Summary

The early promise that backscatter sounding would become a widely used tool in obtaining maximum usable frequencies for commercial circuits has not been realized, owing to

difficulties in interpreting the data. Similarly, the deduction of the ionospheric layer parameters f_o, h_o and y_m by comparing calculated and observed shapes of echo pulses is highly complex and can achieve little. By measuring the angle of arrival of selected parts of the echo pulse, it should be possible to deduce two parameters if the third were known; this could be most useful in observations of sporadic-E.

APPENDIX I

LIST OF PRINCIPAL SYMBOLS

$A = x^2 y_m n^2 / r_o$

$A_o = \sigma_o$

$C = \cos i_o$

c = free-space velocity of electromagnetic waves.

D = ground range to scatter source, $= D_1 + D_2$. *

D_s = skip distance.

$1E_s$ = echo returned by one-hop E_s mode.

F = focusing factor.

1F = echo returned by one-hop F mode.

f = transmitted frequency (always 16 Mc/s here).

f_c = "no field" critical frequency.

f_E = critical frequency of the E ray.

f_H = gyrofrequency.

f_o = critical frequency of the ordinary ray.

G = power gain of aerials for transmission or reception.

$g = \pi/2 - i_o$

H = height of ocean waves.

h_o = true height of base of parabolic layer.

h_o' = virtual height of base of parabolic layer.

i_o = angle of incidence of rays on base of layer.

L = loss of power due to deviative absorption.

n = sin i_o

P_C = calculated relative peak echo power if γ is constant.

P_R = relative power received.

p = phase path-length.

p' = equivalent free-space path-length to scatter source, sometimes referred to as oblique or group range. *

p'_{min} = minimum value of p'.

R = radius of the earth (about 6370 km).

r_o = $R + h_o$

δt = duration of transmitted pulse.

W = windspeed.

X = f_c^2/f^2

x = f / f_o

Y = f_H/f

y_m = semi-thickness of a parabolic layer.

γ = backscatter coefficient, = σ_o / cos φ

Δ = angle of elevation of any ray at the ground.

Δ_k = knee angle in γ (Δ) curve.

Δ_s = angle of elevation of the skip ray.

θ = angle between ray and geomagnetic field.

λ = wavelength (At 16 Mc/s, this is 18.75 m).

ν = collision frequency.

ρ = γ / Ω , also reflection coefficient of F region.

σ_o = radar cross-section per unit area of the ground.

φ = $\pi / 2 - \Delta$

* Subscripts 1 and 2 denote ionospheric and sub-ionospheric contributions respectively.

APPENDIX II

FORMULAS USED TO CALCULATE P_C AND Δ_s

(a) Appleton and Beynon Equations

As given in SHEARMAN (1956b), these are:

$$p_1' = 2x\, y_m \tanh \left(\frac{x \cos i_o}{1 - \frac{x^2\, y_m}{R + h_o} \sin^2 i_o} \right)$$

$$D_1 = \frac{R}{R + h_o} \sin i_o \; p_1'$$

$$p_2' = 2R \frac{\sin (\pi/2 - \Delta - i_o)}{\sin i_o}$$

$$D_2 = 2R (\pi/2 - \Delta - i_o)$$

Using other symbols given in Appendix I, we can simplify the form of these equations. Also, the further formula

$$\frac{R}{\sin i_o} = \frac{R + h_o}{\sin (\pi/2 + \Delta)}$$

enables i_o to be expressed in terms of Δ.

Thus, $\sin i_o = \frac{R}{r_o} \cos \Delta = n$

Also, since $g = \pi/2 - i_o$,

$$\tan g = \cot i_o = \frac{C}{n},$$

so $$g = \tan^{-1} \left(\frac{C}{n}\right)$$

Hence, the equations may be written

$$p_1' = 2 \times y_m \tanh \frac{(x\,C)}{(1 - A)}$$

$$D_1 = \frac{R\,n}{r_o}\, p_1'$$

$$p_2' = 2\,R\,\frac{\sin(g - \Delta)}{n}$$

$$D_2 = 2\,R\,(g - \Delta)$$

(b) To find the penetration angle

By the secant law of ionospheric reflection, at the penetration angle, $x = \sec i_o$.

Then $\cos i_o = 1 / x = \sqrt{1 - n^2}$,

so that $n = \sqrt{1 - 1/x^2}$.

But $\cos \Delta = \frac{r_o\, n}{R}$, hence Δ for penetration can be found; this is the angle of elevation at the ground for which a ray penetrates the ionosphere.

(c) Focusing Factor

(i) First order theory: Re-writing SHEARMAN (1956b), and simplifying,

$$F = \frac{\cot \Delta}{R \sin \frac{D}{R} \frac{dD}{d\Delta}}, \quad \text{where}$$

$$\frac{dD}{d\Delta} = \frac{R}{r_o} \frac{\sin \Delta}{C} \left[2\,R \left\{ A \frac{\left(1 - \frac{2\,x^2 y_m}{r_o} + A\right)}{(1 - A)^2 - x^2 C^2} + 1 \right\} - \frac{C\,D_1}{n} \right] - 2\,R$$

(ii) Second order theory, used at skip distance:

$$F = \frac{10.59 \cdot 10^{-12}}{\lambda^{1/3}} \frac{\cos \Delta}{\sin(\frac{D}{R}) \left(\frac{\sin \Delta}{R} \frac{\partial^2 D}{\partial \Delta^2}\right)^{2/3}}$$

$$D = D_s$$

(d) Echo power

SHEARMAN (1956b) has the equivalent of

$$P_R \propto \int_{D-\delta D}^{D} G^2 F^2 A_o R \sin \frac{D}{R} \, dD$$

For a single hop, $R \sin \frac{D}{R}$ is approximately equal to D, to within 2% and this leads to an error of only 0.1 dB in P_R. Making this approximation, and replacing A_o by $\gamma \sin \Delta$, we have

$$P_R \propto \int_{D-\delta D}^{D} G^2 F^2 \gamma \sin \Delta \, D \, dD$$

In the calculations, γ was assumed constant, giving the result

$$P_C \propto \int_{D-\delta D}^{D} G^2 F^2 \sin \Delta \, D \, dD$$

APPENDIX III

LIST OF PUBLICATIONS

STEELE J.G. 1964 "The effect of the ground back-scatter coefficient on observations of sporadic-E over sea, land and mountains".
J. Atmos. Terrest. Phys. 26, 322.

STEELE J.G. 1965 "Measurement of Antenna Radiation Patterns Using a Tethered Balloon".
Trans. I.E.E.E. AP-13. In press.

REFERENCES

A.R.R.L. 1956 The A.R.R.L. Antenna Book. American Radio Relay League, West Hartford, Connecticut, U.S.A.

ADAM A.E. and WHITEHEAD J.D. 1960 Proc. Inst. Radio Engrs. 48, 1172.

APPLETON E.V. and BEYNON W.J.G. 1940 Proc. Phys. Soc. 52, 518.

BECKMANN P. and SPIZZICHINO A. 1963 The Scattering of Electromagnetic Waves from Rough Surfaces. Pergamon Press, Oxford.

BENNER A.H. 1949 Proc. Inst. Radio Engrs. 37, 44.

BIXBY L.H. JR 1953 Calculation of High Frequency Radio Field Intensity over a 4000-Kilometer Ionospheric Path. Radio Propagation Laboratory, Stanford University.

BLAKE L.V. 1950 Proc. Inst. Radio Engrs. 38, 303.

BREMMER H. 1948 Terrestrial Radio Waves. Elsevier Publishing Company, Amsterdam.

BROWN W.E. JR 1960 J. Geophys. Res. 65, 3087.

BRUECKMANN H. 1955 Electronics. 28, 134.

BRUECKMANN H. 1963 Trans. I.E.E.E. AP-11, 147.

C.R.P.L. 1948 Ionospheric Radio Propagation. U. S. Nat. Bur. Stand. Circular 462.

CLAPP R.E. 1946 MIT Rad. Lab. Report. No. 1024.

COSGRIFF R.L., PEAKE W.H. and TAYLOR R.C. 1960 Engineering Experiment Station Bulletin No. 181, The Ohio State University.

CROMBIE D.D. 1955 Nature. 175, 681.

DAVIES H. 1954 Proc. Instn Elect. Engrs IV, 101, 209.

DAVIES H.	1955	Proc. Instn Elect. Engrs Pt C, 102, 148.
DAVIES H. and MACFARLANE G.G.	1946	Proc. Phys. Soc. 58, 717.
DAVIS J.R. and ROHLFS D.C.	1964	J. Geophys. Res. 69, 3257.
de BETTENCOURT	1952	Trans. Inst. Radio Engrs. AP-3, 202.
DIEMINGER W.	1951	Proc. Phys. Soc. B, 64, 142.
DOMINICI P.	1962	Technical Note 9, Radioelectrico Sperimentale "G. Marconi", Rome.
DOMINICI P.	1963	Ann. Geofis. 16, 121.
DOWDEN R.L.	1957	J. Atmos. Terrest. Phys. 11, 111.
EGAN R.D.	1960	Some Ionospheric Results Obtained During the International Geophysical Year. Page 231. Edited by W.J.G. Beynon. Elsevier Publishing Company, Amsterdam.
EGAN R.D. and PETERSON A.M.	1961	Stanford Technical Report No. 2.
EGAN R.D. and PETERSON A.M.	1962	Ionospheric Sporadic E. Eds, Smith E.K. and Matsushita S. Pergamon Press, Oxford.
EVANS J.V. and PETTENGILL G.H.	1963	J. Geophys. Res. 68, 423 and 5093.
HAGFORS T.	1961	J. Geophys. Res. 66, 777.
HAGN G.	1962	Stanford Research Institute Project 2909, Final Report II.
HEISLER L.H. and WHITEHEAD J.D.	1964	J. Atmos. Terrest. Phys. 26, 437.
INGALLS R.P. and STONE M.L.	1957	Trans. Inst. Radio Engrs. AP-5, 164. (Abstract from IRE-URSI Symposium).

KATZ I. and SPETNER L.M. 1958 App. Phys. Lab. Report CF-2700. The Johns Hopkins University.

KATZ I. and SPETNER L.M. 1960 J. Res. Nat. Bur. Stand. 64-D, 483.

KATZIN M. 1957 Proc. Inst. Radio Engrs. 45, 44.

KEAY C.S.L. and GRAY R.E. 1964 Electronic Engng. 36, 322.

KERR D.E. 1951 Propagation of Short Radio Waves. McGraw-Hill Book Company, Inc., New York.

KNIGHT P., DAVIES R.E. and MANTON R.G. 1964 Proc. Instn Elect. Engrs. 111, 421.

LEWIS C. and CAMPBELL J.D. (Eds) 1951 The Oxford Atlas. Oxford University Press.

LYNN V.H., SCHIGIAN M.D. and CROCKER E.A. 1964 J. Geophys. Res. 69, 781.

MACDONALD F.G. 1956 Convention Record, Inst. Radio Engrs, 4, 29.

McCUE C.G. 1956 Austral. J. Phys. 9, 454.

NIELSON D., HAGN G., RORDEN L. and CLARK N. 1960 Stanford Research Institute Project 2909, Final Report.

PEAKE W.H. 1957a Antenna Lab. Report 694-3, Ohio State University Research Foundation.

PEAKE W.H. 1957b Antenna Lab. Report 694-7, Ohio State University Research Foundation.

PEAKE W.H. 1958 Antenna Lab. Report 898-2, Ohio State University Research Foundation.

PETERSON A.M. 1951 J. Geophys. Res. 56, 221.

PETERSON A.M. 1956 Annals of the International Geophysical Year. 3, Part IV, 361. Pergammon Press.

PETTENGILL G.H.	1960	Proc. Inst. Radio Engrs. 48, 933.
RANZI I. and DOMINICI P.	1959	Scientific Note 1, Centro Radioelectrico Sperimentale "G. Marconi", Rome.
RATCLIFFE J.A.	1959	The Magneto-Ionic Theory and Its Applications to the Ionosphere. Cambridge University Press, London.
SCHMERLING E.R. and VENTRICE C.A.	1959	J. Atmos. Terrest. Phys. 14, 242.
SHEARMAN E.D.R.	1956a	Proc. Instn Elect. Engrs. 103B, 203.
SHEARMAN E.D.R.	1956b	Proc. Instn Elect. Engrs. 103B, 210.
SHEARMAN E.D.R.	1961	Proc. Instn Elect. Engrs. 108B, 361.
SHEARMAN E.D.R.	1963	Proc. International Conference on the Ionosphere, Imperial College, London, 1962. Page 294. Inst. Phys. and Phys. Soc., London.
SILBERSTEIN R.	1954	Trans. Inst. Radio Engrs. AP-2, 56.
SMITH N.	1945	Nat. Bur. Stand. Report IRPL-R9.
STEELE J.G.	1964	J. Atmos. Terrest. Phys. 26, 322.
TAIEB C.	1962	Ann. Geophys. 18, 227.
THOMAS J.A.	1961	Nature. 191, 792.
THOMAS J.A.	1962a	Scientific Report No. 6, Project 5631, Radio Research Section, University of Qld.
THOMAS J.A.	1962b	Scientific Report No. 8, Project 5631, Radio Research Section, University of Qld.
THOMAS J.A.	1964	J. Res. Nat. Bur. Stand. 68D, 419.

THOMAS J.A. and McINNES B.A.	1962	Scientific Report No. 10, Project 5631, Radio Research Section, University of Qld.
THOMAS J.A. and McINNES B.A.	1964	Radio Science. Nat. Bur. Stand. In press.
THOMAS J.A. and McNICOL R.W.E.	1960a	Nature. 187, 398.
THOMAS J.A. and McNICOL R.W.E.	1960b	Scientific Report No. 1, Project 5631, Radio Research Section, University of Qld.
THOMAS J.A. and McNICOL R.W.E.	1962	Scientific Report No. 5, Project 5631, Radio Research Section, University of Qld.
THOMAS J.A., DEARDEN E.W., MATTHEW E.M., McNICOL R.W.E., McINNES B.A., SINGLETON D.G., GOODWIN G.L., LYNCH G.J.E. and CROUCHLEY J.	1962	Scientific Report No. 16, Project 5631, Radio Research Section, University of Qld.
U.S.A.F.	1960	Handbook of Geophysics. The Macmillan Company, New York.
VILLARD O.G. JR and PETERSON A.M.	1952a	Trans. Inst. Radio Engrs. AP-3, 186.
VILLARD O.G. JR and PETERSON A.M.	1952b	Science. 116, 221.
WILKINS A.F. and SHEARMAN E.D.R.	1957	J. Brit. Instn Radio Engrs. 17, 601.
WILLIAMS H.P.	1950	Antenna Theory and Design, Vol. II. Pitman, London.
WINTER D.F.	1962	J. Res. Nat. Bur. Stand. 66D, 215.

UNCLASSIFIED
Security Classification

DOCUMENT CONTROL DATA - R&D

(Security classification of title, body of abstract and indexing annotation must be entered when the overall report is classified)

1. ORIGINATING ACTIVITY *(Corporate author)*
Stanford Electronics Laboratories
Stanford University, Stanford, California

2a. REPORT SECURITY CLASSIFICATION
UNCLASSIFIED

2b. GROUP

3. REPORT TITLE
BACKSCATTER OF RADIO WAVES FROM THE GROUND

4. DESCRIPTIVE NOTES *(Type of report and inclusive dates)*
Technical Report

5. AUTHOR(S) *(Last name, first name, initial)*
J. G. Steele

6. REPORT DATE	7a. TOTAL NO. OF PAGES	7b. NO. OF REFS
June 1965	195	75

8a. CONTRACT OR GRANT NO.	9a. ORIGINATOR'S REPORT NUMBER(S)
ONR Contract Nonr-225(64)	Technical Report No. 109
b. PROJECT NO. and ARPA Order 196-65	SU-SEL-65-064
c.	9b. OTHER REPORT NO(S) *(Any other numbers that may be assigned this report)*
d.	

10. AVAILABILITY/LIMITATION NOTICES
Qualified requesters may obtain copies of this report from DDC. Foreign announcement and dissemination by DDC not authorized.

11. SUPPLEMENTARY NOTES	12. SPONSORING MILITARY ACTIVITY
Covers research conducted at the U. of Queensland, Brisbane, Australia under sponsorship of Australian Radio	Research Board

13. ABSTRACT At 16 Mcs, the backscatter coefficient for sea is found to be 10 dB higher than for land for angles of elevation between 25° and 15°. At lower angles there is a knee effect, and the backscatter coefficient decreases very rapidly. The knee angle is lower for sea than for land. For a given surface, and at angles above the knee, the variation of backscatter coefficient with elevation angle is consistent with the type of scatter expected from upright objects such as trees or wave crests, and the fading of the echoes is ascribed to the Doppler movement of these objects.

The frequency of observation of Sporadic-E by backscatter sounding is strongly influenced by whether the backscatter occurs on the land or on the sea. Sporadic-E itself appears to be uniformly distributed. In observations of F region propagation by the backscatter technique, the nature of the terrain should be taken into account. This is particularly important in the case of trans-equatorial one-hop propagation. The experimental procedures developed here include a new method of measuring the vertical radiation patterns of large high frequency antennas, a computer program to calculate the power of backscatter echoes, and the application of vertical incidence data to oblique propagation. New insights are gained into the interpretation of backscatter records.

DD FORM 1 JAN 64 1473

UNCLASSIFIED
Security Classification

UNCLASSIFIED

Security Classification

14. KEY WORDS	LINK A		LINK B		LINK C	
	ROLE	WT	ROLE	WT	ROLE	WT
BACKSCATTER OF RF FROM LAND AND SEA						

INSTRUCTIONS

1. ORIGINATING ACTIVITY: Enter the name and address of the contractor, subcontractor, grantee, Department of Defense activity or other organization *(corporate author)* issuing the report.

2*a*. REPORT SECURITY CLASSIFICATION: Enter the overall security classification of the report. Indicate whether "Restricted Data" is included. Marking is to be in accordance with appropriate security regulations.

2*b*. GROUP: Automatic downgrading is specified in DoD Directive 5200.10 and Armed Forces Industrial Manual. Enter the group number. Also, when applicable, show that optional markings have been used for Group 3 and Group 4 as authorized.

3. REPORT TITLE: Enter the complete report title in all capital letters. Titles in all cases should be unclassified. If a meaningful title cannot be selected without classification, show title classification in all capitals in parenthesis immediately following the title.

4. DESCRIPTIVE NOTES: If appropriate, enter the type of report, e.g., interim, progress, summary, annual, or final. Give the inclusive dates when a specific reporting period is covered.

5. AUTHOR(S): Enter the name(s) of author(s) as shown on or in the report. Enter last name, first name, middle initial. If military, show rank and branch of service. The name of the principal author is an absolute minimum requirement.

6. REPORT DATE: Enter the date of the report as day, month, year; or month, year. If more than one date appears on the report, use date of publication.

7*a*. TOTAL NUMBER OF PAGES: The total page count should follow normal pagination procedures, i.e., enter the number of pages containing information.

7*b*. NUMBER OF REFERENCES: Enter the total number of references cited in the report.

8*a*. CONTRACT OR GRANT NUMBER: If appropriate, enter the applicable number of the contract or grant under which the report was written.

8*b*, 8*c*, & 8*d*. PROJECT NUMBER: Enter the appropriate military department identification, such as project number, subproject number, system numbers, task number, etc.

9*a*. ORIGINATOR'S REPORT NUMBER(S): Enter the official report number by which the document will be identified and controlled by the originating activity. This number must be unique to this report.

9*b*. OTHER REPORT NUMBER(S): If the report has been assigned any other report numbers *(either by the originator or by the sponsor)*, also enter this number(s).

10. AVAILABILITY/LIMITATION NOTICES: Enter any limitations on further dissemination of the report, other than those imposed by security classification, using standard statements such as:

(1) "Qualified requesters may obtain copies of this report from DDC."

(2) "Foreign announcement and dissemination of this report by DDC is not authorized."

(3) "U. S. Government agencies may obtain copies of this report directly from DDC. Other qualified DDC users shall request through _____."

(4) "U. S. military agencies may obtain copies of this report directly from DDC. Other qualified users shall request through _____."

(5) "All distribution of this report is controlled. Qualified DDC users shall request through _____."

If the report has been furnished to the Office of Technical Services, Department of Commerce, for sale to the public, indicate this fact and enter the price, if known.

11. SUPPLEMENTARY NOTES: Use for additional explanatory notes.

12. SPONSORING MILITARY ACTIVITY: Enter the name of the departmental project office or laboratory sponsoring *(paying for)* the research and development. Include address.

13. ABSTRACT: Enter an abstract giving a brief and factual summary of the document indicative of the report, even though it may also appear elsewhere in the body of the technical report. If additional space is required, a continuation sheet shall be attached.

It is highly desirable that the abstract of classified reports be unclassified. Each paragraph of the abstract shall end with an indication of the military security classification of the information in the paragraph, represented as *(TS)*, *(S)*, *(C)*, or *(U)*.

There is no limitation on the length of the abstract. However, the suggested length is from 150 to 225 words.

14. KEY WORDS: Key words are technically meaningful terms or short phrases that characterize a report and may be used as index entries for cataloging the report. Key words must be selected so that no security classification is required. Identifiers, such as equipment model designation, trade name, military project code name, geographic location, may be used as key words but will be followed by an indication of technical context. The assignment of links, roles, and weights is optional.

UNCLASSIFIED